Synthesis, Properties and Catalytic Activities for CO_2 Reduction of Porphyrins and Porphyrin Complexes Bearing π-Conjugated Substituents

OKABE YUKI

Doctor of Philosophy

Department of Structural Molecular Science
School of Physical Sciences
SOKENDAI (The Graduate University for Advanced Studies)

Synthesis, Properties and Catalytic Activities for CO_2 Reduction of Porphyrins and Porphyrin Complexes Bearing π-Conjugated Substituents

Okabe, Yuki

SOKENDAI (The Graduate University for Advanced Studies)

School of Physical Sciences
Department of Structural Molecular Science

Contents

General Introduction

CO_2 Reduction

The development of sustainable energy conversion system is strongly required in recent years due to the exhaustion of fossil fuels and environmental problems in the world. In nature, efficient sustainable energy conversion is achieved by photosynthetic reactions. In natural photosynthetic reactions, carbon dioxide (CO_2) is converted into chemical energy (glucose) by utilizing solar energy. In this context, the development of artificial photosynthesis,[1, 2] which mimics the natural photosynthetic reaction, is an attractive research subject. As well as natural photosynthesis, clean chemical energy can be obtained from the abundant source on the earth in artificial photosynthesis. The catalytic reduction of CO_2 is a representative example of artificial photosynthetic reactions. As shown in Scheme 1, CO_2 can be reduced to various kinds of chemical fuels such as carbon monoxide (CO), formic acid, formaldehyde, methanol and methane. These reactions are advantageous because the decrease in the amount of CO_2 in the atmosphere and the generation of clean chemical energy source can be achieved at the same time.[3] In particular, CO is greatly useful carbon source which is utilized in the synthesis of liquid fuels kind of liquid hydrocarbons by the Fischer-Tropsch process.[4] Therefore, the development of catalytic system which can convert CO_2 to CO is a crucially important research target.

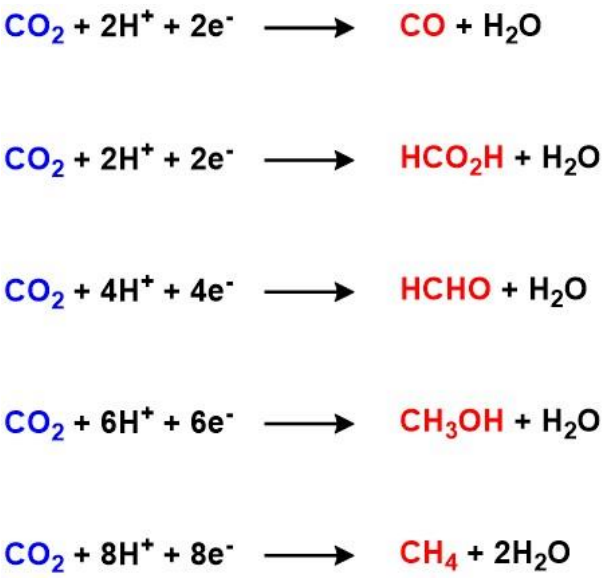

Scheme 1. CO_2 reduction reactions to produce chemical fuels.

Porphyrin Derivatives

Porphyrin is an aromatic macrocyclic molecule which have large π-electronic system. The synthesis and physical properties of porphyrin and its derivatives have been widely studied from the end of the 19th century.[5] These molecules have following four features which are potentially important for the catalytic CO_2 reduction (Figure 1).

At first, porphyrin derivatives have a metal binding site at the center of the macrocycle (Figure 1a). Porphyrin derivatives which have a metal ion at the binding site are called metalloporphyrins, and are known to serve as catalysts for several catalytic reactions. In natural systems, an oxidoreductase superfamily called cytochrome P450, which exist in livers of animals, includes Heme, a kind of iron porphyrins complex, in its structure. This class of enzymes can catalyze various oxidation reactions, and metal centers of Heme function as active centers in these reactions.[6] Metalloporphyrins are used as catalysts in artificial systems as well, and the many kinds of organic reactions including hydroxylation, amination, and epoxidation are catalyzed by metalloporphyrins with variety of metal ions.[7]

Second, porphyrin derivatives have high light-harvesting ability (Figure 1b). Chlorophyll, which is green pigments found in cyanobacteria and the chloroplasts of algae and plants, contains a porphyrin skeleton and function as a light harvesting unit in the natural photosynthetic reaction. In artificial systems, light-harvesting ability of porphyrin derivatives are also widely used. For instance, zinc porphyrin derivatives are employed as photosensitizers in several model compounds to study photoinduced electron transfer processes.[8]

Third feature is redox flexibility (Figure 1c). Porphyrins exhibit redox activity, and are possible to proceed reversible multi-redox reaction utilizing π electrons highly delocalized on the macrocycle.[9] Additionally, the introduction of appropriate substituents to their *meso*-positions, sp^3 carbons bridged by pyrroles, enables the further control over the redox properties. The modification of the *meso*-positions is synthetically straightforward and possible to install not only electron-donating and -withdrawing group but also redox active substituents like ferrocenyl[10] and quinolyl group.[11]

Fourth feature is that porphyrin macrocycle bear highly symmetric and rigid π-planar structure (Figure 1d). π-Planes of porphyrins often exhibit intermolecular

interaction such π-π and CH-π interaction and form assembled structures both in solution[12] and in the solid phase.[13] Such assembled structures usually display hydrophobicity due to the large π-planes of porphyrins and are expected to have high affinity with non-polar CO_2 molecules.

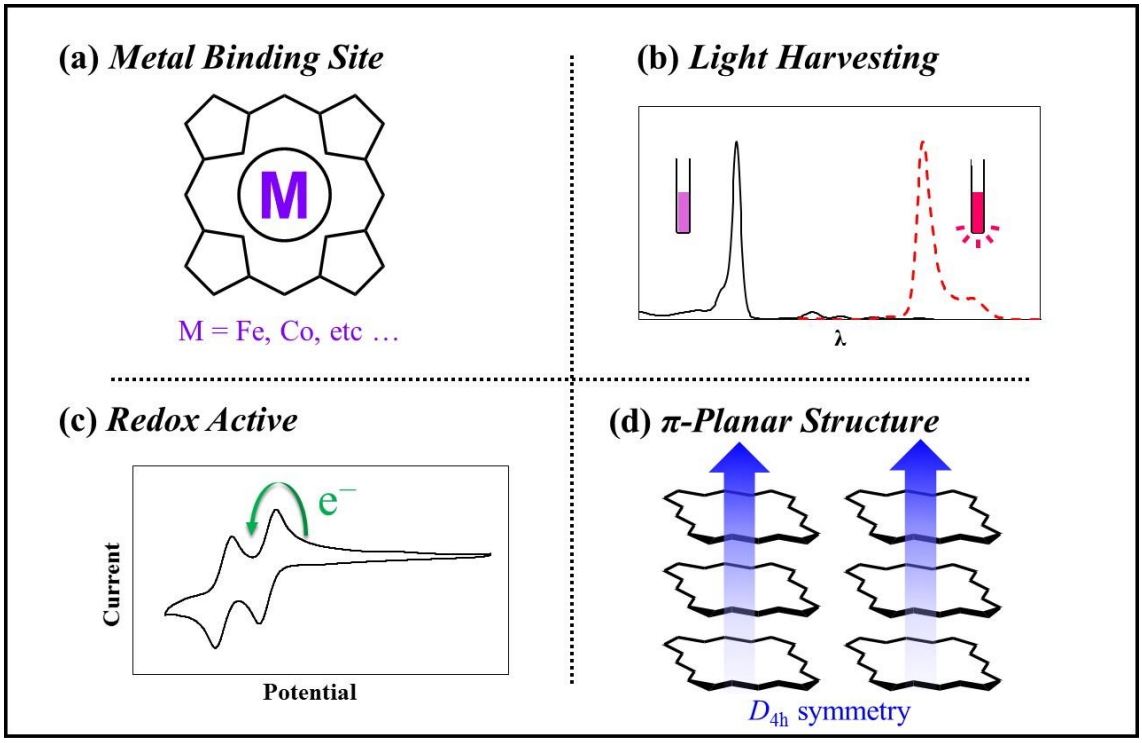

Figure 1. Four important features of porphyrin derivatives for CO_2 reduction.

Metalloporphyrin-Catalyzed CO_2 Reduction

As described in the previous section, porphyrin can form metal complexes, metalloporphyrins, and the metal centers of metalloporphyrins can serve as catalytic centers for various reactions (Figure 1a). Inspired by the feature, the catalytic activity of metalloporphyrin for CO_2 reduction has been studied. In 1988, Savéant *et al*. reported the electrochemical reduction of CO_2 reduction catalyzed by an iron tetraphenylporphyrin complex (**Fe-TPP,** Figure 2a) for the first time.[14] In this catalytic reaction, CO was obtained as a major product. The proposed catalytic cycle of **Fe-TPP** is shown in Scheme 2.[15] In this mechanism, Fe(0) species formed by the three electron reduction of **Fe-TPP** can serve as an active species for the reaction, which indicates that the high redox flexibility of the porphyrin derivative (Figure 1c) is essential to promote the reaction. It should be also noted that the existence of Lewis acids or Brønsted acids can enhance the catalytic activity of **Fe-TPP**.[15, 16]

After the discovery of catalytic activity of **Fe-TPP**, the development of iron porphyrin-based catalysts for electrochemical reduction of CO_2 has begun to explore and various kinds of iron-porphyrins for electrocatalysts for CO_2 reduction have been reported up to date[17] (for representative examples, see Figure 2a). Savéant *et al*. found that the introduction of proton reservoir sites into the porphyrin moiety of **Fe-TPP** can improve the catalytic activity.[15, 16] More recently, it is reported that an unsymmetrical iron porphyrin complex bearing both 2,6-dihydroxyphenyl groups as proton reservoir sites and 2,3,4,5,6-pentafluorophenyl groups as withdrawing groups exhibits superior activity. It is also found that a water soluble iron porphyrin bearing trimethylammonium groups able to convert CO_2 into CO with a little amount of H_2 under neutral pH conditions.[18] Sun *et al* reported the effect of the position of methoxycarbonyl group introduced to the phenyl moieties on the catalytic activity.[19]

It is noteworthy that iron porphyrin complexes undergoes photocatalytic CO_2 reduction and the examples of iron porphyrin-based photocatalysts are shown in Figure 2b.[20] Initially, Neta *et al*. reported that photolysis of **Fe-TPP** in DMF solutions containing 5% of triethylamine as a sacrificial electron donor resulted in the formation of CO.[21] The turnover number of the reaction was approximately 40. In these reactions, **Fe-TPP** functions not only as a catalyst but also as a photo absorbing unit utilizing its high

light harvesting ability (Figures 1b). The authors also investigated the photoreduction of CO_2 in aqueous media using tetrakis(N-methyl-2-pyridyl)porphyrin iron(III) chloride as a catalyst.

The cobalt porphyrin complexes are also known to catalyze CO_2 reduction both under electrochemical and photochemical conditions (Figures 2c, d). The cobalt complex of tetraphenylporphyrin, **Co-TPP** and its derivative bearing trifluoromethyl groups are known to undergo electrocatalytic CO_2 reduction.[22] Photocatalytic activity of **Co-TPP** was also examined and it is found that the addition of *p*-terphenyl as a photosensitizer or trimethylamine as sacrificial electron donor can enhance the catalytic activity of the system.[23]

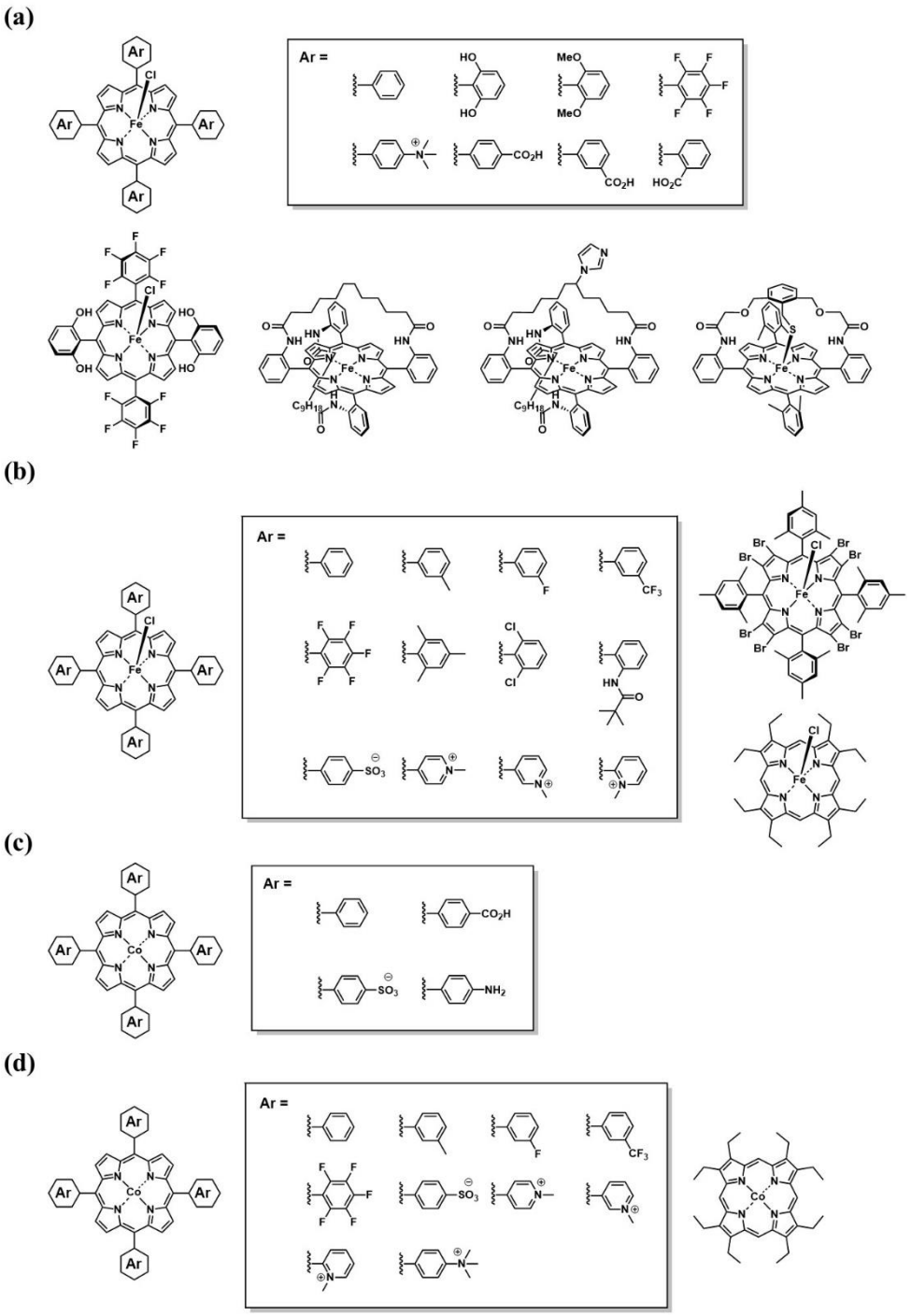

Figure 2. Examples of (a) iron porphyrin complexes catalysts for electrochemical CO_2 reduction (b) iron porphyrin complexes catalysts for photochemical CO_2 reduction (c) cobalt porphyrin complexes catalysts for electrochemical CO_2 reduction (d) cobalt porphyrin complexes catalysts for photochemical CO_2 reduction.

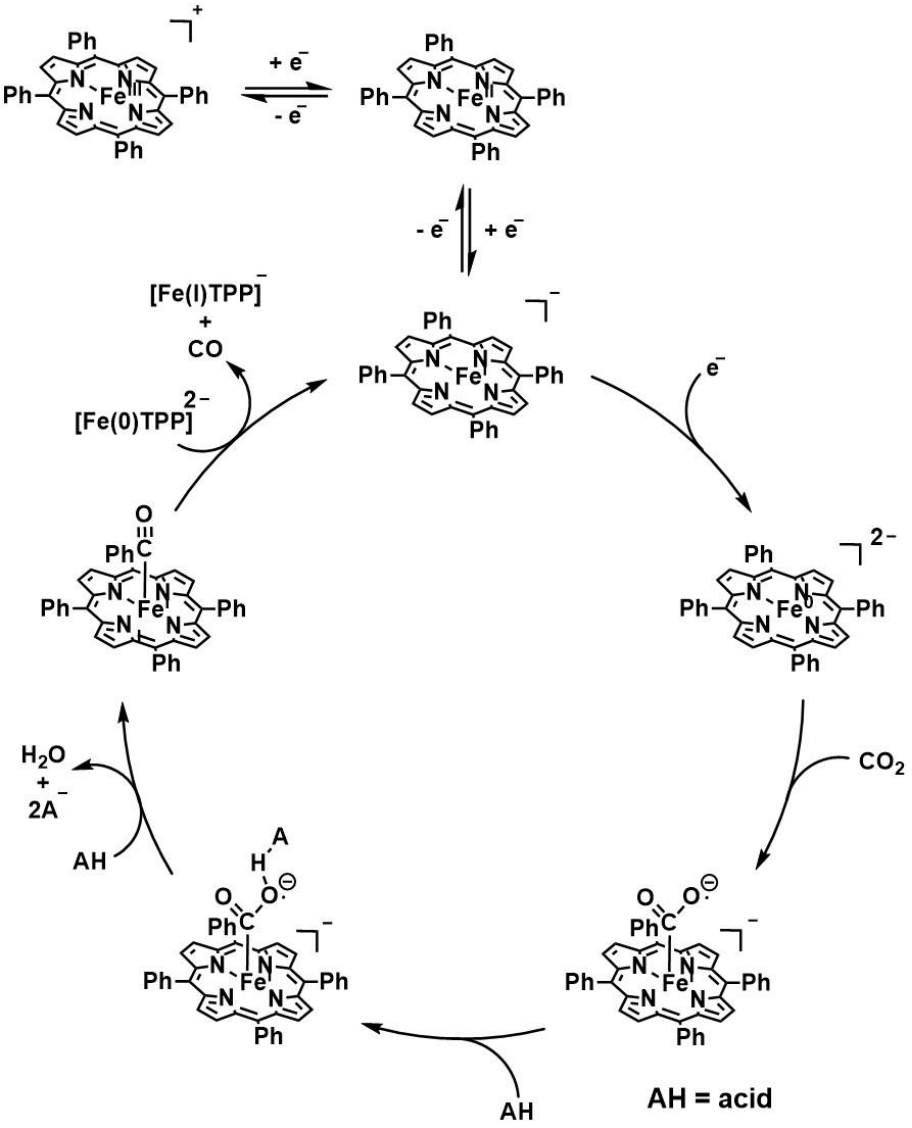

Scheme 2. Proposed mechanism of catalytic CO_2 reduction by **Fe-TPP**.

CO_2 Adsorption in Porphyrin-based Framework

In the atmospheric condition, the concentration of CO_2 is quite low. However, it is very difficult for the currently developed catalysts for CO_2 reduction to proceed the reaction under the ambient condition and most of the system requires the highly concentrated CO_2 gas for the reaction. Therefore, the development of the system which can accumulate CO_2 gas nearby catalytic centers is an important research target.

Metal organic frameworks (MOF)[24] and covalent organic frameworks (COF)[25] are an intriguing class of materials for the accumulation of CO_2. MOFs and COFs have a highly ordered porous network structure constructed by the self-assembly of organic linkers and metal ions (MOFs) or organic linkers (COFs). It is also noteworthy that the size of and the hydrophilicity/ hydrophobicity of pores can finely be tuned by changing the molecular structure of organic linkers which construct the framework, which results in the selective accommodation of gas molecules.[26] Additionally, the functional moieties such as catalytic centers and sensing sites can easily be integrated into the frameworks.[27] These features of MOFs and COFs differentiate them from the conventional porous materials such as activated carbon and zeolites.

Porphyrin derivatives are known to serve as building units for porous materials due to their highly symmetric and rigid structures (Figure 1d). In 1994, Robson *et al*., reported that two kinds of copper(II) porphyrin complexes can form the porous framework via non-covalent interaction between complexes. After the discovery of MOFs and COFs, porphyrin derivatives have started to be used as organic linkers and various kinds of structures are reported so far.[28]

In these reports, the several frameworks are found to be capable to adsorb CO_2 gas in their pores.[29] Ma *et al*. have constructed a MOF composed of cobalt ions and tetrakis(3,5-dicarboxyphenyl)porphine cobalt(II) (Co(II)tdcpp) as an organic linker, $\{[Co(II)_3(OH)(H_2O)]_4(Co(II)tdcpp)_3\}$ (**MMPF-2**, Figure 3a)).[30] The authors concluded that high density of the coordinatively unsaturated cobalt atoms within the porphyrin macrocycles contributed to the excellent CO_2 adsorption properties of the MOF. Jiang *et al*. prepared imine-linked COFs bearing 5,10,15,20-tetraphenylporphyrin moiety (Figure 3b).[31] They systematically controlled the properties of pore surface by introducing diverse functional groups with controllable loading contents via click reaction.

More recently, Yaghi *et al.* has succeeded in developing a COF that can catalyse CO_2 reduction using cobalt porphyrin complexes as organic linkers (Figure 4).[32] The COF developed by the group exhibited 26 times higher catalytic activity for CO_2 reduction in aqueous media compared with the corresponding discrete system. They also found that the expansion of pore size resulted in the higher activity. These reports strongly suggest that the utilization of porous framework can be a powerful tool to develop a highly efficient catalytic system for CO_2 reduction.

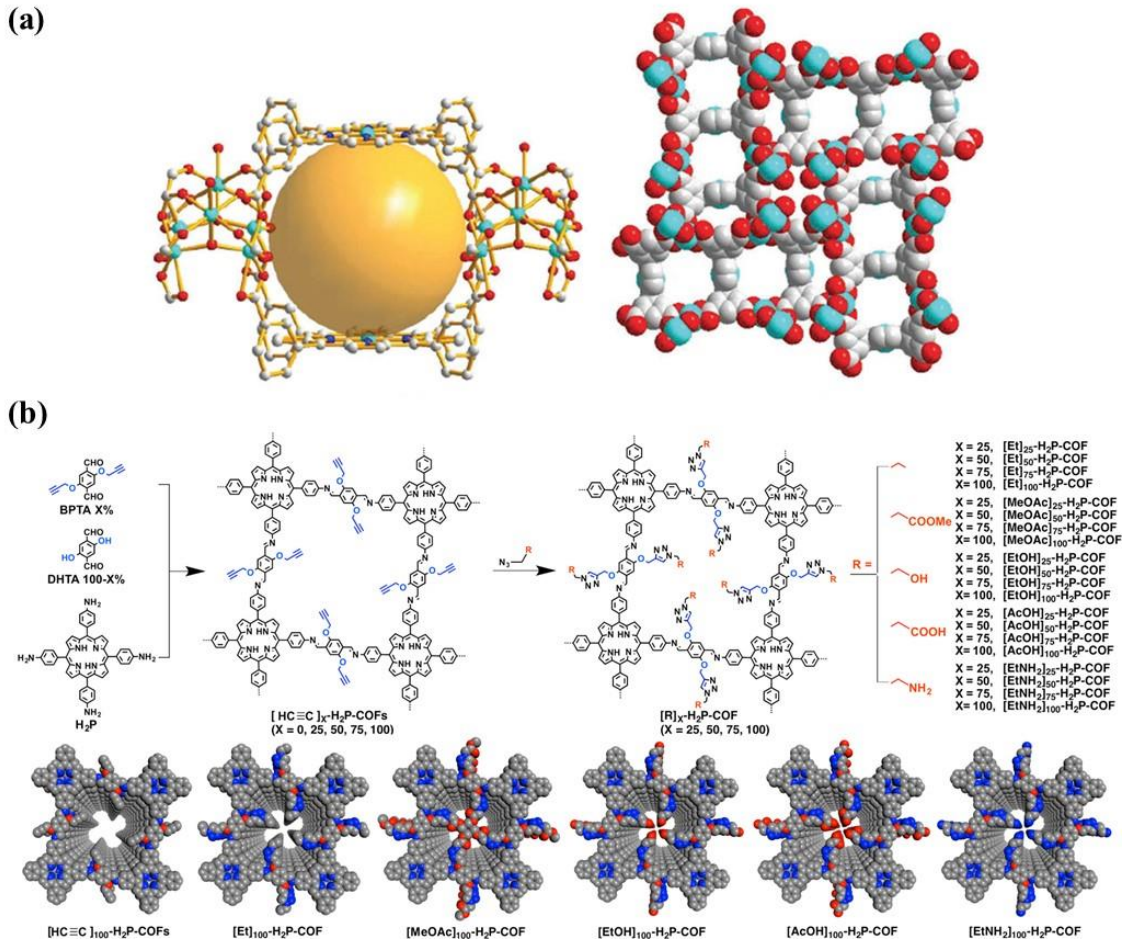

Figure 3. (a) (left) Three cobalt porphyrins located in the "face-to-face" configuration in **MMPF-2**; (right) space filling model of three types of channels in **MMPF-2** viewed from the *c* direction. Reproduced with permission from Ma *et al*.[30] (b) A Schematic illustration of pore surface engineering of imine-linked COFs with various functional groups via click reactions. Reproduced with permission from Jiang *et al*.[31]

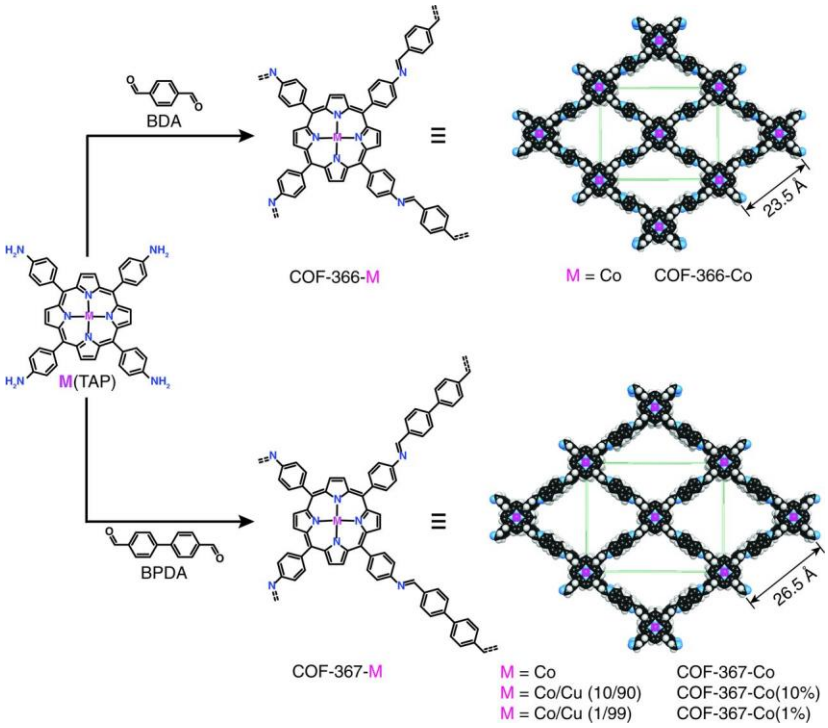

Figure 4. Design and synthesis of metalloporphyrin-derived 2D covalent organic frameworks. Reproduced with permission from Yaghi *et al*.[32]

The Aim of This Thesis

Metalloporphyrin complexes can serve as catalysts CO_2 reduction to generate CO. However, it is still difficult to perform the catalytic reaction with the low concentration of CO_2 as the atmospheric condition (0.04 %). Therefore, it is necessary for the highly effective CO_2 conversion system to develop novel catalytic systems, in which the reaction can proceed under quite low partial pressure of CO_2 gas. To achieve such a goal, the introduction of reaction field to accumulate CO_2 molecules nearby catalytic centers can potentially be interesting and attractive research target.

In this thesis, I aimed to construct novel metalloporphyrin-based catalytic systems with reaction fields. I employed two approaches; (i) a discrete system and (ii) an assembled framework system (Figure 5). Both systems are designed to create hydrophobic reaction field close to the metal centers of porphyrin complexes because non-polar CO_2 molecules are known to be accumulated in such a field. The installation of hydrophobic field is expected to be achieved by introducing substituents with large π-plane to porphyrin moieties. This study investigates the effect of the introduction of π-conjugated substituents into metalloporphyrin complex on their physical properties. The study can give some knowledge about (i) design and synthesis of porphyrin molecules which is able to form the hydrophobic space (ii) the effect of the hydrophobic space on the catalytic activity of the complex, and (iii) the substituents advantageous for the construction of a high ordered molecular assembly.

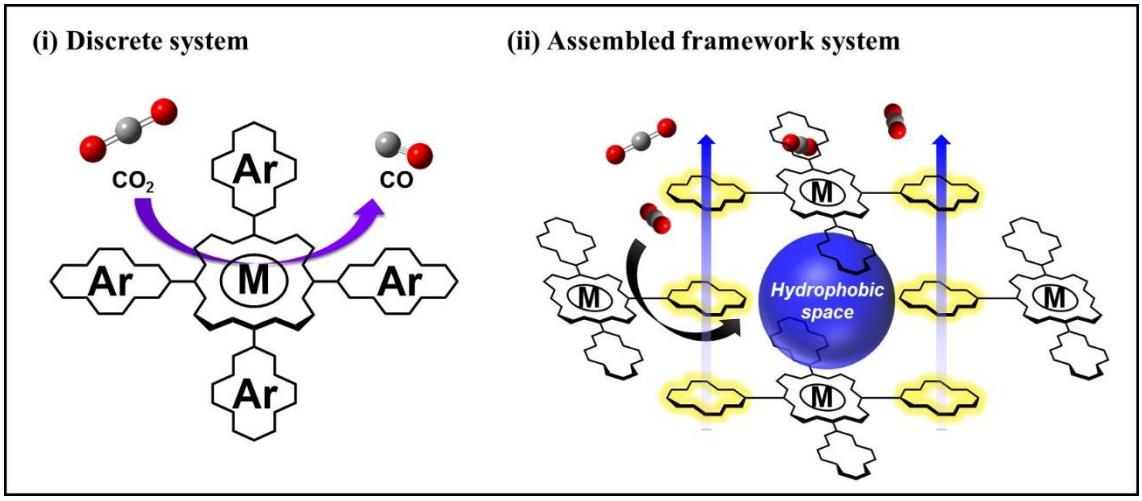

Figure 5. Schematic illustration of the targeted catalytic system (i) discrete system and (ii) assembled framework system.

Survey of This Thesis

Chapter 1 describes the syntheses, crystal structures and physical properties of free-base porphyrins and porphyrin complexes bearing various kinds of substituents at the *meso*-positions of porphyrin moiety. The synthetic procedures were successfully established for free-base porphyrins with electron-donating (**H-TMP**), -withdrawing (**H-EDB**), π-conjugated (**H-PEPy** and **H-PA**) and redox active (**H-FcN**) substituents (Figure 6) and metal complexes bearing the synthesized free-base porphyrins as ligands. The electronic states of the obtained compounds were investigated by UV-vis absorption spectroscopy, electrochemical measurement and transient absorption spectroscopy. Additionally, some crystal structures of free-base porphyrins were also reported, and the intermolecular interactions in each crystal packing were investigated.

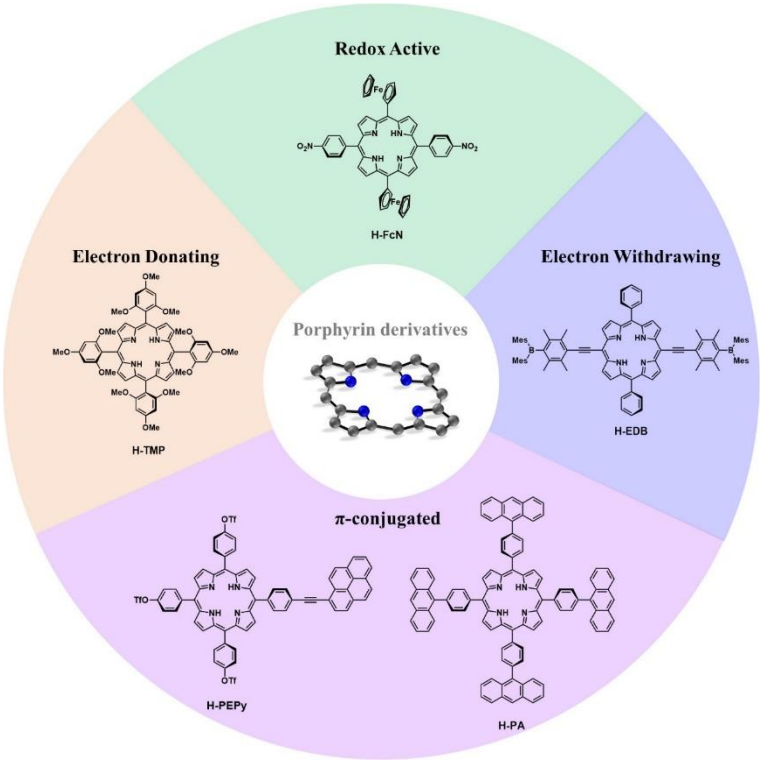

Figure 6. Molecular structures of the porphyrin derivatives investigated in chapter 1.

Chapter 2 describes the syntheses and the spectroscopic and electrochemical properties of iron porphyrin complexes with π-conjugated substituents at the *meso*-position (Figure 7). Three novel iron complexes, (5,10,15,20-tetrakis(pyren-1-yl)porphyrinato iron(III) chloride (**Fe-Py**), (5,10,15,20-tetrakis((1,1'-biphenyl)-4-yl)porphyrinato iron(III) chloride (**Fe-PPh**), and (5,10,15,20-tetrakis(4-(pyren-1-yl)phenyl)porphyrinato iron(III) chloride (**Fe-PPy**)**,** were synthesized by the reaction of the corresponding free-base porphyrins 5,10,15,20-tetrakis(pyren-1-yl)porphyrin (**H-Py**), 5,10,15,20-tetrakis((1,1'-biphenyl)-4-yl)porphyrin (**H-PPh**), and 5,10,15,20-tetrakis(4-(pyren-1-yl)phenyl)porphyrin (**H-PPy**) with iron(II) chloride tetrahydrate in DMF or *N*-methyl-2-pyrrolidone (NMP) and were characterized by elemental analyses and UV-vis absorption spectroscopy.

The electrochemical analyses of the complexes under an Ar atmosphere indicated that the introduction of the π-conjugated substituents rarely affects the electronic structures and redox properties of the iron porphyrin complexes. However, the electrochemical studies under CO_2 revealed that the catalytic activity of **Fe-Py** for CO_2 reduction was found to be much higher than that of 5,10,15,20-tetrakis(phenyl)porphyrinato iron(III) chloride (**Fe-Ph**). These results indicate that the introduction of large π-conjugated substituents directly to the *meso*-positions of a porphyrin moiety could provide a hydrophobic space suitable for the accumulation of CO_2 molecules, which resulted in the superior catalytic activity of the complex.

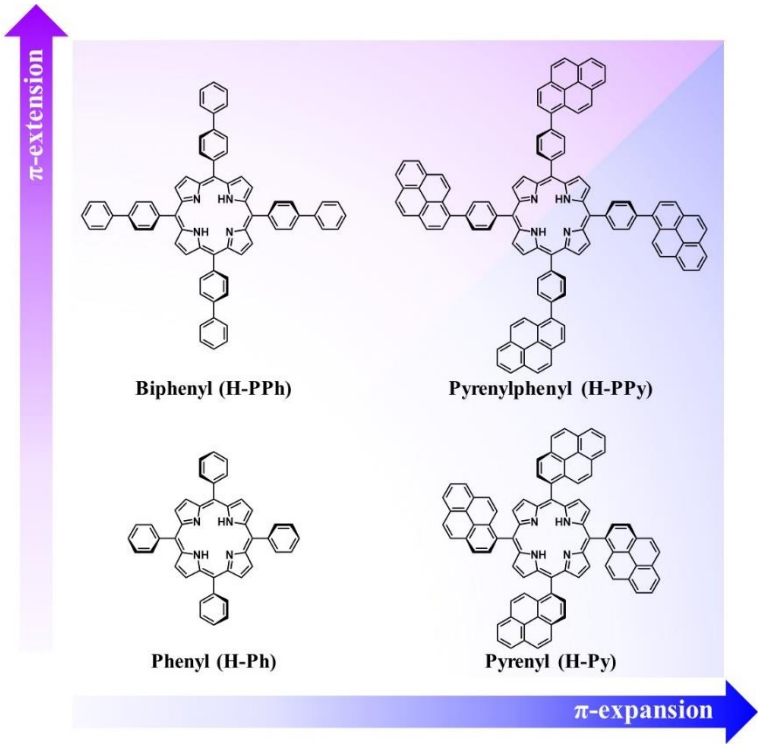

Figure 7. Chemical structures of the porphyrin derivatives investigated in chapter 2.

Chapter 3 describes the synthesis, physical properties and crystal structure of porphyrin derivatives for the construction of framework structure with hydrophobic channels. A novel free-base porphyrin, 5,10,15,20-tetrakis(4-(7-(*tert*-butyl)pyren-2-yl)phenyl)porphyrin (**H-BPPy**), which possesses four pyrenylphenyl moieties at the *meso*-positions of a porphyrin ring, were newly designed. The pyrene units installed in this molecules are known to exhibit both face-to-face (π-π) interaction and face-to-edge (CH-π) interaction and easily form the relatively strong assembled structure due to their planar polyaromatic feature. Furthermore, **H-BPPy** has four-fold symmetry and high planarity, which are advantageous for the construction of a highly ordered structure. Therefore, it is expected that the robust framework structure with hydrophobic pores are constructed by the self-assembly of the **H-BPPy** based metal complexes at room temperature, which will lead to the development of a novel catalytic system for CO_2 reduction.

The synthesis of **H-BPPy** was accomplished by the condensation reaction of pyrrole with the corresponding aldehyde derivative and the subsequent oxidation by 2,3-dichloro-5,6-dicyano-p-benzoquinone (DDQ). **H-BPPy** was further reacted with cobalt (II) acetate tetrahydrate under microwave heating condition and the corresponding cobalt porphyrin complex, **Co-BPPy**, was successfully obtained. The electrochemical studies of **Co-BPPy** under a CO_2 atmosphere revealed the increase of an irreversible current, which implies the catalytic activity of **Co-BPPy** for CO_2 reduction. Finally, the construction of framework structure via the self-assemble of **Co-BPPy** was examined. **Co-BPPy** exhibited high solubility in various organic solvents thanks to the *tert*-butyl moiety introduced at the 7-position of the pyrene unit, and the single crystals were obtained the slow diffusion of hexane to the THF solution of **Co-BPPy**. The structural analysis of the obtained single crystal revealed that porous structure with the pore entrance size of 9.03 × 8.64 $Å^2$ was formed via the CH-π interaction between the pyrene units. These pores are expected to function as channels to accumulate CO_2 molecules because the pores should exhibit hydrophobic nature surrounded by aromatic ring and the size of pores is large enough to accommodate CO_2 (Figure 8).

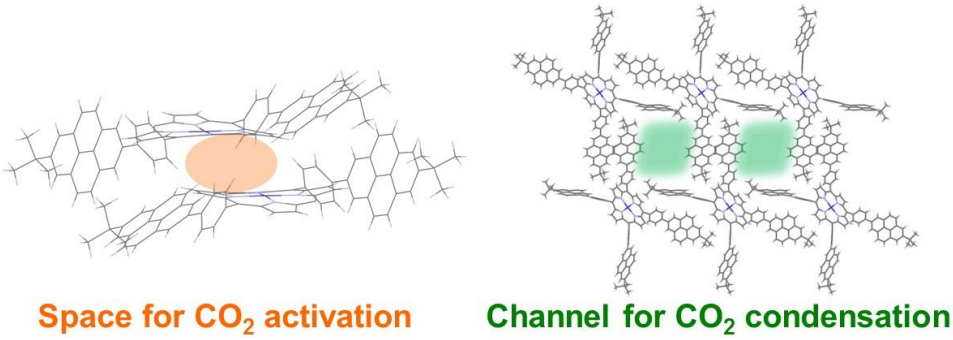

Figure 8. Crystal structures of the framework developed in the study described in chapter 3.

References

1. (a) S. W. Gersten, G. J. Samuels, T. J. Meyer, *J. Am. Chem. Soc*., **1982**, *104*, 4029. (b) T. Wada, K. Tsuge, K. Tanaka, *Angew. Chem. Int. Ed*., **2000**, *39*, 1479. (c) S. Masaoka, K. Sakai, *Chem. Lett*., **2009**, *38*, 182. (d) M. Okamura, M. Kondo, R. Kuga, Y. Kurashige, T. Yanai, S. Hayami, V. K. K. Praneeth, M. Yoshida, K. Yoneda, S. Kawata, S. Masaoka, *Nature*, **2016**, *530*, 465.
2. (a) D. V. Yandulov, R. R. Schrock, *Science*, **2003**, *301*, 76. (b) K. Arashiba, Y. Miyake, Y. Nishibayashi, *Nature Chemistry*, **2011**, *3*, 120. (c) J. S. Anderson, J. Rittle, J. C. Peters, *Nature*, **2013**, *501*, 84. (d) S. Kuriyama, K. Arashiba, K. Nakajima, Y. Matsuo, H. Tanaka, K. Ishii, K. Yoshizawa, Y. Nishibayashi, *Nature Communications*, **2016**, *7*, 12181.
3. N. S. Lewis, D. G. Nocera, *Proc. Natl. Acad. Sci. U.S.A.*, **2006**, *103*, 15729.
4. (a) H. Schulz, *Appl. Catal. A-Ge*n., **1999**, *186*, 3. (b) A. Y. Khodakov, W. Chu, P. Fongarland, *Chem. Rev*., **2007**, *107*, 1692. (c) E. van Steen, M. Claeys, *Chem. Eng. Technol*., **2008**, *31*, 655.
5. (a) J. E. Ranking, G. L. Pardington, *The Lancet*, **1890**, *136*, 607. (b) P. Rothemund, *J. Am. Chem. Soc*., **1939**, *61*, 2912. (c) P. Rothemund, A. R. Menotti, *J. Am. Chem. Soc*., **1941**, *63*, 267. (d) S. Aronoff, M. Calvin, *J. Org. Chem*., **1943**, *8*, 205. (e) R. H. Ball, G. D. Dorough, M. Calvin, *J. Am. Chem. Soc*., **1946**, *68*, 2278.
6. I. G. Denisov, T. M. Makris, S. G. Sligar, I. Schlichting, *Chem. Rev*., **2005**, *105*, 2253.
7. (a) J. P. Collman, X. Zhang, V. J. Lee, E. S. Uffelman, J. I. Brauman, *Science*, **1993**, *261*, 1404. (b) C-M. Che, V. K-Y. Lo, C-Y. Zhou, J-S. Huang, *Chem. Soc. Rev*., **2011**, *40*, 1950.
8. (a) D. Kuciauskas, P. A. Liddell, S. Lin, T. E. Johnson, S. J. Weghorn, J. S. Lindsey, A. L. Moore, T. A. Moore, D. Gust, *J. Am. Chem. Soc*., **1999**, *121*, 8604. (b) D. Kim, A. Osuka, *J. Phys. Chem. A*, **2003**, *107*, 8791. (c) Y. Nakamura, N. Aratani, A. Osuka, *Chem. Soc. Rev*. **2007**, *36*, 831. (d) G. Kodis, P. A. Liddell, L. de la Garza, P. C. Clausen, J. S. Lindsey, A. L. Moore, T. A. Moore, D. Gust. *J. Phys. Chem. A*, **2002**, *106*, 2036. (e) H. Imahori, Y. Sekiguchi, Y. Kashiwagi, T. Sato, Y. Araki, O. Ito, H. Yamada, S. Fukuzumi, *Chem. Eur. J*., **2004**, *10*, 3184. (f) H. Imahori, T. Umeyama, S. Ito, *Acc. Chem. Res*., **2009**, *42*, 1809. (g) A. Yella, H-W. Lee, H. N. Tsao, C. Yi, A. K. Chandiran, Md. K. Nazeeruddin, E. W-G. Diau, C-Y Yeh, S. M. Zakeeruddin, M. Grätzel, *Science*, **2011**, *334*, 629.
9. T. Dhanasekaran, J. Grodkowski, P. Neta, P. Hambright, E. Fujita, *J. Phys. Chem. A*, **1999**, 103, 7742.

10. (a) H. Imahori, D. M. Guldi, K. Tamaki, Y. Yoshida, C. Luo, Y. Sakata, S. Fukuzumi, *J. Am. Chem. Soc*., **2001**, *123*, 6617. (b) S. J. Dammer, P. V. Solntsev, J. R. Sabin, V. N. Nemykin, *Inorg. Chem*., **2013**, *52*, 9496. (c) A. Vecchi, P. Galloni, B. Floris, S. V. Dudkin, V. N. Nemykin, *Coord. Chem. Rev*. **2015**, *291*, 95.
11. (a) H. Grennberg, S. Faizon, J-E. Bäckvall, *Angaw. Chem. Int. Ed. Engl*., **1993**, *32*, 263. (b) M. Schreiber, C. Fuchs, R. Scholz, *J. Lumin*., **1998**, *76*, 482. (c) A. Wiehe, M. O Senge, A. Schäfer, M. Speck, S. Tannert, H. Kurreck, B. Röder, *Tetrahedron*, **2001**, *57*, 10089. (d) F. D'Souza, G. R. Deviprasad, *J. Org. Chem*., **2001**, *66*, 4601.
12. (a) M. Shirakawa, S. Kawano, N. Fujita, K. Sada, S. Shinkai, *J. Org. Chem*., **2003**, *68*, 5037. (b) T. Hasobe, S. Fukuzumi, P. V. Kamat, *J. Am. Chem. Soc*., **2005**, *127*, 11884.
13. (a) K-J. Lin, *Angew. Chem. Int. Ed*., **1999**, *38*, 2730. (b) I. Goldberg, *Chem. Commun*., **2005**, 1243. (c) H. Liu, J. Xu, Y. Li, Y. Li, *Acc. Chem. Res*., **2010**, *43*, 1496.
14. M. Hammouche, D. Lexa, J-M. Savéant, M. Momenteau, *J. Electroanal. Chem. Interfacial Electrochem*., **1988**, *249*, 347.
15. C. Costentin, S. Drouet, G. Passard, M. Robert, J-M. Savéant, *J. Am. Chem. Soc*., **2013**, *135*, 9023.
16. (a) I. Bhugun, D. Lexa, J-M. Savéant, *J. Am. Chem. Soc*., **1994**, *116*, 5015, (b) I. Bhugun, D. Lexa, J-M. Savéant, *J. Am. Chem. Soc*., **1996**, *118*, 1769, (c) I. Bhugun, D. Lexa, J-M. Savéant, *J. Phys. Chem.*, **1996**, *100*, 19981, (d) C. Costentin, S. Drouet, M. Robert, J-M. Savéant, *Science*, **2012**, *338*, 90.
17. (a) C. Costentin, G. Passard, M. Robert, J-M. Savéant, *Proc. Natl. Acad. Sci. U.S.A.*, **2014**, *111*, 14990. (b) H-Z. Zhao, Y-Y. Chang, C. Liu, *J. Solid. State. Electr*., **2013**, *17*, 1657. (c) K. Alenezi, S. K. Ibrahim, P. Li, C. J. Pickett, *Chem. Eur. J*., **2013**, *19*, 13522. (d) E. A. Mohamed, Z. N. Zaharan, Y. Naruta, *Chem. Commun.*, **2015**, *51*, 16900. (e) R. B. Ambre, Q. Daniel, T. Fan, H. Chen, B. Zhang, L. Wang, M. S. G. Ahlquist, L. Duan, L. Sun, *Chem. Commun*., **2016**, *52*, 14478. (f) J. Choi, T. M. Benedetti, R. Jalili, A. Walker, G. G. Wallace, D. L. Officer, *Chem. Eur. J*., **2016**, *22*, 14158.
18. C. Costentin, M. Robert, J-M. Savéant, A. Tatin, *Proc. Natl. Acad. Sci. U. S. A*., **2015**, *112*, 6882.
19. L. Sun, *Chem. Commun*., **2016**, *52*, 14478.
20. A. J. Morria, G. J. Meyer, E. Fujita, *Acc. Chem. Res*., **2009**, *42*, 1983.
21. J. Grodkowski, D. Behar, P. Neta, P. Hambright, *J. Phys. Chem. A*, **1997**, *101*, 248.
22. (a) D. Behar, T. Dhanasekaran, P. Neta, C. M. Hosten, D. Ejeh, P Hambright, E. Fujita, *J. Phys. Chem. A*, **1998**, *102*, 2870. (b) D. Quezada, J. Honores, M. Garcia, F.

Armijo, M. Isaacs, *New J. Chem*., **2014**, *38*, 3606. (c) K. Takahashi, K. Hiratsuka, H. Sasaki, S. Toshima, *Chem. lett*., **1979**, 305. (d) T. Atoguchi, A. Aramata, A. Kazusaka, M. Enyo, *J. Chem. Soc., Chem. Commun*., **1991**, 156.

23. T. Dhanasekaran, J. Grodkowski, P. Neta, P. Hambright, E. Fujita, *J. Phys. Chem. A*, **1999**, 103, 7742.
24. (a) S. Kitagawa, R. Kitaura, S. Noro, *Angew. Chem. Int. Ed*., **2004**, *43*, 2334, (b) O. M. Yaghi, M. O'Keeffe, N. W. Ockwig, H. K. Chae, M. Eddaoudi, J. Kim, *Nature*, **2003**, *423*, 705.
25. S-Y. Ding, W. Wang, *Chem. Soc. Rev*., **2013**, *42*, 548.
26. (a) J. A. Johnson, Q. Lin, L-C. Wu, N. Obaidi, Z. L. Olson, T. C. Reeson, Y-S. Chen, J. Zhang, *Chem. Commun*., **2013**, *49*, 2828. (b) W-Y. Gao, Z. Zhang, L. Cash, L. Wojtas, S. Ma, *CrystEngComm*., **2013**, *15*, 9320. (c) W-Y. Gao, L. Wojtas, S. Ma, *Chem. Commun*., **2014**, *50*, 5316. (d) S. Hamad, N. C. Hernandez, A. Aziz, A. R. Ruiz-Salvador, S. Calero, R. Grau-Crespo, *J. Mater. Chem. A*, **2015**, *3*, 23458. (e) A. Modak, M. Pramanik, S. Inagaki, A. Bhaumik, *J. Mater. Chem. A*, **2014**, *2*, 11642.
27. (a) N. Kornienko, Y. Zhao, C. S. Kley, C. Zhu, D. Kim, S. Lin, C. J. Chang, O. M. Yaghi, P. Yang, *J. Am. Chem. Soc*., **2015**, *137*, 14129. (b) I. Hod, M. D. Sampson, P. Deria, C. P. Kubiak, O. K. Farha, J. T. Hupp, *ACS Catal*., **2015**, *5*, 6302.
28. (a) B. F. Abrahams, B. F. Hoskins, D. M. Michail, R. Robson, *Nature*, **1994**, *369*, 727. (b) P. D. W. Boyd, C. A. Reed, *Acc. Chem. Res*., **2005**, *38*, 235. (c) K. S. Suslick, P. Bhyrappa, J-H. Chou, M. E. Kosal, S. Nakagaki, D. W. Smithenry, S. R. Wilson, *Acc. Chem. Res*., **2005**, *38*, 283. (d) L. Chen, Y. Yang, D. Jiang, *J. Am. Chem. Soc*., **2010**, *132*, 9138. (e) S. Wan, F. Gándara, A. Asano, H. Furukawa, A. Saeki, S. K. Dey, L. Liao, M. W. Ambrogio, Y. Y. Botros, X. Duan, S. Seki, J. F. Stoddart, O. M. Yaghi, *Chem. Mater*., **2011**, *23*, 4094. (f) A. Fateeva, P. A. Chater, C. P. Ireland, A. A. Tahir, Y. Z. Khimyak, P. V. Wiper, J. R. Darwent, M. J. Rosseinsky, *Angew. Chem. Int. Ed*., **2012**, *51*, 744. (g) W. Morris, B. Volosskiy, S. Demir, F. Gándara, P. L. McGrier, H. Furukawa, D. Cascio, J. F. Stoddart, O. M. Yaghi, *Inorg. Chem*., **2012**, *51*, 6443. (h) S. Kandambeth, D. B. Shinde, M. K. Panda, B. Lukose, T. Heine, R. Banerjee, *Angew. Chem. Int. Ed*., **2013**, *52*, 13052. (i) M. Calik, F. Auras, L. M. Salonen, K. Bader, I. Grill, M. Handloser, D. D. Medina, M. Dogru, F. Löbermann, D. Trauner, A. Hartschuh, T. Bein, *J. Am. Chem. Soc*., **2014**, *136*, 17802. (j) Z-S. Wu, L. Chen, J. Liu, K. Parvez, H. Liang, J. Shu, H. Sachdev, R. Graf, X. Feng, K. Müllen, *Adv. Mater*., **2014**, *26*, 1450. (k) M. Zhao, S. Ou, C-D. Wu, *Acc. Chem. Res*., **2014**, *47*, 1199. (a) Z. Guo, B. Chen, *Dalton Trans*., **2015**, *44*, 14574. (b) S. Huh, S-J. Kim, Y. Kim, *CrystEngComm*., **2016**, *18*, 345.

29. S. Kumar, M. Y. Wani, C. T. Arranja, J. A. e Silva, B. Avula, A. J. F. N. Sobral, *J. Mater. Chem. A*, **2015**, *3*, 19615.
30. X-S. Wang, M. Chrzanowski, C. Kim, W-Y. Gao, L. Wojtas, Y-S. Chen, X. P. Zhang, S. Ma, *Chem. Commun*., **2012**, *48*, 7173.
31. N. Huang, R. Krishna, D. Jiang, *J. Am. Chem. Soc*., **2015**, *137*, 7079.
32. S. Lin, C. S. Diercks, Y-B. Zhang, N. Kornienko, E. M. Nichols, Y. Zhao, A. R. Paris, D. Kim, P. Yang, O. M. Yaghi, C. J. Chang, *Science*, **2015**, *349*, 6253.

Chapter 1

Synthesis, crystal structures and physical properties of porphyrins and porphyrin complexes

Introduction

Porphyrin and its metal complexes are an intriguing class of molecules that shows rich redox chemistry and unique photophysical properties arising from highly delocalized π system. The first synthesis of a porphyrin derivative was achieved by Rothemund in 1935.[1] He reported the synthesis of tetraphenyl porphyrin from pyrrole and benzaldehyde. However, the isolated yield of the target compound was quite low, and this method is not suitable for the practical use. Latterly, Adler *et al.*, discovered the more convenient synthetic procedure to obtain tetraphenyl porphyrin and the yield of the synthetic reaction has dramatically improved.[2] However, this method is applicable only for the synthesis of symmetrical tetra-substituted porphyrin derivatives, and the selective synthesis of unsymmetrical porphyrins, which requires the condensation of pyrrole with more than two kinds of aldehyde derivatives, was quite difficult. To overcome such a problem, Lindsey *et al.*, developed an alternative synthetic route.[3] In their method, the diluted reaction condition was used to decrease the amount of an undesired side product, polypyorrylmethane, forms upon the condensation step and the formation of the desired porphyrin skelton became thermodynamically favorable. Additionally, they examined the syntheses of several unsymmetrical porphyrin derivatives via stepwise synthetic route, and succeeded in increasing the selectivity of the desired compounds.[4] After the discovery of these synthetic methods, the studies on porphyrin derivatives has explosively accelerated, which afforded various kinds of porphyrin-based functional materials.[5]

This chapter describes the syntheses and physical properties of porphyrins and porphyrin complexes bearing substituents at the *meso*-positions. I employed electron-donating and withdrawing, π-conjugated and redox active substituents. The synthetic route suitable for each substituents was successfully established. The obtained

compounds were studied by UV-vis absorption spectroscopy and electrochemical measurements to clarify the effect of the substituents on the electronic state of the molecules. The crystal structure of two compounds were also reported. The chemical structures of molecules investigated in this chapter is shown in Figure 1.

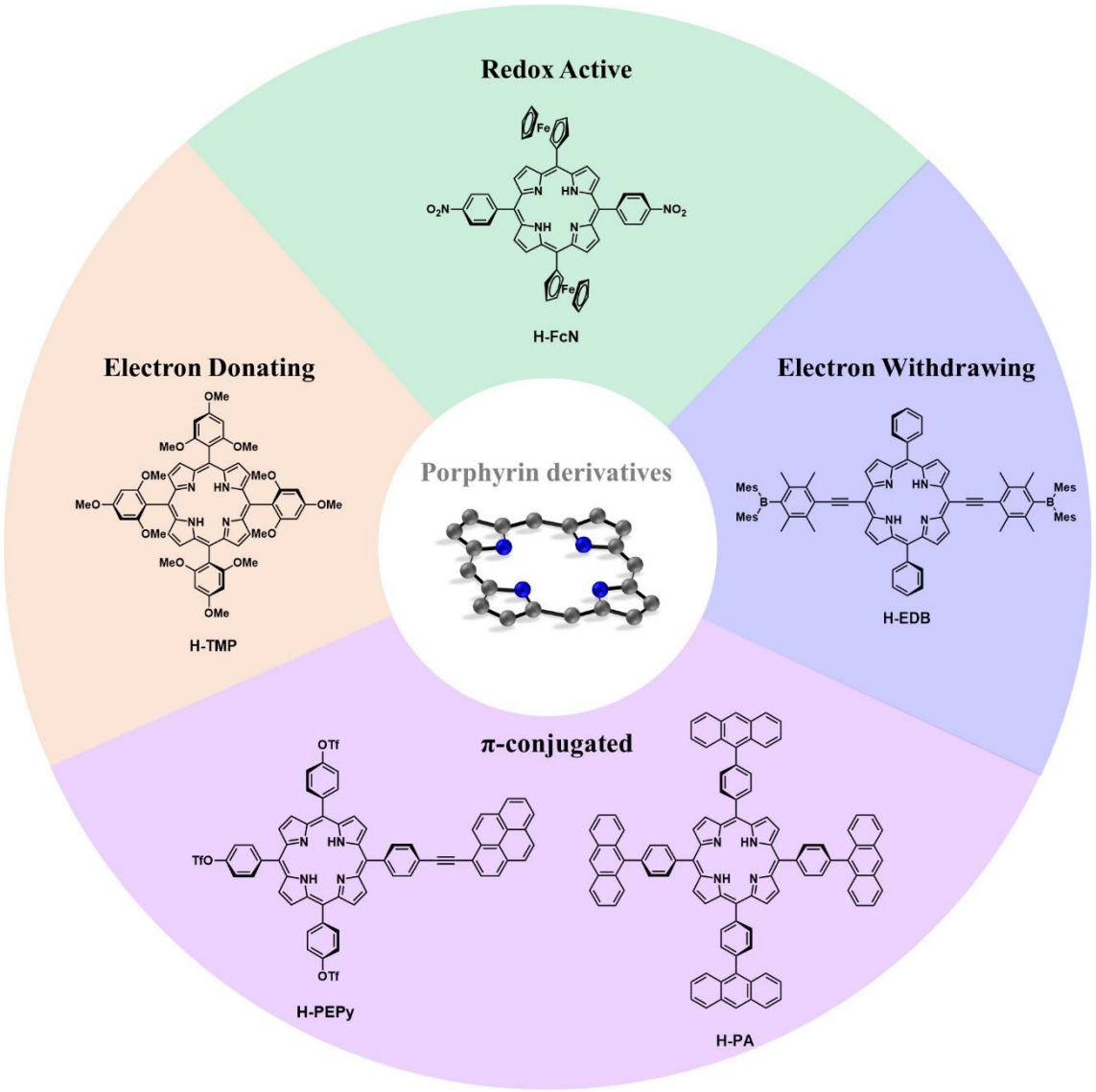

Figure 1. Molecular structure of the porphyrin derivatives investigated in this study.

Results and Discussion

Syntheses of Porphyrin Derivatives with Electron-Donating Substituents

The syntheses of a free-base porphyrin bearing four electron-donating substituents, 5,10,15,20-tetrakis(2,4,6-trimethoxyphenyl)porphyrin (**H-TMP**) and its iron complex, 5,10,15,20-tetrakis(2,4,6-trimethoxyphenyl)porphyrinato iron(III) chloride (**Fe-TMP**) are shown in Scheme 1. I assume that 2,4,6-trimethoxybenzaldehyde has lower reactivity compared to benzaldehyde due to the electron withdrawing nature of 2,4,6-trimethoxyphenyl group. Therefore, the stepwise synthetic route involving the isolation of the corresponding dipyrromethane derivative was employed. The synthesis of 5-(2,4,6-trimethoxyphenyl)dipyrromethane was performed by reacting 2,4,6-trimethoxybenzaldehyde with an excess amount of pyrrole and the desired compound was obtained in 22% yield. Subsequently, the obtained dipyrromethane was reacted with 2,4,6-trimethoxybenzaldehyde in dichloromethane (DCM), and the further oxidation of the corresponding porphyrinogen using chloranil as an oxidant affords the desired free-base porphyrin, **H-TMP**, in 38% yield. **H-TMP** was characterized by ^{1}H NMR spectroscopy.

The synthesis of the iron complex, **Fe-TMP**, was performed by reacting **H-TMP** with iron(II) chloride tetrahydrate (6.2 eq.) in dimethyl sulfoxide (DMSO) under reflux condition for 1h. The isolated yield of **Fe-TMP** was 73%. **Fe-TMP** was characterized by elemental analysis.

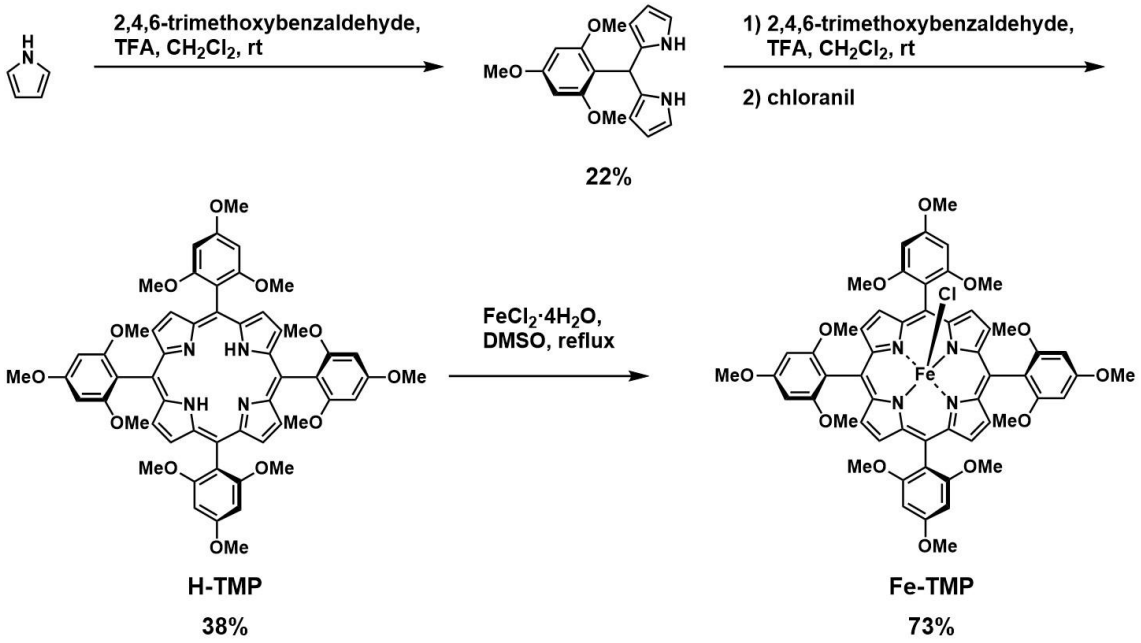

Scheme 1. Synthetic routes for **H-TMP** and **Fe-TMP**.

Synthesis of a Porphyrin Derivative with Electron-Withdrawing Substituents

The synthesis of a free-base porphyrin bearing with two electron-withdrawing substituents, trans-5,15-bis(dimesithylborylduryletheynyl)-10,20-bisphenyl porphyrin (**H-EDB**) is shown in Scheme 2. (4-ethynyl-2,3,5,6-tetramethylphenyl)dimesitylborane (**EDDB**) was synthesized as follows.[6] 1,2,4,5-Tetramethylbenzene was brominated using bromine in DCM to afford 1,4-dibrmo-2,3,5,6-tetramethylbenzene in 80% yield. The obtained compound was dehalogenated using *n*-butyllithium at −20 °C and the further boronation by dimesitylfluoroborane afforded (4-bromo-2,3,5,6-tetramethylphenyl)bis(2,4,6-trimethylphenyl)borane in 97% yield. The bromo group of the obtained compound was converted to an iodo group via the dehalogenation by *t*-butyllithium and the subsequent reaction with iodine, and (4-iodo-2,3,5,6-tetramethylphenyl)bis(2,4,6-trimethylphenyl)borane was obtained in 92% yield. Further Sonogashira cross coupling reaction of the compound with trimethylsilylacetylene and the deprotection of the trimethylsilyl affords **EDDB**.

The synthesis of porphyrin skeleton was performed as follows. First, the reaction of pyrrole and formaldehyde under acidic condition affords dipyrromethane in 49% yield. Dipyrromethane was condensed with benzaldehyde om the presence of triflluoroacetic acid (TFA) and an unsymmetrical porphyrin, 5, 15-bis(phenyl)porphyrin, was obtained (yield:30%). The *meso*-positions of 5, 15-bis(phenyl)porphyrin was brominated with *N*-bromosuccinimide (NBS) and *trans*-5,15-bisbromo-10,20-bisphenyl porphyrin was obtained (yield:95%). Finally, Sonogashira cross coupling of *trans*-5,15-bisbromo-10,20-bisphenyl porphyrin and **EDDB** afforded the desired porphyrin derivative, **H-EDB**, in 43% yield. **H-EDB** was characterized by ^{1}H NMR spectroscopy.

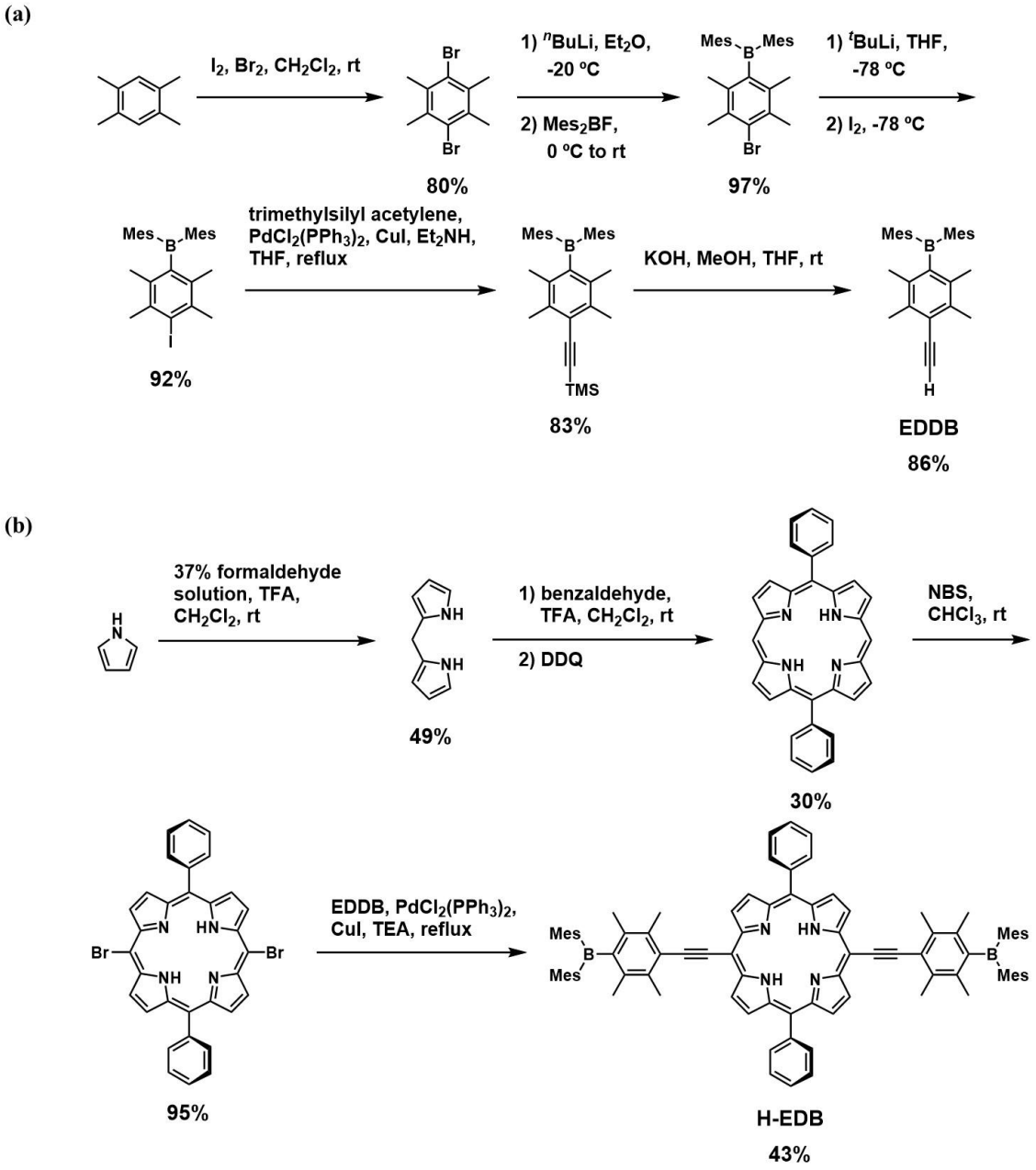

Scheme 2. Synthetic routes for (a) **EDDB** and (b) **H-EDB.**

Syntheses of Porphyrin Derivatives with π-Conjugated Substituents

The syntheses of free-base porphyrins bearing π-conjugated substituents, and their iron complexes are shown in Schemes 3 and 4. A free-base porphyrin bearing four anthracenylphenyl groups, 5,10,15,20-tetrakis(4-(anthracen-9-yl)phenyl)porphyrin **(H-PA**), was synthesized using 9-bormoanthracene as a starting substrate. Pd-catalyzed Suzuki-Miyaura cross coupling of the compound with 4-formylphenylboronic acid affords 4-(anthracen-9-yl)benzaldehyde in high yield (93%). The obtained aldehyde was condensed with pyrrole under modified Lindsey condition, and **H-PA** was obtained in 23% yield. **H-PA** was characterized by ^{1}H NMR spectroscopy.

The metalation to **H-PA** was performed by reacting **H-PA** with iron(II) chloride tetrahydrate (6.1 eq.) in *N*,*N*-dimethlyformamide (DMF) under reflux condition for 1h. The correponding iron complex, 5,10,15,20-tetrakis(4-(anthracen-1-yl)phenyl)porphyrinato iron(III) chloride, (**Fe-PA**) was obtained in 71% yield. **Fe-PA** was characterized by elemental analysis.

The syntheses of free-base porphyrins bearing pyrenylphenyl groups, 5,10,15,20-tetrakis(4-(pyren-1-ylethynyl)phenyl)porphyrin **(H-PEPy$_4$)**, were also examined. 4-Formylphenyl trifluoromethanesulfonate was obtained by the triflation of 4-hydroxybenzaldehyde using trifluoromethanesulfonic anhydride in basic condition at 0 °C. Following condensation reaction of the aldehyde with pyrrole was conducted in two different condition, Lindsey (Path 1, Scheme 4) and Adler condition (Path 2), and the Lindsey method gave 5,10,15,20-tetrakis(4-trifluoromethansulfonylphenyl)porphyrin (**H-PT**) in higher yield than that of Path 2. This is because the lower concentration of substrates in Path 1 prevented the undesired side reaction, the polymerization of pyrrole. As a final step, a palladium catalyzed Sonogashira coupling reaction of **H-PT** with 1-ethynylpyrene was performed to obtain **H-PEPy$_4$**. However, only the mono-substituted porphyrin (**H-PEPy**) was obtained as a main product. **H-PEPy** was characterized by ^{1}H NMR spectroscopy. The metalation to **H-PEPy** was performed by reacting **H-PEPy** with iron(II) chloride tetrahydrate (6.0 eq.) in *N*,*N*-dimethlyformamide (DMF) under reflux condition for 1h. The correponding iron complex, 5,10,15-tris(4-trifluoromethansulfonylphenyl)-20-(4-(pyren-1-ylethynyl)phenyl)porphyrinato iron(III)

chloride, (**Fe-PEPy**) was obtained in 75% yield. **Fe-PEPy** was characterized by elemental analysis.

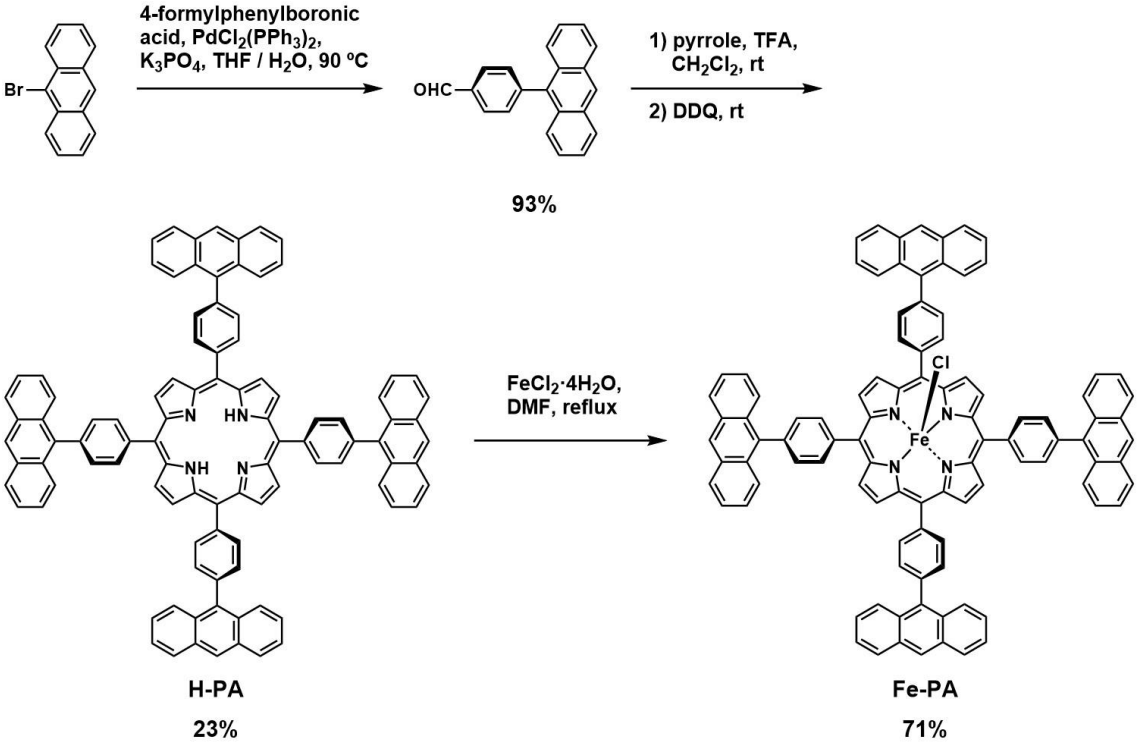

Scheme 3. Synthetic routes for **H-PA** and **Fe-PA.**

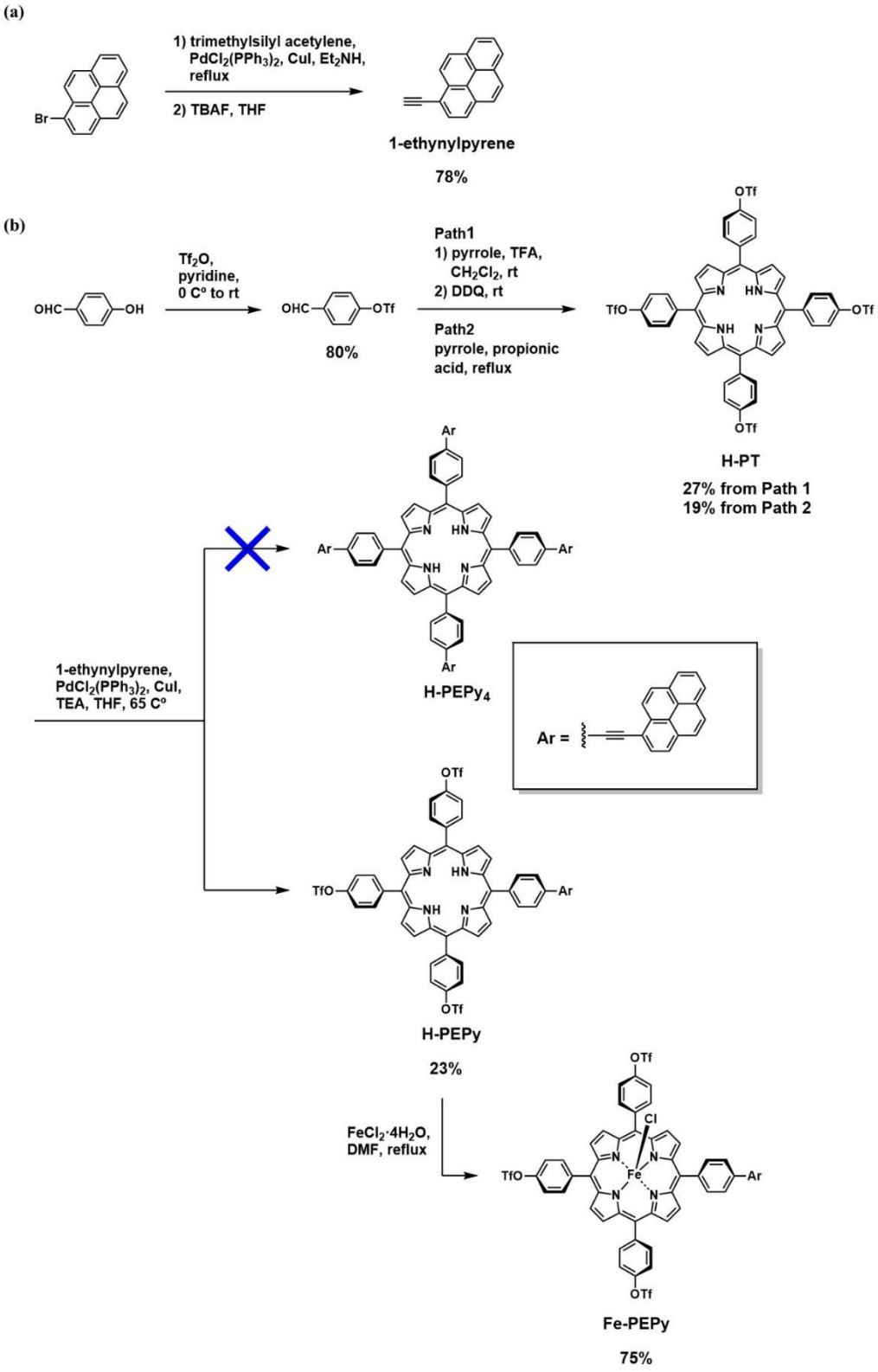

Scheme 4. Synthetic routes for (a) 1-ethynylpyrene and **(b) H-PEPy** and **Fe-PEPy**.

Synthesis of a Porphyrin with Redox Active Substituents

The synthesis of a free-base porphyrin bearing redox active substituents, trans-5,15-bisferrocenyl-10,20-bis(4-nitrophenyl) porphyrin (**H-FcN**) is shown in Scheme 5. [7, 8] Due to the strong electron donating ability of ferrocenyl group, **H-FcN** was synthesized via the stepwise synthetic route involving the isolation of the corresponding dipyrromethane derivative, which is similar to the synthesis of **H-TMP** (*vide supra*). Ferrocenecarbaldehyde was condensed with an excess amount of pyrrole to give 5-ferrocenyldipyrromethane (**Fc-DP**) in 88% yield. The dipyrromethane derivative was further condensed with an equal amount of 4-nitrobenzaldehyde in acidic condition. After the construction of macrocyclic porphyrin skeleton, it was aromatized by using 2,3-dichloro-5,6-dicyano-p-benzoquinone (DDQ) as an oxidant, which afforded *trans*-5,15-bisferrocenyl-10,20-bis(4-nitrophenyl)porphyrin (**H-FcN**) in 4% yield. I also tried an alternative synthetic route to improve the reaction yield. In this alternative route, the condensation reaction with 4-nitrobenzaldehyde and pyrrole was initially performed to obtain 5-(4-nitrophenyl)dipyrromethane (**NO_2-DP**) in 89% yield. Subsequently, **NO_2-DP** was condensed with ferrocenecalbaldehyde under the similar reaction condition as described above, and the desired product, **H-FcN**, was obtained in higher yield than the previous attempt. The formation of the desired unsymmetrical porphyrin was confirmed by ^{1}H NMR and elemental analysis. The ^{1}H-NMR spectra of **H-FcN** in $CDCl_3$ shows two doublet peaks of pyrrole β-position's proton at δ 9.86 and 8.55 ppm due to unsymmetrical porphyrin structure. Multiplet peaks at δ 8.61-8.64 and 8.32-8.35 ppm are assigned to the protons of the 4-nitrophenyl substituents. Signals attributed to the cyclopentadienyl (Cp) ring which is directly connected to porphyrin ring located at δ 5.49 and 4.84 ppm as triplet peaks, and the unsubstituted Cp ring showed only one singlet peak at δ 4.11 ppm. In higher magnetic field, a typical broad singlet signal which corresponds to the internal N-H of the porphyrin moiety was observed.

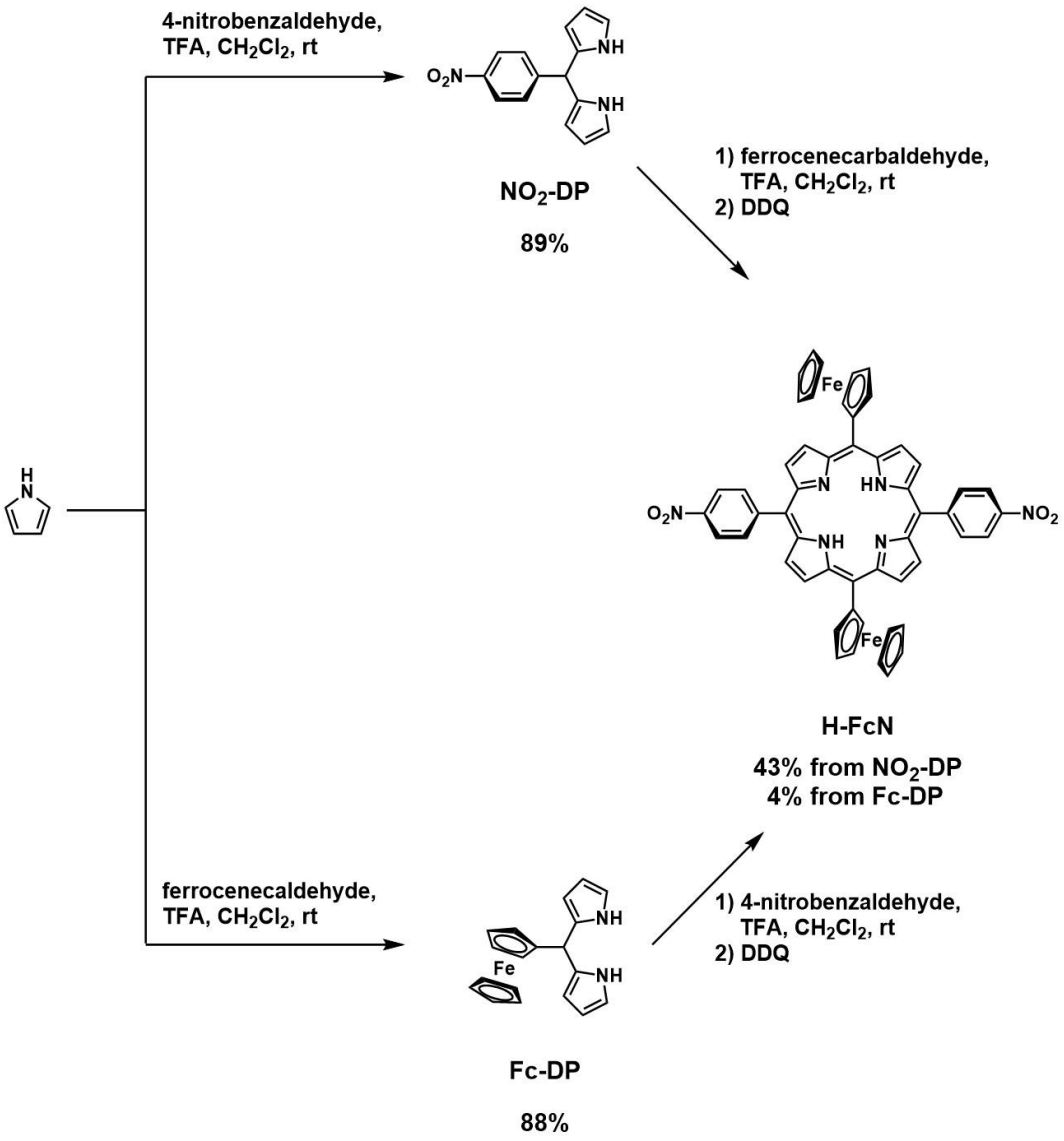

Scheme 5. Synthetic routes for **H-FcN** through **NO_2-DP** and **Fc-DP**.

UV-vis absorption spectra

UV-vis absorption spectroscopy of the synthesized free-base porphyrins was conducted to investigate the effect of electron-donating and –withdrawing, π-conjugated and redox active substituents on the electronic states. UV-vis absorption spectra of the free-base porphyrins in 1,2-dichlorobenzene and the summary of absorption bands are shown in Figure 2 and Table 1, respectively. Note that the spectral data for 5,10,15,20-tetraphenylporphin (**H-Ph**) as a reference compound was also presented.

All free-base porphyrins present a strong absorption band at approximately 422-455 nm and four weaker bands widely located at approximately 516-702 nm. These spectral features are caused by porphyrin macrocycle-based π-π* transitions described by Gouterman's four orbital model.[9] The former band in the shorter wavelength region is assigned to the $S_0 \rightarrow S_2$ transition (Soret band), and the latter bands are attributed to the $S_0 \rightarrow S_1$ transition (Q bands). In addition to these porphyrin-based absorption bands, bands attributed to the π-π* transition of the substituents at the *meso*-position are also observed in the UV region for all compounds. The Soret bands of **H-TMP**, **H-FcN**, **H-PEPy** and **H-PA** are slightly red shifted compared to that of **H-Ph**, indicating that the effect of the substituents on the electronic structure of the porphyrin moieties is relatively small. In contrast, the Soret band of **H-EDB** (λ_{max} = 455 nm) is largely shifted to the longer wavelength region compared to that of **H-Ph** (λ_{max} = 422 nm). Similarly, the Q-bands of **H-EDB** are largely red shifted compared to those of **H-Ph**, whereas the Q-bands of **H-TMP**, **H-PEPy** and **H-PA** are located almost similar position as those of **H-Ph**. These results indicate that electron-withdrawing nature of the dimesityldurylborane moieties largely affects the electronic structure of the porphyrin unit. In the case of **H-FcN**, broad Q bands at lower wavelength region compared to **H-Ph** was observed. This is because the smaller location barrier of ferrocenyl moieties compared to benzene rings.[10]

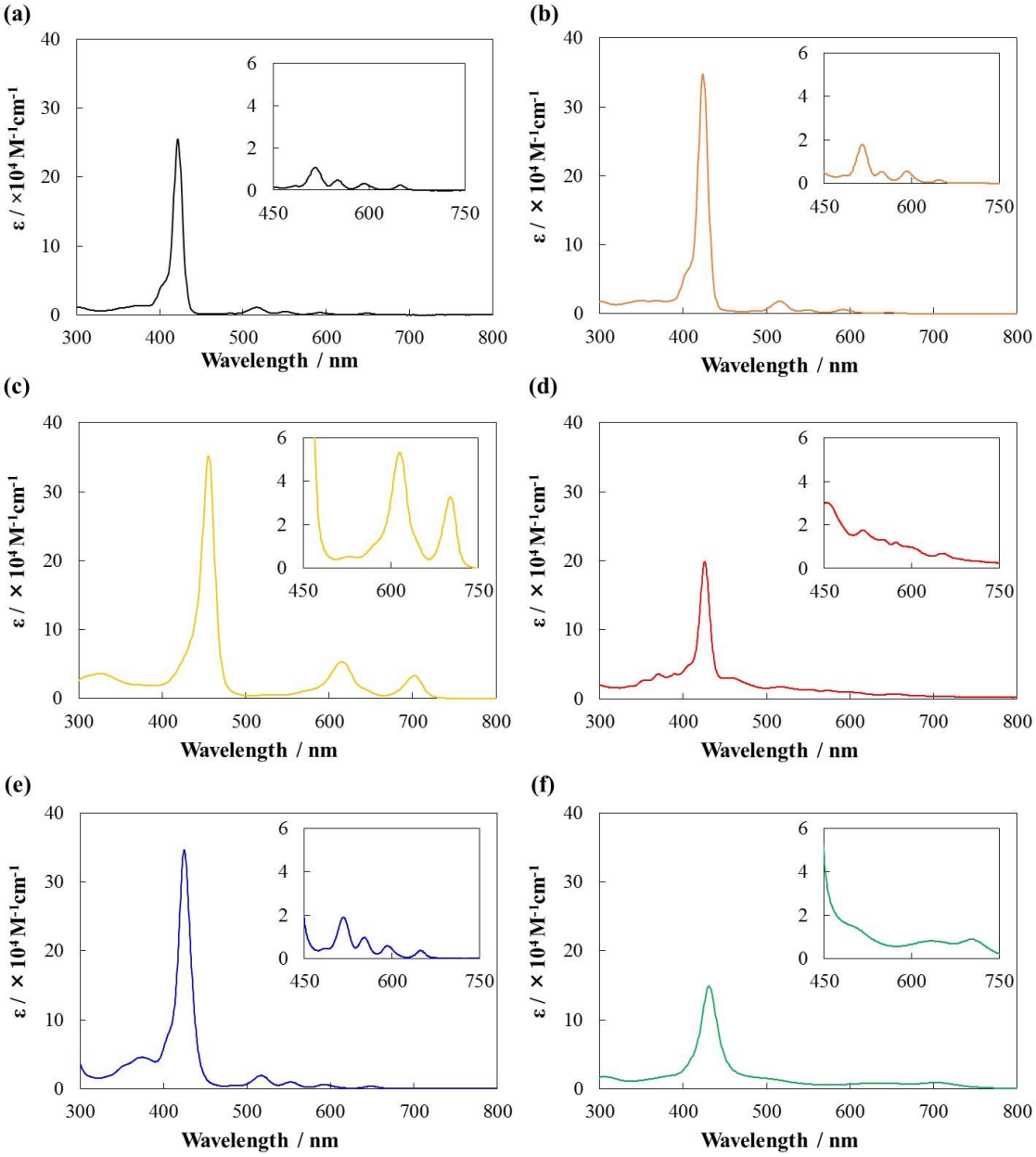

Figure 2. UV-vis absorption spectra of the free-base porphyrins in 1,2-dichlorobenzene (a) **H-Ph**, (b) **H-TMP**, (c) **H-EDB**, (d) **H-PA**, (e) **H-PEPy** and (f) **H-FcN**. (Insets) Enlarged UV-vis absorption spectra at Q-band regions.

Table 1. Summary of the absorption spectra for the free-base porphyrins in 1,2-dichlorobenzene.

Compound	λ_{max} / nm ($\varepsilon/10^4$ M^{-1} cm^{-1})		
	Substituent's bands	**Soret-band**	**Q-bands**
H-Ph	373 (1.30)	422 (25.52)	516 (1.08), 551 (0.48), 593 (0.30), 649 (0.24)
H-TMP	366 (1.88)	424 (34.78)	515 (1.80), 549 (0.54) 591 (0.58), 644 (0.18)
H-EDB	326 (3.60)	455 (35.24)	615 (5.34), 702 (3.28)
H-PA	335 (1.80), 352.5 (2.66), 370.5 (3.58), 389.5 (3.60)	426 (19.9)	516.5 (1.76), 546 (1.32) 573 (1.20), 656.5 (0.70)
H-PEPy	375 (4.56)	424.5 (34.64)	517 (1.90), 553 (0.98), 592 (0.58), 649 (0.38)
H-FcN	302 (1.76)	431 (14.86)	br, 629 (0.82), 698 (0.88)

Cyclic Voltammetry

Cyclic voltammograms of the free-base porphyrins are shown in Figure 3, and the redox potentials are summarized in Table 2. Electrochemical data of **H-Ph** as a reference compound was also presented. All measurements were performed in 0.1 M tetra-*n*-butylannmonium perchlorate (TBAP)/DMF solutions under an Ar atmosphere. As shown in Figure 3(a), **H-Ph** exhibits two reversible redox waves, which are assigned to the two-step one electron reduction of the porphyrin ring.[11] Similar two reversible waves were observed for **H-TMP** and **H-EDB**. The half wave potentials ($E_{1/2}$ / V vs. ferrocene/ferrocenium (Fc/Fc^+)) of **H-TMP** ($E_{1/2}$ = −1.82 (first reduction) and −2.25 V (second reduction)) are shifted to the negative potential compared to those of **H-Ph** ($E_{1/2}$ = −1.54 (first reduction) and −1.99 V (second reduction)), reflecting the electron-donating nature of 2,4,6-trimethoxyphenyl groups. In contrast, the half wave potentials of **H-EDB**, which possesses electron-withdrawing groups, are shifted to the positive potential region ($E_{1/2}$ = −1.26 (first reduction) and −1.77 V (second reduction)). These observation indicates that the introduction of the electron-donating and electron-withdrawing groups largely affects the LUMO and LUMO+1 level of the porphyrins. In the case of **H-PA**, three redox waves were observed at $E_{1/2}$ = −1.53, −1.94, and −2.42 V. The first two waves are attributed to the reduction process of the porphyrin ring and the potentials are similar to those of **H-Ph**. The third wave at −2.42 V is assignable to the reduction of the anthracenylphenyl groups.[12] **H-PEPy** exhibits one reversible reduction wave at −1.43 V, which may be attributed to the reduction of the porphyrin ring. However, the second wave at −1.8 V became irreversible possibly due to the reduction of the substituents at the *meso*-positions.

Cyclic voltammograms of the iron porphyrin complexes in 0.1 M TBAP/DMF solutions under Ar and the summary of the redox potentials are shown in Figure 4 and Table 3, respectively. Electrochemical data of 5,10,15,20-tetrakis(phenyl)porphyrinato iron(III) chloride (**Fe-Ph**) as a reference compound was also presented. **Fe-Ph** displayed three reversible redox waves at −0.63, −1.51 and −2.15 V, which are assigned to be Fe(III)/Fe(II), Fe(II)/Fe(I) and Fe(I)/Fe(0) redox couples.[13] As shown in Figure 4b, **Fe-TMP** exhibited similar three reversible waves and the half-wave potentials are $E_{1/2}$ = −0.63, −1.51 and −2.15 V. All of the potentials were shifted to the negative potential

region compared to **Fe-Ph**, which was similar tendency as observed in the corresponding free-base porphyrin, **H-TMP**. In the cyclic voltammogram of **Fe-PA**, three redox waves attributed to the reduction of the porphyrin moiety at −0.74, −1.54 and −2.13 V, and one additional wave attributed to the anthracenylphenyl groups was observed at −2.41 V. The redox potential of this forth wave was almost identical to that of the third wave observed in **H-PA** (−2.42 V).

The cyclic voltammogram of **H-FcN**, which has redox active substituents, in a 0.1 M TBAP/1,2-dichlorobenzene solution under Ar and the summary of the redox potentials are shown in Figure 5 and Table 4, respectively. Note that 1,2-dichlorobezene was used in this measurement because of the low solubility of the compound in DMF. **H-FcN** exhibited one quasi-reversible wave at −0.19 V, which is assignable to the oxidation of the ferrocenyl groups. In the negative potential region, one reversible two-electron redox wave at −1.85 V and one reversible one-electron redox wave at −2.01 V were observed. The cyclic voltammogram of nitrobenzene exhibits reversible wave at −1.98 V (Figure 5c). Therefore, the wave at −1.85 V can be assigned to the reduction of the nitrophenyl moieties of **H-FcN**. The wave at −2.01 V is attributed to the reduction of the porphyrin ring. It should be noted that the second reduction of the porphyrin ring became unfavourable in **H-FcN** because of the two electron reduction at the nitrophenyl moieties.

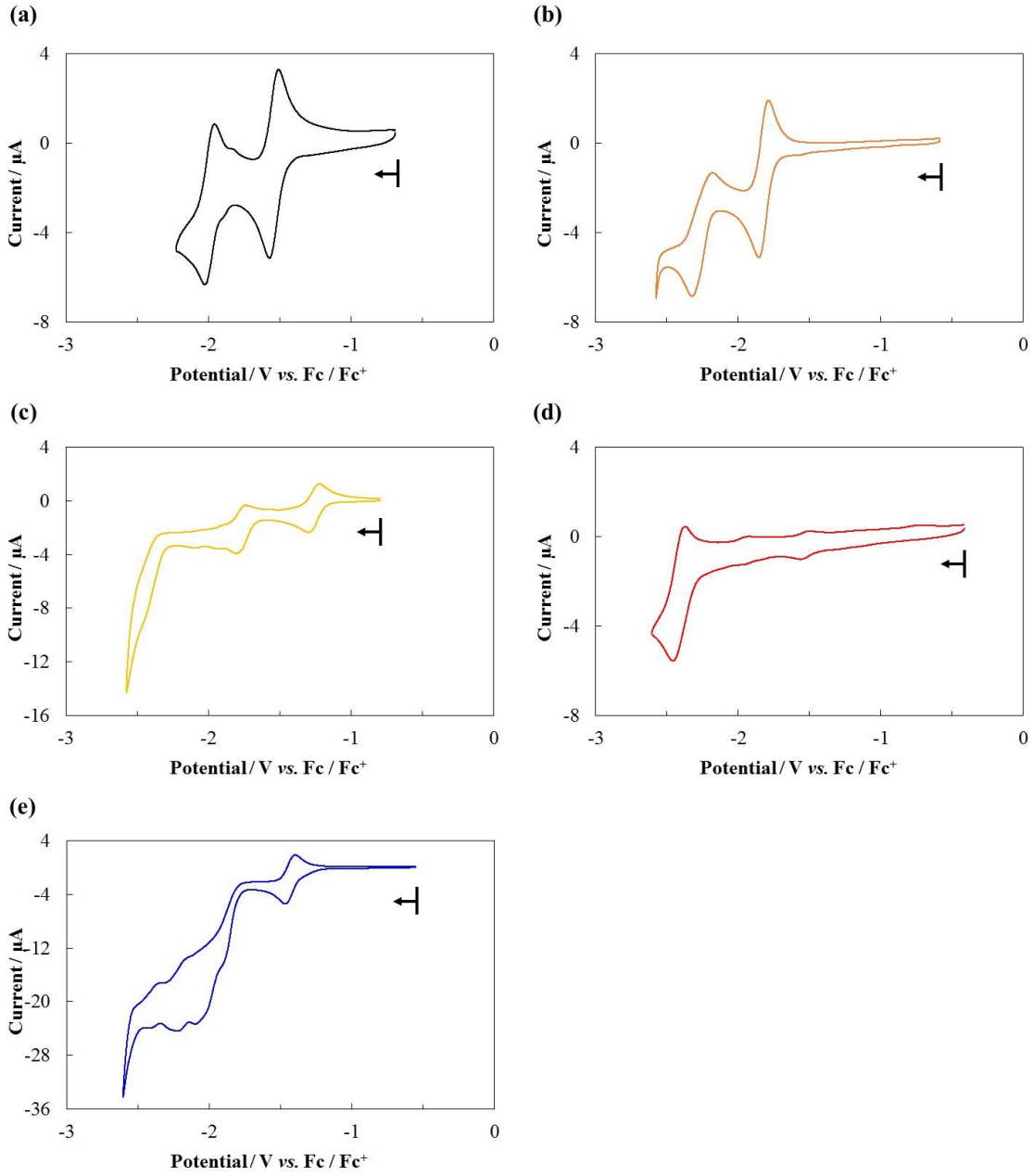

Figure 3. Cyclic voltammograms of the free-base porphyrins ((a) **H-Ph**, (b) **H-TMP**, (c) **H-EDB**, (d) **H-PA** and (f) **H-PEPy**, 1.0 mM) in a 0.1 M TBAP/DMF solution under an Ar atmosphere (WE: GC; CE: Pt wire; RE: Ag^{+}/Ag; scan rate: 20 mV s^{-1}). Potential sweeps were started from the open circuit potential −0.69 V (**H-Ph**), −0.59 V (**H-TMP**), −0.80 V (**H-EDB**), −0.41 V (**H-PA**) and −0.55 V (**H-PEPy**). Arrows in the voltammograms indicate the direction of potential sweep.

Table 2. Redox potentials of the prepared free-base porphyrins ($E_{1/2}$ / V vs. Fc/Fc^+) in DMF under an Ar atmosphere.

Compound	$E_{1/2}(1)$ / V	$E_{1/2}(2)$ / V	$E_{1/2}(3)$ / V
H-Ph	−1.54	−1.99	–
H-TMP	−1.82	–2.25	–
H-EDB	−1.26	–1.77	–
H-PA	−1.53	–1.94	–2.42
H-PEPy	−1.43	–	–

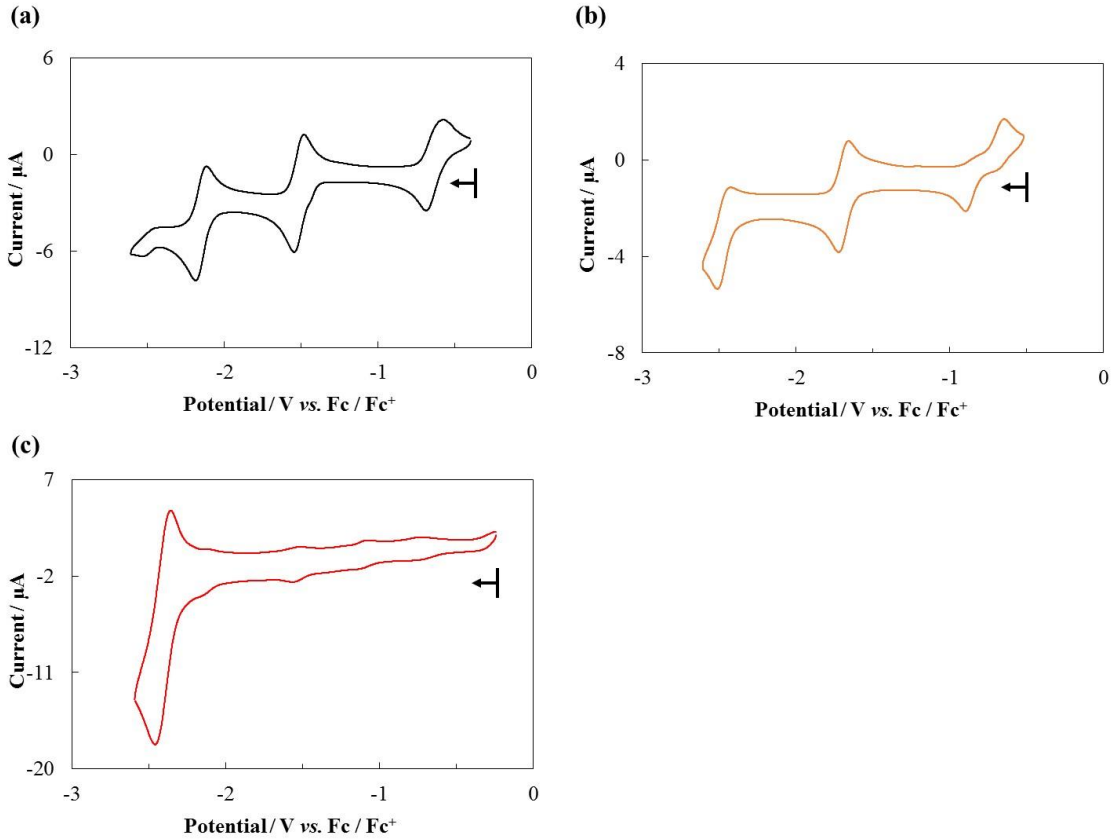

Figure 4. Cyclic voltammograms of the iron porphyrin complexes ((a) **Fe-Ph**, (b) **Fe-TMP**, and (c) **Fe-PA**, 1.0 mM) in a 0.1 M TBAP/DMF solution under an Ar atmosphere (WE: GC; CE: Pt wire; RE: Ag^{+}/Ag; scan rate: 20 mV s^{-1}). Potential sweeps were started from the open circuit potential −0.40 V (**Fe-Ph**), −0.52 V (**Fe-TMP**), and −0.24 V (**Fe-PA**). Arrows in the voltammograms indicate the direction of potential sweep.

Table 3. Redox potentials of the prepared iron porphyrin complexes ($E_{1/2}$ / V vs. Fc/Fc^+) in DMF under an Ar atmosphere.

Compound	$E_{1/2}(1)$ / V	$E_{1/2}(2)$ / V	$E_{1/2}(3)$ / V	$E_{1/2}(4)$ / V
Fe-Ph	−0.63	−1.51	−2.15	−
Fe-TMP	−0.77	–1.69	–2.47	−
Fe-PA	−0.74	−1.54	−2.13	−2.41

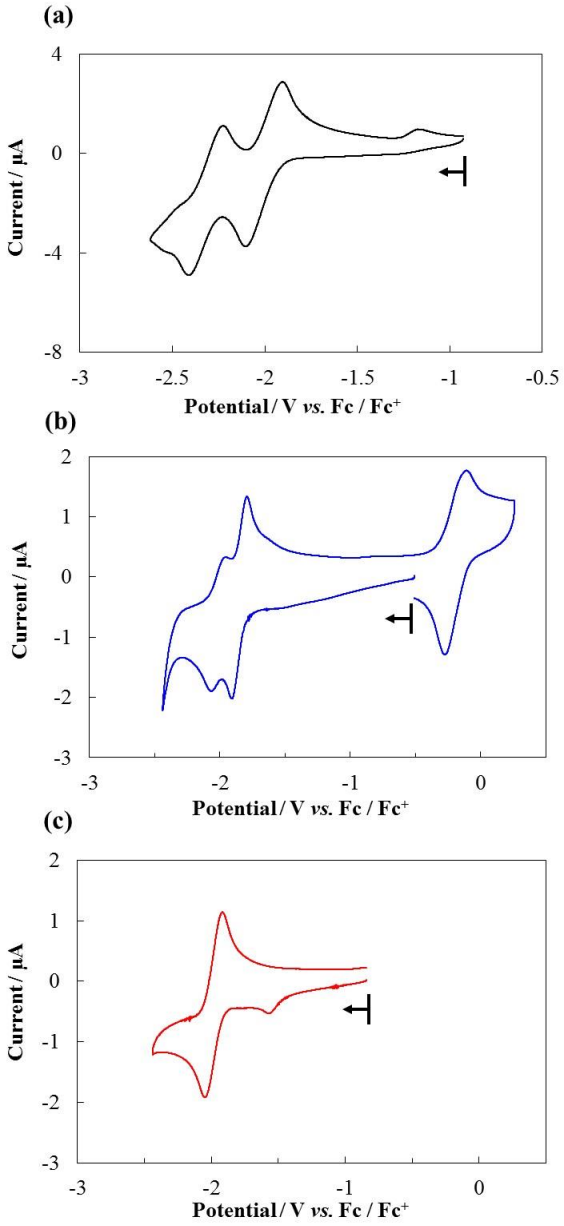

Figure 5. Cyclic voltammograms of the free-base porphyrins and nitrobenzene ((a) **H-Ph**, 1.0 mM (b) **H-FcN** 0.2mM, and (c) nitrobenzene, 0.2mM) in a 0.1 M TBAP/1,2-dichlorobenzene solution under an Ar atmosphere (WE: GC; CE: Pt wire; RE: Ag^{+}/Ag; scan rate: 20 mV s^{-1}). Potential sweeps were started from the open circuit potential −0.93 V (**H-Ph**), −0.51 V (**H-FcN**), and −0.84 V (nitrobenzene). Arrows in the voltammograms indicate the direction of potential sweep.

Table 4. Redox potentials of the prepared free-base porphyrins and nitrobenzene ($E_{1/2}$ / V vs. Fc/Fc^+) in 1,2-dichlorobenzene under an Ar atmosphere.

Compound	$E_{1/2}(1)$ / V	$E_{1/2}(2)$ / V	$E_{1/2}(3)$ / V
H-Ph	−1.54	−1.99	–
H-FcN	−0.19	–1.85	–2.01
Nitrobenzene	-1.98	–	–

Crystal Structure of H-PEPy

Single crystals of **H-PEPy** suitable for single crystal X-ray structural analysis were obtained by the diffusion of methanol into the dichloromethane solution of **H-PEPy**. An ORTEP drawing and packing structures of the obtained crystal are shown in Figure 6 and crystallographic data is summarized in Table 5. The compound crystallized in a monoclinic $P2_1/a$ space group and one crystallographically independent **H-PEPy** molecule was observed in the structure. As shown in Figure 6, **H-PEPy** has one phenyl ring which has ethynylpyrenyl moiety and the remaining three phenyl rings have triflate groups. This observation is consistent with the result of ^{1}H NMR spectroscopy (*vide supra*). The dihedral angle between the phenyl ring and the pyrenyl moiety was 53.7 deg. In the packing structure, CH-π interaction with the distance of 2.60 Å was formed between the phenyl ring and the pyrenyl moiety.

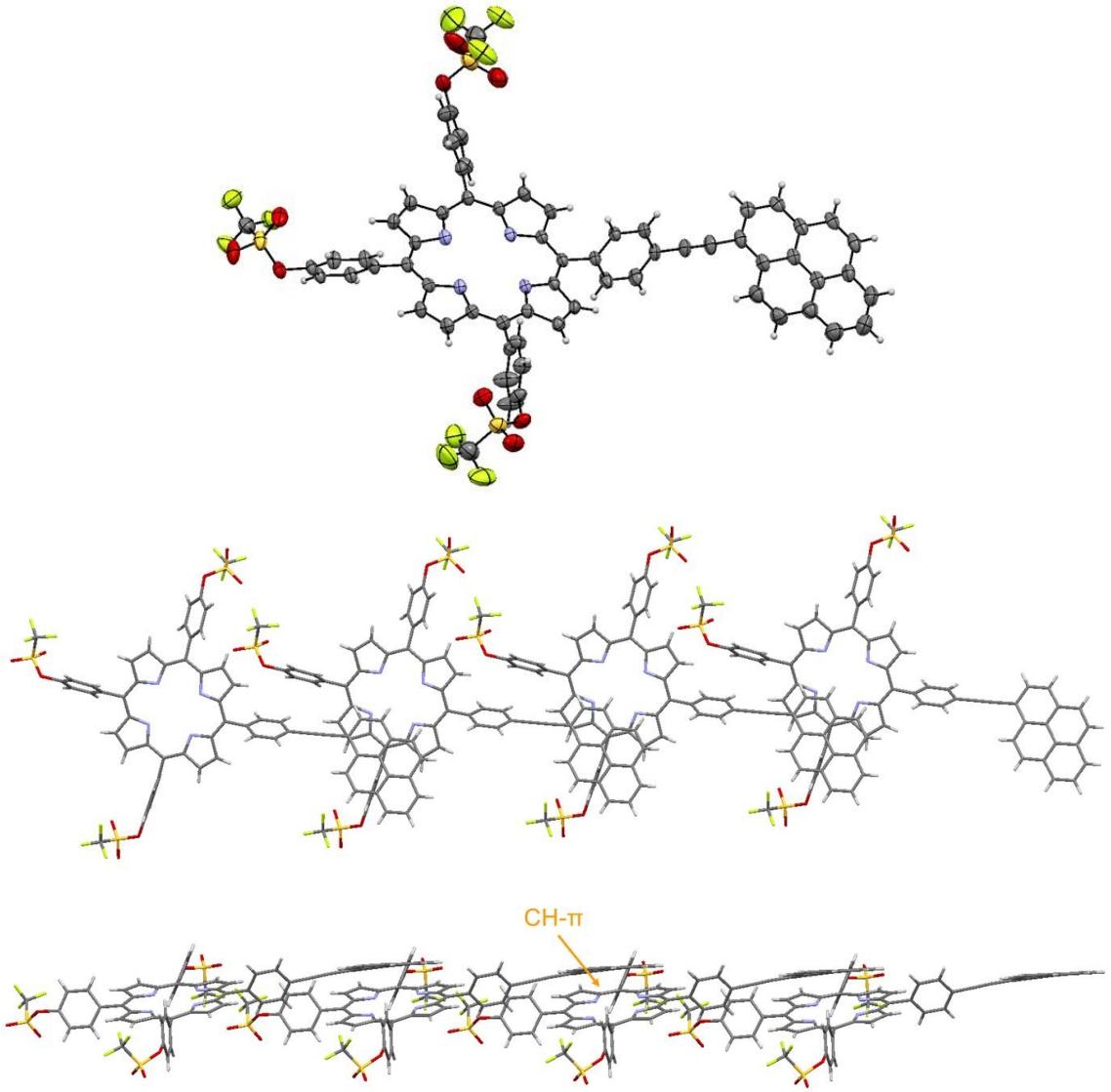

Figure 6. An ORTEP drawing and packing structures of **H-PEPy**. Thermal ellipsoids are shown at the 50% probability level. C = gray, N = pale blue, O= red, F = pale green, S = yellow and H = white.

Table 5. Summary of crystallographic data for **H-PEPy**

Formula	$C_{65}H_{33}F_9N_4O_9S_3$
Fw	1281.13
Color, habit	purple, platelet
Crystal size, mm	0.503 × 0.493 × 0.028
Crystal system	monoclinic
Space group	$P2_1/a$
a (Å)	14.9896(3)
b (Å)	22.0654(5)
c (Å)	18.9156(5)
α (deg)	90
β (deg)	104.2327(7)
γ (deg)	90
V (Å^3)	6064.9(2)
Z	4
T (K)	123(2)
R_1	0.0804
wR_2	0.2625
GOF	1.078

Crystal Structure of H-FcN/TNCEL Co-crystal

Single crystals suitable for single crystal X-ray structure determination were obtained by the diffusion of hexane into the benzene solution of **H-FcN** containing organic acceptor, tetracyanoethylene (**TCNE**). The crystal structure of the obtained single crystal and the summary of crystallographic data are shown in Figure 7 and Table 6, respectively. One **H-FcN** and two 1,2,2-tricyanoethenolate (**TCNEL**) molecules are found as crystallographically asymmetric unit in this structure with triclinic $P\bar{1}$ space group. It was previously reported that **TCNE** molecules can be converted to 1,2,2-tricyanoethenolate (**TCNEL**) via the reduction of **TCNE** and the subsequent reaction with dioxygen [14] or by the hydrolysis of **TCNE** [15] (Figure 8). As a result a co-crystal of **H-FcN** with **TCNEL** (**H-FcN/TNCEL Co-crystal**) is formed. In this structure, the main framework of porphyrin was distorted due to the change of their electronic state upon complexation with **TCNEL**. Judging from this result, we assumed that electron transfer may occur from porphyrin or ferrocenyl substituents to **TCNEL** because Webster and co-workers reported ferrocene is capable to form charge separated complex with **TCNEL**. π-Plane Cp ring of the ferrocenyl substituents in **H-FcN** are tilted about 30° against the porphyrin skeleton due to low energy barrier (< 10.4 kcal mol^{-1}) for the rotation [10]. In contrast, the dihedral angle between the π-Plane of 4-nitrophenyl group the porphyrin skeleton was approximately 50 deg, reflecting the bulkiness of the phenyl ring. For **TCNEL**, bond distances between the sp^2 carbon atoms and the carbon atoms of CN groups are in the range of 1.42−1.52 Å, and the distances between the sp^2 carbon atoms and oxygen atoms are 1.25 and 1.26 Å.

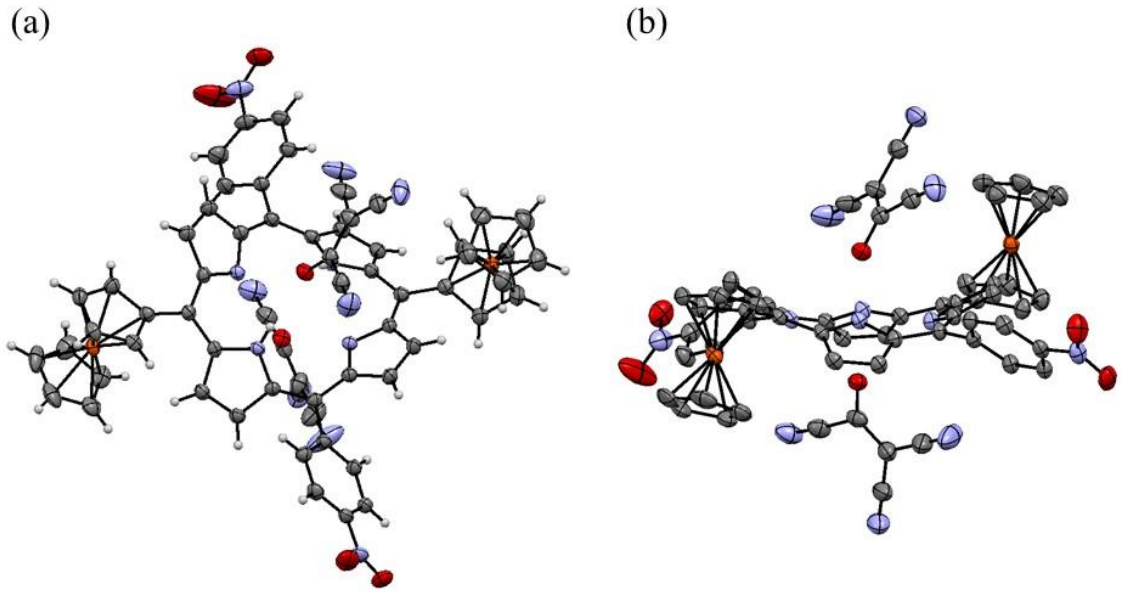

Figure 7. (a) Top and (b) side views of ORTEP drawings of **H-FcN/TNCEL Co-crystal** In the side view (b), hydrogen atoms are omitted for clarity.

Table 6. Summary of crystallographic data for **H-FcN/TNCEL Co-crystal**

Formula	$C_{62}H_{36}Fe_2N_{12}O_6$
Fw	1156.73
Color, habit	navy blue, platelet
Crystal size, mm	0.265 × 0.261 × 0.034
Crystal system	triclinic
Space group	*P*-1
a (Å)	11.4777(3)
b (Å)	14.8574(4)
c (Å)	16.5932(5)
α (deg)	84.3794(8)
β (deg)	86.1232(8)
γ (deg)	69.9196(7)
V (Å^3)	2642.4(1)
Z	2
T (K)	123(2)
R_1	0.0553
wR_2	0.1568
GOF	1.054

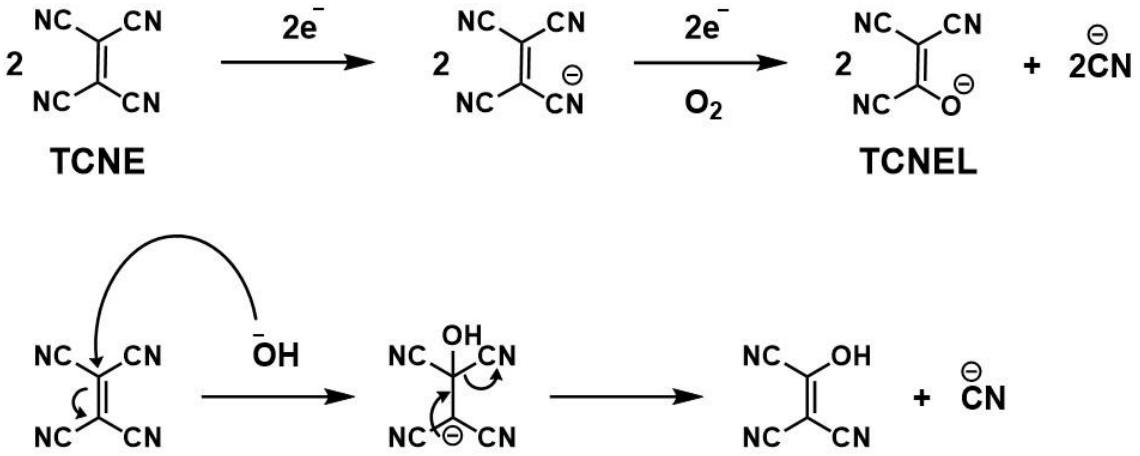

Figure 8. Conversion of **TCNE** to **TCNEL** via (top) the reduction and (bottom) the hydrolysis.

IR spectrum of H-FcN/TNCEL Co-crystal

A fourier transform infrared (FT-IR) spectrum of **H-FcN/TNCEL Co-crystal** was measured to determine their chemical compositions. The IR spectra of **H-FcN/TNCEL Co-crystal**, **H-FcN** and **TCNE** are shown in Figure 9. The powder of **H-FcN** shows symmetrical and antisymmetric N-O stretching vibrations at 1341 and 1516 cm^{-1} which correspond to NO_2 group. Similarly, we assign two peaks at 1343 and 1519 cm^{-1} in the spectrum of **H-FcN/TNCEL Co-crystal** to the symmetrical and antisymmetrical N-O stretching vibrations. In addition to these peaks, the small sharp peaks at 2217 and 2193 cm^{-1}, which are attributed to the C-N stretching vibration which originates from **TCNEL** molecules and are comparable to the previously reported values.[16] The C-N stretching vibration bands of **TCNE** were observed at higher wavenumber region (2264 and 2231 cm^{-1}). The strength of the C-N bonds in **TCNEL** are weakened by the existence of its resonance structures (Figure 10).[16]

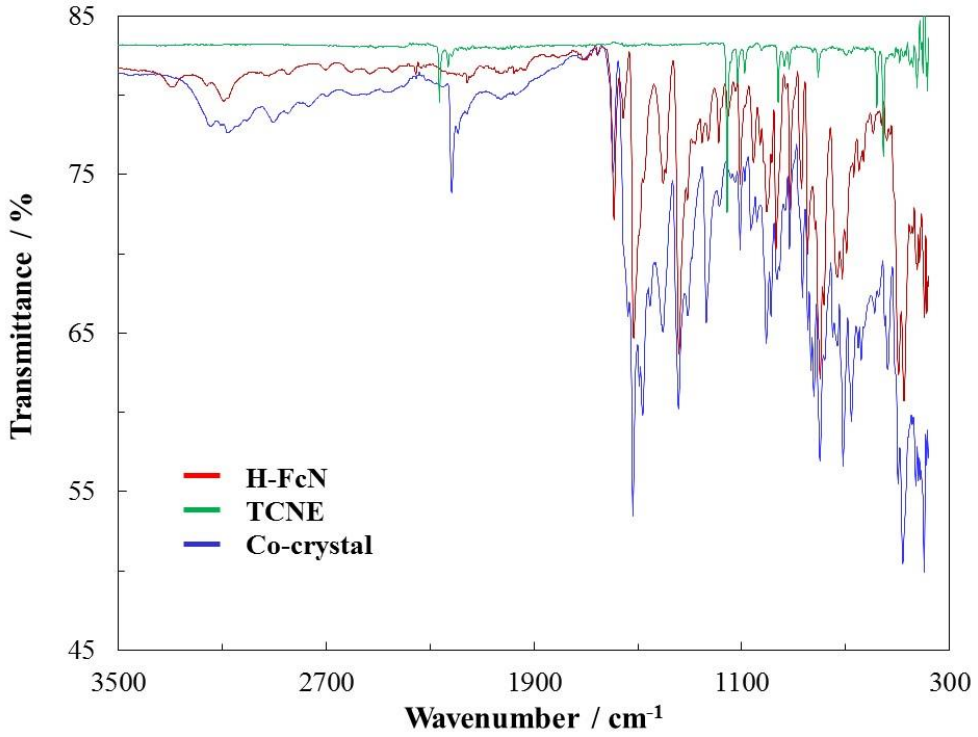

Figure 9. IR spectra of **H-FcN** (red line), TCNE (green line) and **H-FcN/TNCEL Co-crystal** (blue line).

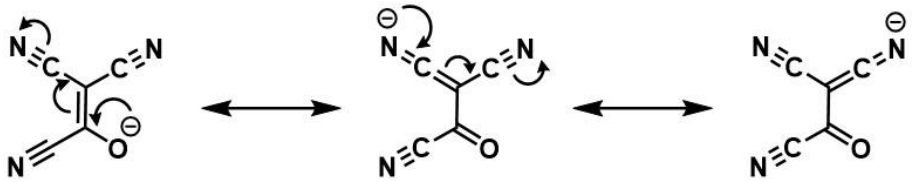

Figure 10. Resonance structures of **TCNEL**.

Diffuse Reflectance Spectrum of H-FcN/TNCEL Co-crystal

UV-vis diffuse reflectance spectra of **H-FcN** and **H-FcN/TNCEL Co-crystal** in the solid state were shown in Figure 11. The spectrum of **H-FcN** exhibits several broad absorption bands from around 300 to 840 nm (Figure 11(a)). The spectral features may be caused by porphyrin macrocycle-based π-π* transitions. The measurement of **H-FcN/TNCEL Co-crystal** was performed in same condition as **H-FcN**, and a new broaden absorption band appeared at longer wavelength region (800 to 1500 nm) in addition to the porphyrin based absorption bands. This result clearly indicates the formation of charge transfer (CT) salt was formed in **H-FcN/TNCEL Co-crystal**. To investigate the origin of the CT absorption band, electronic transitions of the **H-FcN** and co-crystal of **H-FcN/TNCEL Co-crystal** were investigated by the time dependent density functional theory (TD-DFT) calculations using the Gaussian 09 [17] programs with the B3LYP function[18] and 6-31G (d) basis set [19]. The calculated absorption spectra were drawn in Figure 11(b) and the frontier molecular orbitals of **H-FcN/TNCEL Co-crystal** are described in Figure 12. In the spectrum of **H-FcN**, the intense bands in the visible region are assigned to the π-π* transitions of the porphyrin macrocycle and the π-π* transitions of the substituents (Fc to $C_6H_4NO_2$). For **H-FcN/TNCEL Co-crystal**, the absorption bands in the visible region are also corresponds to the π-π* transition between the occupied and unoccupied orbitals widely delocalized on the **H-FcN** molecule. Moreover, the broad absorption band from around 800 nm was obtained by calculation. Major contribution of the transition in longer wavelength was assigned to the transition from HOMO−2 → LUMO (f=0.1019) at 1229.7 nm, and mainly originate from charge transfer from ferrocenyl substituents to **TNCEL** and the porphyrin skeleton (Figure 12).

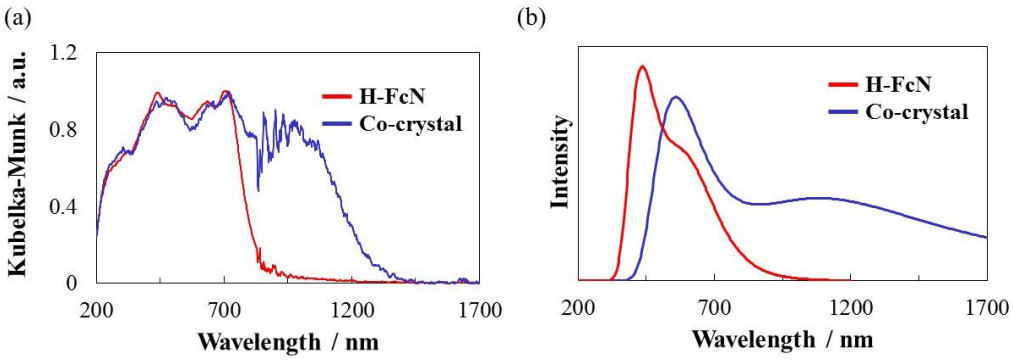

Figure 11. (a) Diffuse reflectance spectra of **H-FcN** (red line) and **H-FcN/TNCEL Co-crystal** (blue line) (b) Simulated absorption spectra of **H-FcN** (red line) and **H-FcN/TNCEL Co-crystal** (blue line).

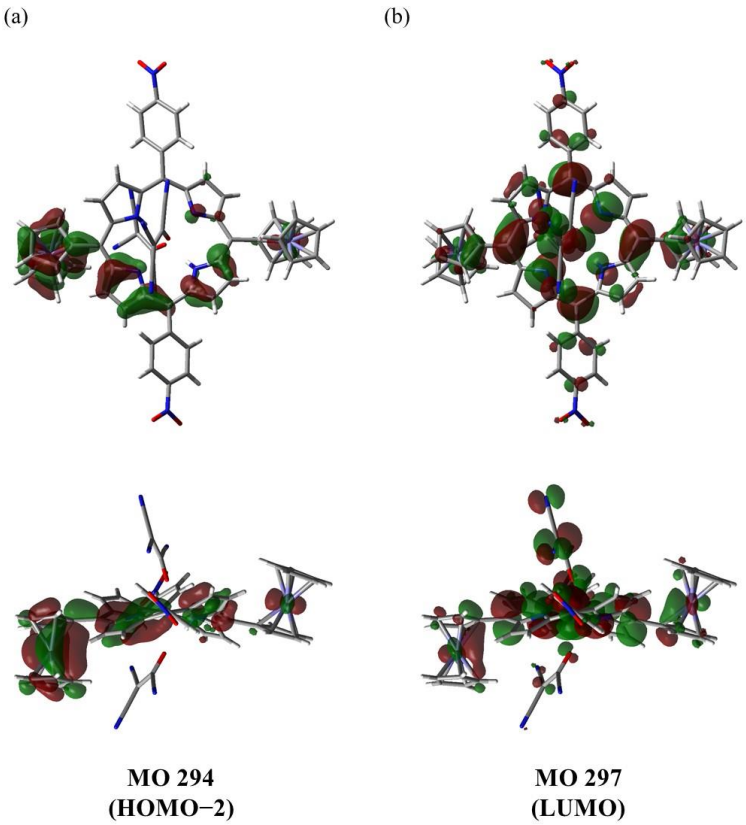

Figure 12. Frontier molecular orbitals of **H-FcN/TNCEL Co-crystal** on the basis of single point DFT calculations.

Conclusion

This chapter described the syntheses of various kinds of porphyrins and metalloporphyrins bearing electron-donating and withdrawing, π-conjugated and redox active substituents at the *meso* positions. The synthetic route to obtain each porphyrin derivatives were successfully optimized by considering the nature of each substituent and five kinds of free-base porphyrins (**H-TMP**, **H-EDB**, **H-PA**, **H-PEPy** and **H-FcN**) and three kinds of iron porphyrin complexes (**Fe-TMP**, **Fe-PA** and **Fe-PEPy**) were obtained. Moreover, UV-vis absorption spectroscopy and electrochemical studies of the obtained compounds were performed. The results of these measurements were compared with the reference compounds, **H-Ph** and **Fe-Ph**, and the effect of the substituents on the electronic structures of the molecules was discussed. I also examined the crystallization of the porphyrin bearing redox active ferrocenyl moieties, **Fc-N**. The crystals of **Fc-N** were obtained as by the recrystallization in the presence of organic acceptor molecules, TCNE. Single crystal X-ray structural analysis revealed that TCNE is reduced to TCNEL and the co-crystal of **Fc-N** and **TCNEL** (**Fc-N/TCNEL Co-crystal**) is formed. The electronic structure of **Fc-N/TCNEL Co-crystal** was investigated using IR spectroscopy, diffuse reflectance UV-vis spectroscopy, TD-DFT calculations, and the charge transfer interaction between **Fc-N** and **TCNEL** was indicated.

Experimental

Materials and Methods

Pyrrole was purchased from Sigma-Aldrich Co., LLC. 9-bromoanthracene, 4-bromobenzaldehyde, *n*-butyllithium (^{n}BuLi), 1,2-dichlorobenzene, dimethylsulfoxide (DMSO), ethyl acetate, diethylamine, trimethylamine, ferrocene (Fc), ferrocenecarbaldehyde, 4-formylphenylboronic acid, iodine, iron(II) chloride tetrahydrate, 1-pyrenecarbaldehyde, trifluoroacetic acid (TFA), bis(triphenylphosphine)palladium(II) dichloride, potassium hydroxide, and tripotassium phosphate were purchased from Wako Pure Chemical Industries, Ltd. Chloroform, hexane (Hex), *N*,*N*-dimethylformamide (DMF) and pyridine were purchased from Kanto Chemical Co., Inc. Tetrabutylammonium fluoride (TBAF) (*ca*. 1 mol/L in tetrahydrofuran), tetra(*n*-butyl)ammonium perchlorate (TBAP), bromine, 1-bromopyrene, *N*-bromosuccinimide, 2,3-dichloro-5,6-dicyano-1,4-benzoquinone, trifluoromethanesulfonic anhydride, formaldehyde solution (37%), 4-hydroxymezaldehyde, dimesitylfluoroborane, trimethylsilylacetylene, 2,4,6-trimethoxybenzaldehyde, 4-nitrobenzaldehyde and 4-phenylbenzaldehyde were purchased from Tokyo Chemical Industry Co., Ltd. Copper iodide was purchased from Nacalai tesque Co., Ltd. $CDCl_3$ was obtained from Cambridge Isotopes, Inc. Diethylamine and trimethylamine were used after distillation. Another reagents were used without further purification. TBAP was recrystallized from absolute ethanol and dried in vacuo. Dichloromethane (DCM) and tetrahydrofuran (THF) were degassed and purified under an N_2 atmosphere using a GlassContour solvent system (Nikko Hansen Co., Ltd.).

^{1}H NMR spectra were recorded on a JEOL 400 MHz instrument. All ^{1}H NMR spectra were referenced against residual proton signals. Elemental analyses were measured on a MICRO CORDER JM10. Electrochemical experiments were performed under argon and CO_2 atmospheres using a BAS ALS Model 650DKMP electrochemical analyzer. Cyclic voltammograms were recorded in 1,2-dichlorobenzene ([complex] = 1.0 mM; 0.1 M TBAP) using a glassy carbon disk, a platinum wire and an Ag^+/Ag electrode (Ag/0.01 M $AgNO_3$) that were used as the working, auxiliary, and reference electrodes, respectively. The redox potentials of the samples were calibrated against the redox signal for the ferrocene/ferrocenium (Fc/Fc^+) couple. UV-vis absorption measurements were

performed on a Shimadzu UV-1800 spectrometer at room temperature.

Syntheses

Synthesis of 5-(2,4,6-trimethoxyphenyl) dipyrromethane: To a mixture of 2,4,6-trimethoxybenzaldehyde (3.0 g, 15 mmol) and pyrrole (27 mL, 0.38 mol) was added TFA (0.12 mL, 1.5 mmol) at rt. The mixture was stirred for 10 min at rt, and the reaction was quenched by 1M NaOH aq. The resulting mixture was extracted with ethyl acetate. The extract was dried over anhydrous Na_2SO_4, and concentrated under reduced pressure. The resulting mixture was purified by column chromatography (DCM:ethyl acetate:Hex = 7:3:1) to afford a desired product (1.0 g, yield 22%). ^{1}H NMR (400 MHz, $CDCl_3$) δ 8.46 (s, 2H), 6.61 (dd, J = 4.3, 2.7 Hz, 2H), 6.17 (s, 2H), 6.07 (q, J = 2.8 Hz, 2H), 6.04 (s, 1H), 5.88 (q, J = 0.8 Hz, 2H), 3.79 (s, 3H), 3.71 (s, 6H) ppm.

Synthesis of 5,10,15,20-tetrakis(2,4,6-trimethoxyphenyl)porphyrin (H-TMP): To a solution of 2,4,6-trimethoxybenzaldehyde (0.40 g, 2.0 mmol) and 5-(2,4,6-trimethoxyphenyl) dipyrromethane (0.62 g, 2.0 mmol) in dry DCM (200 mL) was added TFA (77 μL, 1.0 mmol) at rt. The mixture was stirred for 90 min at rt and then chloranil (0.49 g, 2.0 mmol) was added. After 90 min, the reaction mixture was passed through alumina short column to quench the reaction. The resulting mixture was purified by column chromatography (chloroform) to afford a purple solution. The desired product was recrystallized from chloroform and Hex, and washed by Hex to give a purple solid (0.37 g, yield 38%). ^{1}H NMR (400 MHz, $CDCl_3$) δ 8.68 (s, 8H), 6.53 (s, 8H), 4.06 (s, 12H), 3.47 (s, 24H), −2.56 (s, 2H) ppm.

Synthesis of 5,10,15,20-tetrakis(2,4,6-trimethoxyphenyl)porphyrinato iron(III) chloride (Fe-TMP): To a solution of **H-TMP** (0.10 g, 0.10 mmol) in DMSO (26 mL), a DMSO 15 mL) solution of $FeCl_2 \cdot 4H_2O$ (0.12 g, 0.62 mmol) was added dropwise at room temperature. The mixture was refluxed for 1 h and then cooled to room temperature. After evaporating half volume of the solvent, 6 M HCl was added into the resulting mixture and the solution was filtrated. The desired product was washed by 3 M HCl and then, extraction by DCM was performed. The extract was dried over anhydrous Na_2SO_4, and concentrated under reduced pressure. (80 mg, yield 73%). Anal. Calcd for $C_{56}H_{52}ClFeN_4O_{12} \cdot 2H_2O$: C, 61.13; H, 5.13; N, 5.09. Found: C, 61.11; H, 4.85; N, 5.04%.

Synthesis of (4-ethynyl-2,3,5,6-tetramethylphenyl)dimesitylborane (EDDB): **EDDB** was synthesized according to the published method [6, 10] (yield 51% (5 steps from 1,2,4,5-tetramethylbenzene)). ^{1}H NMR (400 MHz, $CDCl_3$) δ 6.71 (s, 4H), 3.49 (s, 1H), 2.34 (s, 6H), 2.25 (s, 6H), 1.93 (s, 12H) ppm.

Synthesis of dipyrromethane: To a mixture of formaldehyde solution (37%) (2.1 mL, 29 mmol) and pyrrole (50 mL, 0.72 mol) was added TFA (0.22 mL, 2.9 mmol) at rt. The mixture was stirred for 5 min at rt, and the reaction was quenched by 1M NaOH aq. The resulting mixture was extracted with DCM. The extract was dried over anhydrous Na_2SO_4, and concentrated under reduced pressure. The resulting mixture was purified by column chromatography (DCM) to afford a desired product (2.1 g, yield 49%). ^{1}H NMR (400 MHz, $CDCl_3$) δ 7.74 (s, 2H), 6.62 (dd, J = 4.1, 2.6 Hz, 2H), 6.15 (q, J = 2.8 Hz, 2H), 6.03 (t, J = 0.8 Hz, 2H), 3.94 (s, 2H) ppm.

Synthesis of 5, 15-bis(phenyl)porphyrin: To a solution of benzaldehyde (0.15 mL, 1.4 mmol) and dipyrromethane (0.20, 1.4 mmol) in dry DCM (250 mL) was added TFA (62 μL, 0.81 mmol) at rt. The mixture was stirred for 4 h at rt and then DDQ (0.37 g, 1.6 mmol) was added. After 1 h, the reaction was quenched by TEA (2.0 mL, 14 mmol). The resulting mixture was purified by column chromatography (DCM:Hex = 4:1) to afford a purple solution. The desired product was recrystallized from DCM and Hex, and the product was washed with several portions of Hex to give a purple solid (93 mg, yield 30%). ^{1}H NMR (400 MHz, $CDCl_3$) δ 10.31 (s, 2H), 9.39 (d, J = 4.9 Hz, 4H), 9.07 (d, J = 4.6 Hz, 4H), 8.25-8.28 (m, 4H), 7.79-7.81 (m, 6H), −3.13 (s, 2H) ppm.

Synthesis of *trans*-5,15-bisbromo-10,20-bisphenyl porphyrin: To a solution of 5, 15-bis(phenyl)porphyrin (0.27 mg, 0.57 mmol) in mix solution (115 mL) of DCM and MeOH (9:1) was added NBS (0.21 g, 1.2 mmol) at rt. The mixture was stirred for 10 min at rt and the reaction was quenched by acetone (11 mL). After removing volatile, the desired product was collected from the solution (0.34 g, yield 95%). ^{1}H NMR (400 MHz, $CDCl_3$) δ 9.60 (d, J = 4.9 Hz, 4H), 8.82 (d, J = 4.3 Hz, 4H), 8.14 (dd, J = 7.8, 1.4 Hz, 4H), 7.73-7.82 (m, 6H), -2.74 (s, 2H) ppm.

Synthesis of *trans*-5,15-bis(dimesithylborylduryletheynyl)-10,20-bisphenyl porphyrin (H-EDB): To the mixture of *trans*-5,15-bisbromo-10,20-bisphenyl porphyrin (0.25 g, 0.40 mmol), **EDDB** (0.34 g, 0.85 mmol), copper iodide (7.7 mg, 0.040 mmol) and bis(triphenylphosphine)palladium(II) dichloride (14 mg, 0.020 mmol) was added dry TEA (8.1 mL). The mixture was refluxed with stirring for 23 h. After addition of water, the resulting mixture was extracted with DCM, 1 M HCl and brine. The extract was dried over anhydrous Na_2SO_4, and concentrated under reduced pressure. The resulting mixture was purified by column chromatography (DCM:Hex = 3:7) to afford a desired product (0.22 g, yield 43%). ^{1}H NMR (400 MHz, $CDCl_3$) δ 9.73 (d, J = 4.3 Hz, 4H), 8.81 (d, J = 4.3 Hz, 4H), 8.18 (d, J = 7.0 Hz, 4H), 7.76 (d, J = 5.5 Hz, 6H), 6.78 (s, 8H), 2.90 (s, 12H), 2.29 (s, 12H), 2.16 (s, 12H), 2.08 (s, 12H), 2.01 (s, 12H), −1.82 (s, 2H) ppm.

Synthesis of 4-(anthracen-9-yl)benzaldehyde: To the mixture of 9-bromoanthracene (2.3 g, 8.9 mmol), 4-formylphenylboronic acid (2.0 g, 13 mmol), tripotassium phosphate (5.7 g, 27 mmol) and bis(triphenylphosphine)palladium(II) dichloride (0.62 g, 0.89 mmol) was added dry THF (89 mL) and water (10 mL). The mixture was refluxed with stirring for 24 h. The resulting mixture was extracted with DCM, water and brine. The extract was dried over anhydrous Na_2SO_4, and concentrated under reduced pressure. The resulting mixture was purified by column chromatography (DCM/Hex) to afford a desired product (2.3 g, yield 93%). ^{1}H NMR (400 MHz, $CDCl_3$) δ 10.18 (s, 1H), 8.53 (s, 1H), 8.09-8.11 (m, 2H), 8.05 (d, J = 8.5 Hz, 2H), 7.60-7.62 (m, 2H), 7.55 (dd, J = 8.9, 0.9 Hz, 2H), 7.44-7.48 (m, 2H), 7.35 (ddd, J = 8.8, 6.6, 1.3 Hz, 2H) ppm.

Synthesis of 5,10,15,20-tetrakis(4-(anthracen-1-yl)phenyl)porphyrin (H-PA): To a solution of 4-(anthracen-9-yl)benzaldehyde (0.57 g, 2.0 mmol) in dry DCM (300 mL) was added pyrrole (0.14 mL, 2.0 mmol) in one portion at rt. After stirring for 5 min, to the reaction mixture was added TFA (0.47 mL, 6.1 mmol) at rt. The mixture was stirred for 20 h at rt and then DDQ (0.55 g, 2.4 mmol) was added. After 90 min, the reaction was quenched by TEA (0.85 mL, 6.1 mmol). The resulting mixture was purified by column chromatography (DCM) to afford a dark purple solution. The desired product was recrystallized from a tiny amount of THF and diethyl ether to give a purple solid (0.15 mg, yield 23%). ^{1}H NMR (400 MHz, $CDCl_3$) δ 9.29 (s, 8H), 8.65 (s, 4H), 8.55 (d, J = 7.0 Hz, 8H), 8.15-8.19 (m, 16H), 7.90 (d, J = 7.3 Hz, 8H), 7.59-7.63 (m, 16H), −2.48 (s, 2H)

ppm.

Synthesis of 5,10,15,20-tetrakis(4-(anthracen-1-yl)phenyl)porphyrinato iron(III) chloride (Fe-PA): To a solution of **H-PA** (50 mg, 0.038 mmol) in DMF (4.6 mL), a DMF (3.0 mL) solution of $FeCl_2 \cdot 4H_2O$ (45 mg, 0.23 mmol) was added dropwise at room temperature. The mixture was refluxed for 1 h and then cooled to room temperature. After evaporating all the solvent, the resulting mixture was extracted with DCM, water and brine. The extract was dried over anhydrous Na_2SO_4, and concentrated under reduced pressure. The desired product was precipitated from DCM and Hex to give a desired product, and the product was washed with several portions of methanol (46 mg, yield 71%). Anal. Calcd for $C_{100}H_{60}ClFeN_4 \cdot 0.5H_2O$: C, 84.71; H, 4.34; N, 3.95. Found: C, 84.67; H, 4.71; N, 3.88%.

Synthesis of 1-ethynylpyrene: To the mixture of 1-bromopyrene (1.0 g, 3.6 mmol), trimethylsilylacetylene (1.0 mL, 7.1 mmol), copper iodide (68 mg, 0.36 mmol) and bis(triphenylphosphine)palladium(II) dichloride (0.25 g, 0.36 mmol) was added dry Et_2NH (100 mL). The mixture was refluxed with stirring for 23 h. After evaporation of Et_2NH, to reaction mixture was added THF (36 mL) and TBAF (*ca*. 1 mol/L in tetrahydrofuran) (7.1 mL, 7.1 mmol). The mixture was stirred for 1 h at rt and purified by column chromatography (Hex) to afford a desired product (0.62 g, yield 78%). ^{1}H NMR (400 MHz, $CDCl_3$) δ 8.58 (d, J = 9.2 Hz, 1H), 8.15-8.23 (m, 4H), 8.09 (d, J = 7.9 Hz, 2H), 8.00-8.05 (m, 2H), 3.61 (s, 1H) ppm.

Synthesis of 4-formylphenyl trifluoromethanesulfonate: To 4-hydroxybezaldehyde (1.0 g, 8.2 mmol) was anhydrous pyridine (8.2 mL). The mixture was stirred for 5 min at 0 ℃. To the mixture was added trifluoromethanesulfonic anhydride at 0 ℃. After stirring, the reaction mixture was allowed to warm to rt followed by stirring for 12 h. After addition of diethyl ether (21 mL), the mixture was extracted with 1 M $CuSO_4$ aq, water and brine. The extract was dried over anhydrous Na_2SO_4, and concentrated under reduced pressure. The resulting mixture was purified by column chromatography (ethyl acetate:Hex = 1:4) to afford a desired product (1.7 g, yield 80%). ^{1}H NMR (400 MHz, $CDCl_3$) δ 9.99 (s, 1H), 7.96 (dt, J = 9.1, 2.3 Hz, 2H), 7.39-7.43 (m, 2H) ppm.

Synthesis of 5,10,15,20-tetrakis(4-trifluoromethansulfonylphenyl)porphyrin (H-PT) (Path 1): To a solution of 4-formylphenyl trifluoromethanesulfonate (0.34 g, 1.4 mmol) in dry DCM (200 mL) was added pyrrole (94 μL, 1.4 mmol) in one portion at rt. After stirring for 5 min, to the reaction mixture was added TFA (1.0 mL, 14 mmol) at rt. The mixture was stirred for 2 h at rt and then DDQ (0.37 g, 1.6 mmol) was added. After 90 min, the reaction was quenched by TEA (1.9 mL, 14 mmol). The resulting mixture was purified by column chromatography (DCM) to afford a purple solution. The desired product was recrystallized from a DCM and Hex to give a purple solid (0.11 g, yield 27%). ^{1}H NMR (400 MHz, $CDCl_3$) δ 8.80 (s, 8H), 8.27 (d, J = 8.8 Hz, 8H), 7.69 (d, J = 8.4 Hz, 8H), −2.90 (s, 2H) ppm.

(Path 2):

4-formylphenyl trifluoromethanesulfonate (1.3 g, 5.2 mmol) and pyrrole (0.36 mL, 5.2 mmol) was added propionic acid (17 mL) at rt then reflux for 1 h. After cooled to room temperature, resulting mixture was filtrated to give a purple solid (0.30 g, yield 19%). ^{1}H NMR (400 MHz, $CDCl_3$) δ 8.80 (s, 8H), 8.28 (d, J = 8.8 Hz, 8H), 7.69 (d, J = 8.4 Hz, 8H), −2.90 (s, 2H) ppm.

Synthesis of 5,10,15-tris(4-trifluoromethansulfonylphenyl)-20-(4-(pyren-1-ylethynyl)phenyl)porphyrin (H-PEPy): To the mixture of **H-PT** (0.11 g, 0.092 mmol), 1-ethynylpyrene (0.13 g, 0.55 mmol) was added dry Et_2NH (9.2 mL) and dry THF (18 mL). After strring, copper iodide (1.8 mg, 9.2 μmol) and bis(triphenylphosphine)palladium(II) dichloride (6.5 mg, 9.2 μmol) were added in one portion and the mixture was refluxed with stirring for 35 h. The resulting mixture was purified by column chromatography (DCM:Hex = 2:3) to afford a purple solution. The desired product was recrystallized from a DCM and MeOH to give a purple solid (27 mg, yield 23%). ^{1}H NMR (400 MHz, $CDCl_3$) δ 8.97 (d, J = 4.9 Hz, 2H), 8.80-8.86 (m, 6H), 8.21-8.36 (m, 14H), 8.13 (dd, J = 16.9, 9.0 Hz, 4H), 8.06 (t, J = 7.6 Hz, 1H), 7.70 (d, J = 8.5 Hz, 6H), −2.85 (s, 2H) ppm.

Synthesis of 5,10,15-tris(4-trifluoromethansulfonylphenyl)-20-(4-(pyren-1-ylethynyl)phenyl)porphyrinato iron(III) chloride (Fe-PEPy): To a solution of H-PEPy (9.9 mg, 7.7μmol) in DMF (4.0 mL), a DMF (3.7 mL) solution of $FeCl_2 \cdot 4H_2O$ (9.2 mg, 0.046 mmol) was added dropwise at room temperature. The mixture was refluxed for 1 h and then cooled to room temperature. After evaporating all the solvent, the resulting mixture was extracted with DCM. The extract was dried over anhydrous Na_2SO_4, and concentrated under reduced pressure. The desired product was precipitated from DCM and Hex to give a desired product, and the product was washed with several portions of Hex (8.0 mg, yield 75%). Anal. Calcd for $C_{65}H_{33}ClF_9FeN_4O_9S_3 \cdot H_2O$: C, 56.15; H, 2.54; N, 4.03. Found: C, 56.40; H, 2.79; N, 4.02%.

Synthesis of 5-ferrocenyl dipyrromethane (Fc-DP): To a mixture of ferrocenecarbaldehyde (1.0 g, 4.7 mmol) and pyrrole (8.1 mL, 0.12 mol) was added TFA (36 μL, 0.47 mmol) at rt. The mixture was stirred for 5 min at rt, and the reaction was quenched by 1M NaOH aq. The resulting mixture was extracted with DCM. The extract was dried over anhydrous Na_2SO_4, and concentrated under reduced pressure. The resulting mixture was purified by column chromatography (DCM) to afford a brown solid (1.4 g, yield 88%). ^{1}H NMR (400 MHz, $CDCl_3$) δ 7.94 (s, 2H), 6.65 (dd, J = 4.1, 2.6 Hz, 2H), 6.10-6.14 (m, 2H), 5.99 (s, 2H), 5.20 (s, 1H), 4.01-4.13 (m, 9H) ppm.

Synthesis of 5-(4-nitrophenyl) dipyrromethane (NO_2-DP): To a mixture of 4-nitrobenzaldehyde (1.7 g, 11 mmol) and pyrrole (20 mL, 0.28 mol) was added TFA (84 μL, 1.1 mmol) at rt. The mixture was stirred for 10 min at rt, and the reaction was quenched by 1M NaOH aq. The resulting mixture was extracted with DCM and brine. The extract was dried over anhydrous Na_2SO_4, and concentrated under reduced pressure. The resulting mixture was purified by column chromatography (Ethyl acetate:Hex = 2:3) to afford a yellow solid (2.7 g, yield 89%). ^{1}H NMR (400 MHz, $CDCl_3$) δ 8.15 (dt, J = 9.1, 2.3 Hz, 2H), 7.99 (s, 2H), 7.35 (dt, J = 9.1, 2.1 Hz, 2H), 6.73 (td, J = 2.6, 1.5 Hz, 2H), 6.16 (q, J = 3.0 Hz, 2H), 5.84-5.86 (m, 2H), 5.57 (s, 1H) ppm.

Synthesis of *trans*-5,15-bisferrocenyl-10,20-bis(4-nitrophenyl) porphyrin (H-FcN):

To a solution of ferrocenecarbaldehyde (0.29 g, 1.4 mmol) and 5-(4-nitrophenyl)dipyrromethane (0.36 g, 1.4 mmol) in dry DCM (200 mL) was added TFA (62 μL, 0.81 mmol) at rt. The mixture was stirred for 45 h at rt and then DDQ (0.37 g, 1.6 mmol) was added. After 1 h, the reaction was quenched by TEA (0.11 mL, 0.81 mmol). The resulting mixture was purified by column chromatography (DCM:Hex = 4:1) to afford a dark purple solution. The desired product was recrystallized from DCM and Hex, and washed by MeOH to give a dark purple solid (0.26 g, yield 43%). ^{1}H NMR (400 MHz, $CDCl_3$) δ 9.86 (d, J = 4.9 Hz, 4H), 8.61-8.64 (m, 4H), 8.55 (d, J = 4.9 Hz, 4H), 8.32-8.35 (m, 4H), 5.49 (t, J = 1.8 Hz, 4H), 4.84 (t, J = 1.8 Hz, 4H), 4.11 (s, 10H), −1.66 (s, 2H) ppm. Anal. Calcd for $C_{52}H_{36}N_6O_4Fe_2 \cdot H_2O$: C, 66.54; H, 4.08; N, 8.95. Found: C, 66.77; H, 4.06; N, 9.01%.

References

1. (a) P. Rothemund, *J. Am. Chem. Soc*., **1939**, *61*, 2912. (b) P. Rothemund, A. R. Menotti, *J. Am. Chem. Soc.*, **1941**, *63*, 267. (c) S. Aronoff, M. Calvin, *J. Org. Chem.*, **1943**, *8*, 205. (d) R. H. Ball, G. D. Dorough, M. Calvin, *J. Am. Chem. Soc.*, **1946**, *68*, 2278.
2. A. D. Adler, F. R. Longo, W. Shergalis, *J. Am. Chem. Soc*., **1964**, *86*, 3145.
3. (a) J. S. Lindsey, H. C. Hsu, I. C. Schreiman, *Tetrahedron Lett*., **1986**, *27*, 4969. (b) R. W. Wagner, D. S. Lawrence, J. S. Lindsey, *Tetrahedron Lett*., **1987**, *28*, 3069. (c) J. S. Lindsey, I. C. Schreiman H. C. Hsu, P. C. Kearney, A. M. Marguerettaz, *J. Org. Chem*., **1987**, *52*, 827. (d) J. S. Lindsey, R. W. Wagner, *J. Org. Chem*., **1989**, *54*, 828
4. (a) P. D. Rao, S. Dhanalekshmi, B. J. Littler, J. S. Lindsey, *J. Org. Chem*., **2000**, *65*, 7323. (b) C. Clausen, D. T. Gryko, A. A. Yasseri, J. R. Diers, D. F. Bocian, W. G. Kuhr, J. S. Lindsey, *J. Org. Chem*., **2000**, *65*, 7371. (c) G. R. Geier, III, J. S. Lindsey, *Tetrahedron*., **2004**, *60*, 11435.
5. (a) H. L. Anderson, *Chem. Commun*., **1999,** 2323. (b) B. M. J. M. Suijkerbuijk, R. J. M. K. Gebbink, *Angew. Chem. Int. Ed*., **2008**, *47*, 7396. (c) S. Fukuzumi, *Phys. Chem. Chem. Phys*., **2008**, *10*, 2283. (d) M. Li, S. Ishihara, Q. Ji, M. Akada, J. P. Hill, K. Ariga, *Sci. Technol. Adv. Mater*., **2012**, *13*, 053001.
6. S. Yamaguchi, T. Shirasaka, K. Tamao, *Org. Lett*., **2000**, *2*, 4129.
7. (a) B. J. Littler, M. A. Miller, C-H. Hung, R. W. Wagner, D. F. O'Shea, P. D. Boyle, J. S. Lindsey, *J. Org. Chem*., **1999**, *64*, 1391. (b) J. C. Er, M. K. Tang, C. G. Chia, H. Liew, M. Vendrell, Y-T. Chang, *Chem. Sci*., **2013**, *4*, 2168.
8. P. Muthukumar, S. A. John, *Sensor. Actuat. B-Chem*., **2012**, *174*, 74. (b) P. Zhu, P. Ma, Y. Wang, Q. Wang, X. Zhao, X. Zhang, *Eur. J. Inorg. Chem*., **2011**, *27*, 4241.
9. (a) M. Gouterman, *J. Chemi. Phys*., **1959**, *30*, 1139. (b) M. Gouterman, *J. Mol. Spectrosc*., **1961**, *6*, 138.
10. V. N. Nemykin, C. D. Barrett, R. G. Hadt, R. I. Subbotin, A. Y. Maximov, E. V. Polshin, A. Y. Koposov, *Dalton. Trans*., **2007**, 3378.
11. T. Dhanasekaran, J. Grodkowski, P. Neta, P. Hambright, E. Fujita, *J. Phys. Chem. A*, **1999**, *103*, 7742.
12. The half wave potential of 9-phenylanthracene was reported to be $E_{1/2} = -1.93$ V (vs.

SCE) in DMF, 0.5M $TBABF_4$ at Hg electrode, CRC Handbook of Chemistry and Physics, 97th Edition.

13. I. Bhugun, D. Lexa, J-M. Savéant, *J. Am. Chem. Soc*., **1996**, *118*, 1769.
14. (a) B. H. Loo, *J. Mol. Struct*., **2003**, *661*, 451. (b) O.W. Webster, W. Mahler, R.E. Benson, *J. Am. Chem. Soc*., **1962**, *84*, 3678. (c) J. C. Moore, D. Smith, Y. Youhne, J. P. Devlin, *J. Phys. Chem*., **1971**, *75*, 325.
15. (a) W. J. Middleton, E. L. Little, D. D. Coffman, V. A. Engelhardt, *J. Am. Chem. Soc*., **1958**, *80*, 2795. (b) B. W. Sullivan, B. M. Foxman, *Organometallics*, **1983**, *2*, 187.
16. Y. Sato, H. Miyasaka, N. Matsumoto, H. Ōkawa, *Inorganica Chimica Acta*, **1996**, *247*, 57.
17. M. J. Frisch, G. W. Trucks, H. B. Schlegel, G. E. Scuseria, M. A. Robb, J. R. Cheeseman, G. Scalmani, V. Barone, B. Mennucci, G. A. Petersson, H. Nakatsuji, M. Caricato, X. Li, H. P. Hratchian, A. F. Izmaylov, J. Bloino, G. Zheng, J. L. Sonnenberg, M. Hada, M. Ehara, K. Toyota, R. Fukuda, J. Hasegawa, M. Ishida, T. Nakajima, Y. Honda, O. Kitao, H. Nakai, T. Vreven, J. A. Montgomery, Jr. J. E. Peralta, F. Ogliaro, M. Bearpark, J. J. Heyd, E. Brothers, K. N. Kudin, V. N. Staroverov, T. Keith, R. Kobayashi, J. Normand, K. Raghavachari, A. Rendell, J. C. Burant, S. S. Iyengar, J. Tomasi, M. Cossi, N. Rega, J. M. Millam, M. Klene, J. E. Knox, J. B. Cross, V. Bakken, C. Adamo, J. Jaramillo, R. Gomperts, R. E. Stratmann, O. Yazyev, A. J. Austin, R. Cammi, C. Pomelli, J. W. Ochterski, R. L. Martin, K. Morokuma, V. G. Zakrzewski, G. A. Voth, P. Salvador, J. J. Dannenberg, S. Dapprich, A. D. Daniels, O. Farkas, J. B. Foresman, J. V. Ortiz, J. Cioslowski, D. J. Fox, Gaussian 09 (Revision C.01), Gaussian, Inc. Wallingford CT, **2010**.
18. A. D. Becke, *J. Chem. Phys*., **1993**, *98*, 5648.
19. V. A. Rassolov, J. A. Pople, M. A. Ratner, T. L. Windus, *J. Chem. Phys*., **1998**, *109*, 1223.
20. E. Sakuda, Y. Ando, A. Ito, N. Kitamura, *Inorg. Chem*., **2011**, *50*, 1603.

Chapter 2

Synthesis and CO_2 reduction activities of π-expanded/extended iron porphyrin complexes

Journal of Biological Inorganic Chemistry, in press, DOI: 10.1007/s00775-017-1438-3

Introduction

Growing global energy demands and environmental problems, such as climate change and air pollution, currently underpin the broad interest in the development of sustainable energy conversion systems. In natural photosynthetic reactions, renewable but not storable solar energy is successfully converted into storable chemical energy by reducing carbon dioxide. This reductive transformation of carbon dioxide, which results in the production of energy-rich carbon compounds, is a very attractive reaction because this technology will allow us to solve both energy and environmental problems [1, 2]. Based on such considerations, there have been numerous studies that aimed to develop molecular-based artificial catalysts for the reduction of carbon dioxide in recent years [3, 4].

Iron porphyrin complexes are fascinating candidates as catalysts for carbon dioxide reduction [5–8]. One of the advantageous points of the complexes is that we can easily tune their physical properties by introducing various substituents at the *meso*-positions of the porphyrin framework. In fact, several reports revealed that the introduction of appropriate functional groups, such as acidic/basic and electron donating/withdrawing substituents, could affect the catalytic activity [7]. In this context, the introduction of substituents with a large π plane is expected to be one of the ways to control the catalytic activity of the iron porphyrin catalysts because this class of substituents not only could influence the electronic structure but could also provide hydrophobicity, which is preferable for accumulating CO_2 molecules near the active

center, to the molecular catalysts. However, the effect of such substituents on the catalytic activity of iron porphyrin complexes has not been explored.

In this study, we aimed to investigate the properties of iron porphyrin complexes with various types of π-conjugated substituents. We employed 5,10,15,20-tetrakis(phenyl)porphyrin (**H-Ph**, Figure 1), which is known to catalyze electrochemical CO_2 reduction [8], as a basic framework and derivatized its structure with π-expanded substituents, π-extended substituents, and π-expanded and extended substituents to afford 5,10,15,20-tetrakis(pyren-1-yl)porphyrin (**H-Py**), 5,10,15,20-tetrakis((1,1'-biphenyl)-4-yl)porphyrin (**H-PPh**) and 5,10,15,20-tetrakis(4-(pyren-1-yl)phenyl)porphyrin (**H-PPy**), respectively. Described herein are the syntheses, UV-vis absorption properties, and electrochemical properties of the free-base porphyrins and iron porphyrin complexes. In addition, the catalytic activities of the iron porphyrin complexes for electrochemical CO_2 reduction are also presented.

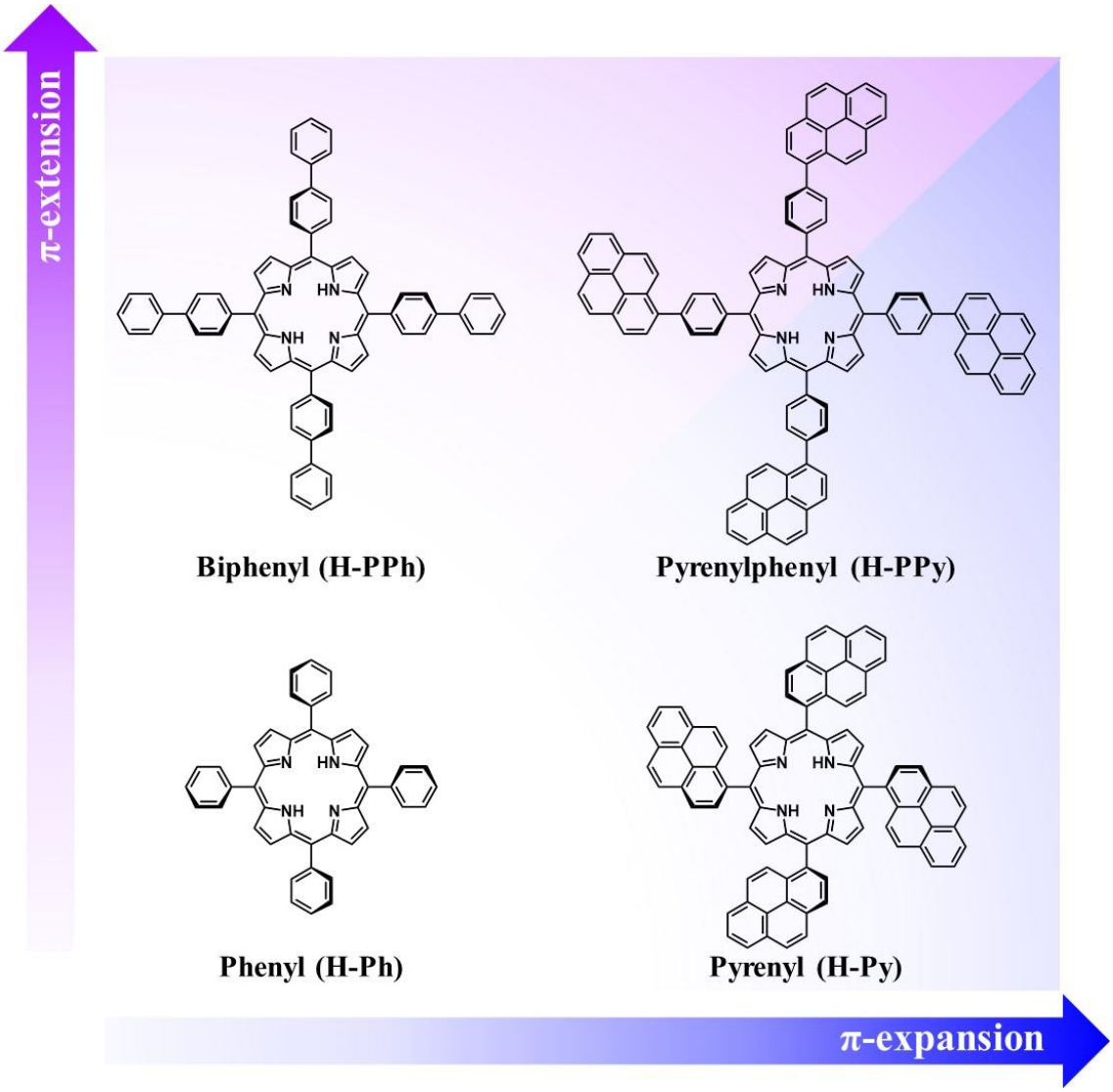

Figure 1. Chemical structures of the porphyrin derivatives investigated in this study.

Results and Discussion

Syntheses

Syntheses of the free-base porphyrins

Four types of free-base porphyrins were prepared following the synthetic routes shown in Scheme 1. The porphyrin with a basic structure, **H-Ph**, was obtained in moderate yield (19%) using Adler's method [9], in which benzaldehyde and pyrrole were refluxed in propionic acid under an air atmosphere. The π-expanded (**H-Py**) and the π-extended (**H-PPh**) derivatives were also previously synthesized using Adler's method [10, 11]. Therefore, we initially attempted the syntheses of these compounds under the same conditions as the synthesis of **H-Ph**, and the formation of the macrocyclic porphyrin skeleton was confirmed by ^{1}H NMR. However, the isolation of the desired products (**H-Py** and **H-PPh**) from the reaction mixture using column chromatography was unsuccessful due to the generation of numerous types of side products. Therefore, we adopted Lindsey's method [12, 13], in which porphyrin derivatives were obtained by the condensation of aryl aldehydes with pyrrole and the subsequent aromatization of the porphyrinogen intermediate by oxidation, as an alternative synthetic route. Aryl aldehydes (1-pyrenecarbaldehyde or 4-phenylbenzaldehyde) were reacted with pyrrole (1.0 eq.) in dichloromethane (DCM) at room temperature in the presence of trifluoroacetic acid (TFA), and 2,3-dichloro-5,6-dicyano-*p*-benzoquinone (DDQ) was added to the resultant reaction mixture as an oxidant. Under these reaction conditions, the amounts of impurities, such as polymeric pyrrole, were lower compared to the previous reaction conditions. Thus, the desired compounds were successfully isolated after their purification by silica gel column chromatography. The isolated yields were 6% and 7% for **H-Py** and **H-PPh**, respectively. Note that the synthesis of **H-PPh** by a similar method has been reported previously [14]. Since the acid-catalyzed condensation reaction using Lindsey's method was effective, the synthesis of the π-expanded and extended derivative (**H-PPy**) was performed using the same method. An aryl aldehyde with a pyrenylphenyl moiety, 4-(pyren-1-yl)benzaldehyde, was prepared by a Pd-catalyzed Suzuki-Miyaura cross-coupling reaction between 1-pyrenecarbaldehyde and 4-formylphenylboronic acid, and 4-(pyren-1-yl)benzaldehyde was obtained in 77% yield. The obtained aryl aldehyde was then condensed with pyrrole, and the porphyrinogen intermediate was further

oxidized by 1.2 eq. of DDQ at room temperature for 90 min. The resulting reaction mixture was quenched by triethylamine (TEA) and then purified by silica gel chromatography to afford **H-PPy** with a 16% yield. The obtained free-base porphyrins, **H-Ph**, **H-Py**, **H-PPh**, and **H-PPy**, were characterized by ^{1}H NMR spectroscopy and elemental analysis.

In the ^{1}H NMR spectra of the free-base porphyrins in $CDCl_3$, the broad singlet signal attributed to the internal N-H moieties was observed below 0 ppm (Figure 2) because of the ring current associated with the aromatic porphyrin. The chemical shifts of the signals were –2.80, –1.98, –2.69 and –2.51 ppm for **H-Ph**, **H-Py**, **H-PPh**, and **H-PPy**, respectively. Note that these chemical shifts were largely different depending on the substituent at the *meso*-positions. The order of chemical shifts was **H-Py** > **H-PPy** > **H-PPh** > **H-Ph**, which can be explained by considering the ring current from the aromatic substituents.

In addition to the singlet peaks of the internal N-H proton, the peaks originating from the aromatic substituents and the protons at the *β*-position of pyrrole rings (*β*-protons) were observed in the aromatic region. The signal of the *β*-protons was obtained as a singlet peak for **H-Ph** (8.82 ppm), **H-PPh** (8.96 ppm) and **H-PPy** (9.21 ppm), whereas the *β*-protons of **H-Py** were observed as multiplets at 8.75-8.86 ppm and 8.39-8.42 ppm. Generally, the symmetrical tetra-substituted porphyrin structure affords a singlet peak for the *β*-protons, and the asymmetric porphyrins give more complicated peaks. Therefore, the multiplet signals observed for **H-Py** indicate the presence of four stereoisomers formed due to the asymmetric structure and the large steric hindrance of the pyrenyl moiety. For **H-PPy**, a singlet peak for the *β*-protons was observed despite the asymmetric structure of the pyrenylphenyl moiety. This is because the phenylene linker allows the free rotation of the pyrenyl moiety, which results in the averaged symmetric structure in solution.

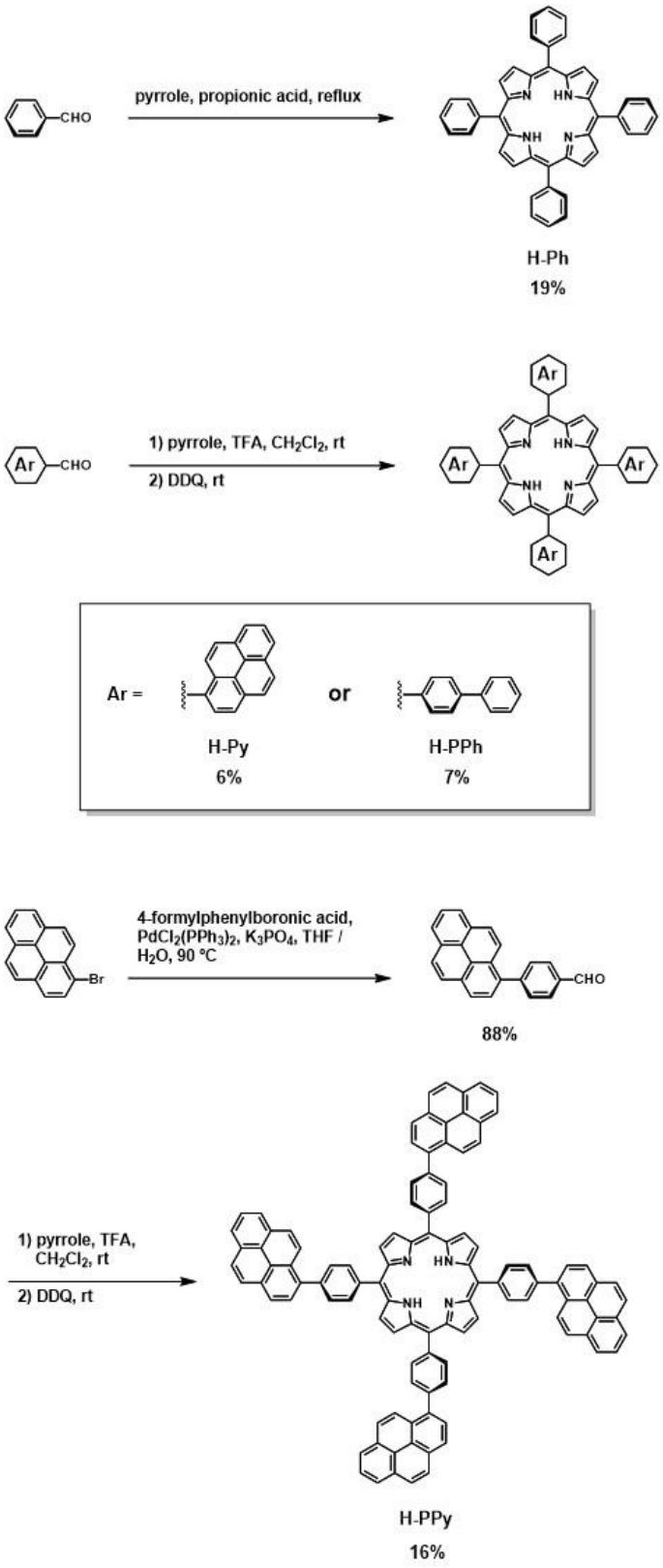

Scheme 1. Synthetic routes for the free-base porphyrins, **H-Ph**, **H-Py**, **H-PPh**, and **H-PPy**.

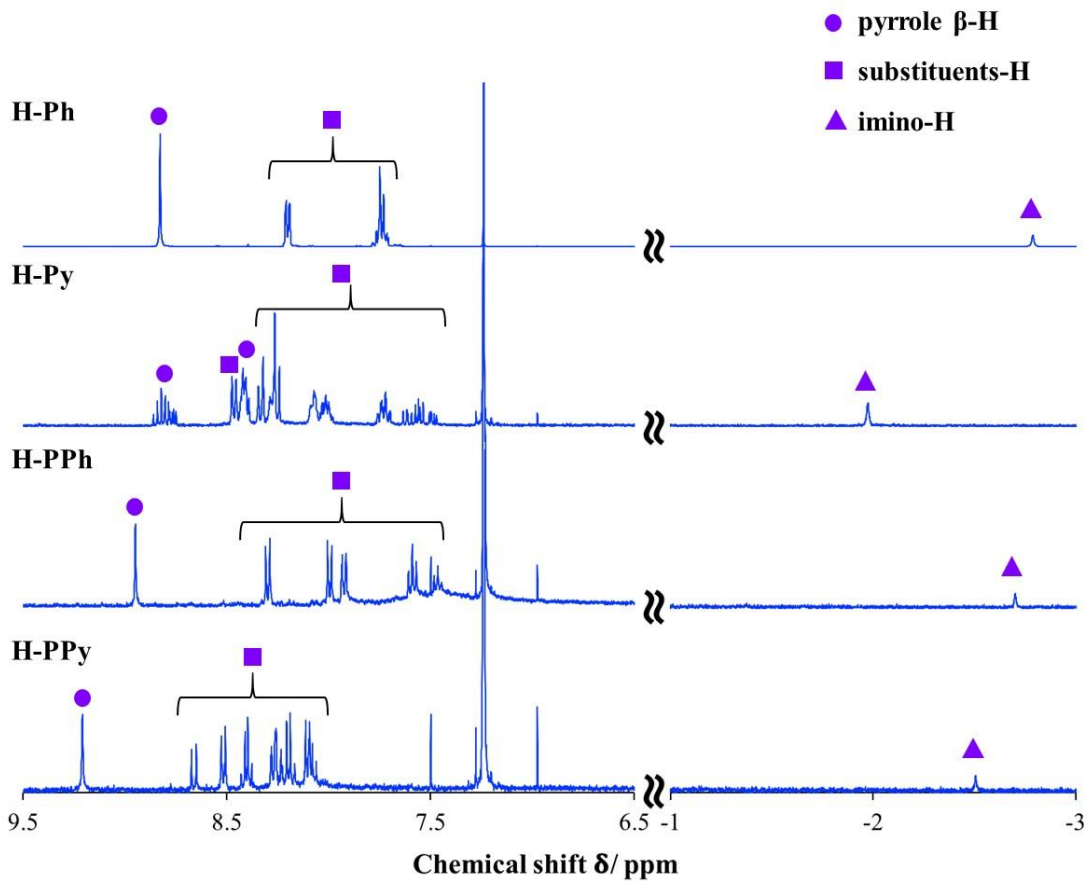

Figure 2. ^{1}H NMR spectra of **H-Ph, H-Py, H-PPh,** and **H-PPy** (400 MHz, $CDCl_3$).

Syntheses of iron porphyrin complexes

All free-base porphyrins were converted into the iron porphyrin complexes by a reaction with iron(II) chloride tetrahydrate in DMF or *N*-methylpyrrolidone (NMP). The synthetic scheme employed to obtain the iron complexes is shown in Scheme 2. The reaction conditions were optimized using **H-Ph** as a ligand. In the procedure previously reported in the literature [15, 16], the iron salt was gradually added to the reaction mixture in several portions within a given time period, and it is a slightly cumbersome procedure. To simplify the experimental operation, we first attempted the reaction by adding the solid iron salt in one portion. However, the reaction yield (trace) became lower than the previous report (97%) [16]. This might be because the oxidation of the iron salt to give iron(III) species is promoted upon the heating of the metal salt in the solid state, which prevents the metalation reaction. To avoid such a situation, in the modified method, a solution of iron(II) chloride was prepared beforehand and added to a solution of **H-Ph** dropwise before heating the solution. This modified synthetic strategy resulted in the formation of the desired complex, 5,10,15,20-tetrakis(phenyl)porphyrinato iron(III) chloride (**Fe-Ph**), in high yield (93%). The metalation of **H-Py** was also performed using the same reaction conditions, and the desired product, 5,10,15,20-tetrakis(pyren-1-yl)porphyrinato iron(III) chloride (**Fe-Py**), was obtained quantitatively. However, the iron complex was not formed at all when **H-PPh** was reacted under the same reaction conditions due to the low solubility of the ligand in DMF. Therefore, the reaction solvent was changed to NMP and the iron complex, 5,10,15,20-tetrakis((1,1'-biphenyl)-4-yl)porphyrinato iron(III) chloride (**Fe-PPh**), was obtained with moderate yield (66%). In the case of **H-PPy**, it took almost 24 h to complete the metalation in DMF and several decomposed compounds, which formed by heating the porphyrin for a long time, were obtained. Based on this observation, we changed the reaction solvent to NMP which possesses a higher boiling point than DMF, to shorten the reaction time. As a result, the iron complex, 5,10,15,20-tetrakis(4-(pyren-1-yl)phenyl)porphyrinato iron(III) chloride (**Fe-PPy**), was successfully obtained with high yield (87%). In all cases, the progress of the iron insertion reaction and the consumption of starting material were monitored by TLC and by checking the decrease of the number of Q bands in UV-vis absorption spectra (for the assignments of absorption bands, see section 2.2). All iron porphyrin complexes,

Fe-Ph, **Fe-Py**, **Fe-PPh** and **Fe-PPy**, were characterized by UV-vis absorption spectroscopy, electrochemical measurements and elemental analyses. The characterization by ^{1}H NMR measurement was difficult due to the paramagnetic nature of the complexes.

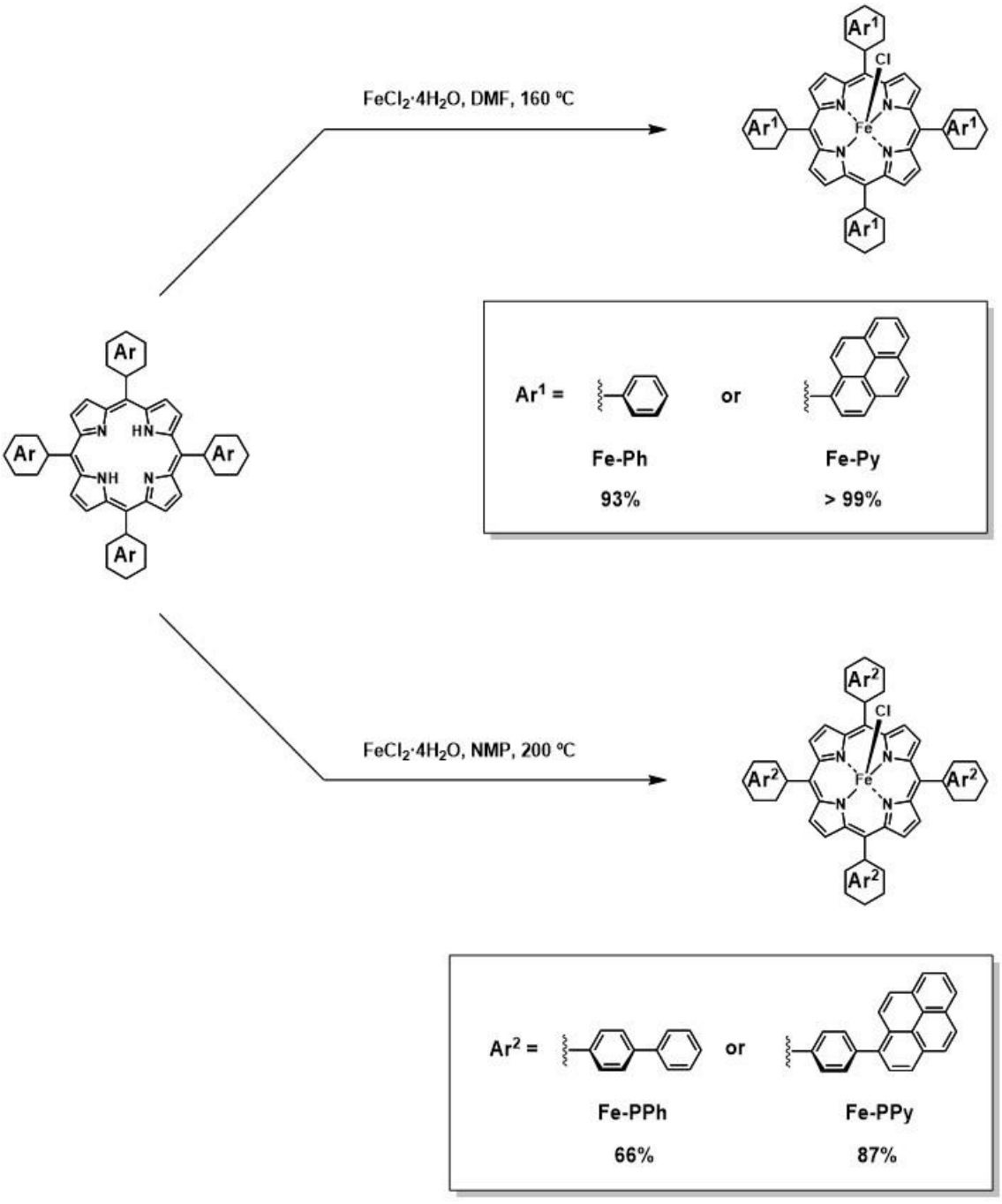

Scheme 2. Synthetic routes for the iron porphyrin complexes, **Fe-Ph, Fe-Py, Fe-PPh** and **Fe-PPy**.

UV-vis absorption properties of free-base and iron porphyrins

UV-vis absorption spectra of the free-base porphyrins and the iron complexes are shown in Figure 3, and the spectroscopic data are summarized in Table 1. All free-base porphyrins present a strong absorption band at approximately 422-436 nm and four weaker bands widely located at approximately 516-654 nm. These spectral features are caused by porphyrin macrocycle-based π-π* transitions described by Gouterman's four orbital model [17, 18]. The former band in the shorter wavelength region is assigned to the $S_0 \rightarrow S_2$ transition (Soret band), and the latter bands are attributed to the $S_0 \rightarrow S_1$ transition (Q bands). The Soret and Q bands of **H-Py, H-PPh**, and **H-PPy** are slightly red shifted compared with those of **H-Ph**, but located at a quite similar position. This result indicates that the electronic structure of the porphyrin moieties was not affected by the introduction of the aromatic substituents and is consistent with the results of the electrochemical measurements (*vide infra*). In addition to the typical porphyrin-based absorption bands, several absorption bands were observed at shorter wavelength (< 384 nm) in the case of **H-Py** and **H-PPy**, and assigned to the π-π* transitions of the aromatic substituents [19–22].

All iron porphyrin complexes show a strong absorption band at approximately 420-431 nm (Soret band) and weaker bands located in a wider region between 510-695 nm (Q bands). The decrease in the number of Q bands is due to the degeneration of the HOMO and the HOMO–1 for each porphyrin, thus indicating the generation of more symmetric structures via metalation [23]. There is no significant change in the absorption maxima of the Soret bands upon metalation, which was characteristic of iron porphyrin complexes [16].

Table 1. Summary of the absorption spectra for the free-base porphyrins and the iron porphyrin complexes in 1,2-dichlorobenzene.

Compound	λ_{max} / nm ($\varepsilon/10^4$ M^{-1} cm^{-1})		
	Substituent's bands	**Soret-band**	**Q-bands**
H-Ph	373 (1.30)	422 (25.52)	516 (1.08), 551 (0.48) 593 (0.30), 649 (0.24)
H-Py	328 (6.78), 340 (7.46)	436 (19.56)	524 (1.78), 555 (1.26), 604 (0.76), 658 (3.56)
H-PPh	311 (2.08), 377 (2.20)	427 (44.14)	520 (1.80), 557 (1.32), 596 (0.56), 653 (0.66)
H-PPy	349 (10.54)	429 (28.12)	520 (1.82), 556 (1.34), 596 (0.72), 654 (0.84)
Fe-Ph	378 (2.38)	420 (5.20)	510 (0.56), 575 (0.10), 691 (0.12)
Fe-Py	346 (7.74)	431 (5.74)	513 (1.32)
Fe-PPh	383 (2.78)	426 (6.30)	513 (0.74), 695 (0.18)
Fe-PPy	351 (11.22)	427 (11.66)	512 (1.48), 694 (0.34)

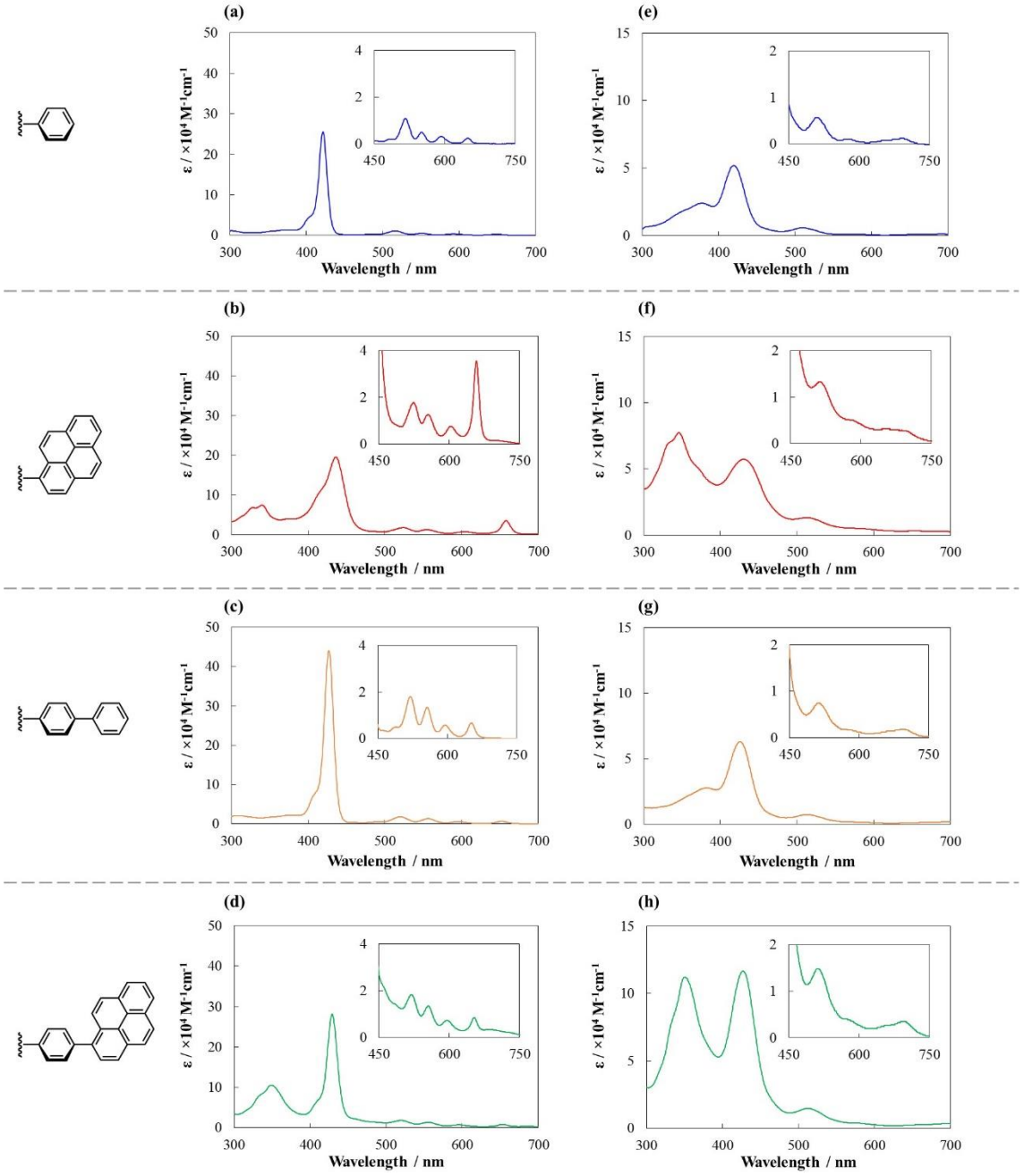

Figure 3. UV-vis absorption spectra of the free-base porphyrins in 1,2-dichlorobenzene (a) **H-Ph**, (b) **H-Py**, (c) **H-PPh**, (d) **H-PPy**, (e) **Fe-Ph**, (f) **Fe-Py**, (g) **Fe-PPh** and (h) **Fe-PPy**. (Insets) Enlarged UV-vis absorption spectra at Q-band regions.

Electrochemical properties

The cyclic voltammograms (CVs) of the free-base porphyrins (**H-Ph**, **H-Py**, **H-PPh**, and **H-PPy**) and the iron porphyrin complexes (**Fe-Ph**, **Fe-Py**, **Fe-PPh**, and **Fe-PPy**) are shown in Figure 4 and the redox potentials of these compounds are summarized in Table 2. The CVs were measured with 0.1 M tetrabutylammonium perchlorate (TBAP) in 1,2-dichlorobenzene. The concentrations of the free-base porphyrins and iron porphyrin complexes were 1.0 mM except for **H-PPh**. The CV of **H-PPh** was measured using a saturated solution due to its low solubility in the electrolyte solution. All free-base porphyrins displayed two reversible waves, which are assigned to the two-step one electron reduction of the porphyrin ring [6b]. The half wave potentials ($E_{1/2}$ (1) / V vs. ferrocene/ferrocenium (Fc/Fc^{+})) for the first reduction were –2.01 (**H-Ph**), –1.99 (**H-Py**), –1.97 (**H-PPh**) and –1.99 V (**H-PPy**), and those for the second reduction ($E_{1/2}$ (2)) were –2.32 (**H-Ph**), –2.38 (**H-Py**), –2.27 (**H-PPh**) and –2.28 V (**H-PPy**), respectively. The redox potentials of the free-base porphyrins are quite similar to each other, indicating almost no electronic interaction between the porphyrin framework and the substituent. In the cases of the iron porphyrin complexes, three reversible reduction peaks, which are possibly assigned to be Fe(III)/Fe(II), Fe(II)/Fe(I) and Fe(I)/Fe(0) redox couples according to the previous report [8b], were observed [24]. Similar to the results of the CVs of the free-base porphyrins, the redox potentials of the iron complexes are located at almost identical positions, reflecting the similar electronic structure of the ligands.

Table 2. Redox potentials of the prepared free-base porphyrins and the iron porphyrin complexes ($E_{1/2}$ / V vs. Fc/Fc^+) in 1,2-dichlorobenzene under an Ar atmosphere.

Compound	$E_{1/2}(1)$ / V	$E_{1/2}(2)$ / V	$E_{1/2}(3)$ / V
H-Ph	−2.01	−2.32	–
H-Py	−1.99	−2.38	–
H-PPh	−1.97	−2.27	–
H-PPy	−1.99	−2.28	–
Fe-Ph	−1.14	−1.88	−2.49
Fe-Py	−1.18	−1.89	−2.52
Fe-PPh	−1.12	−1.86	−2.45
Fe-PPy	−1.19	−1.93	−2.52

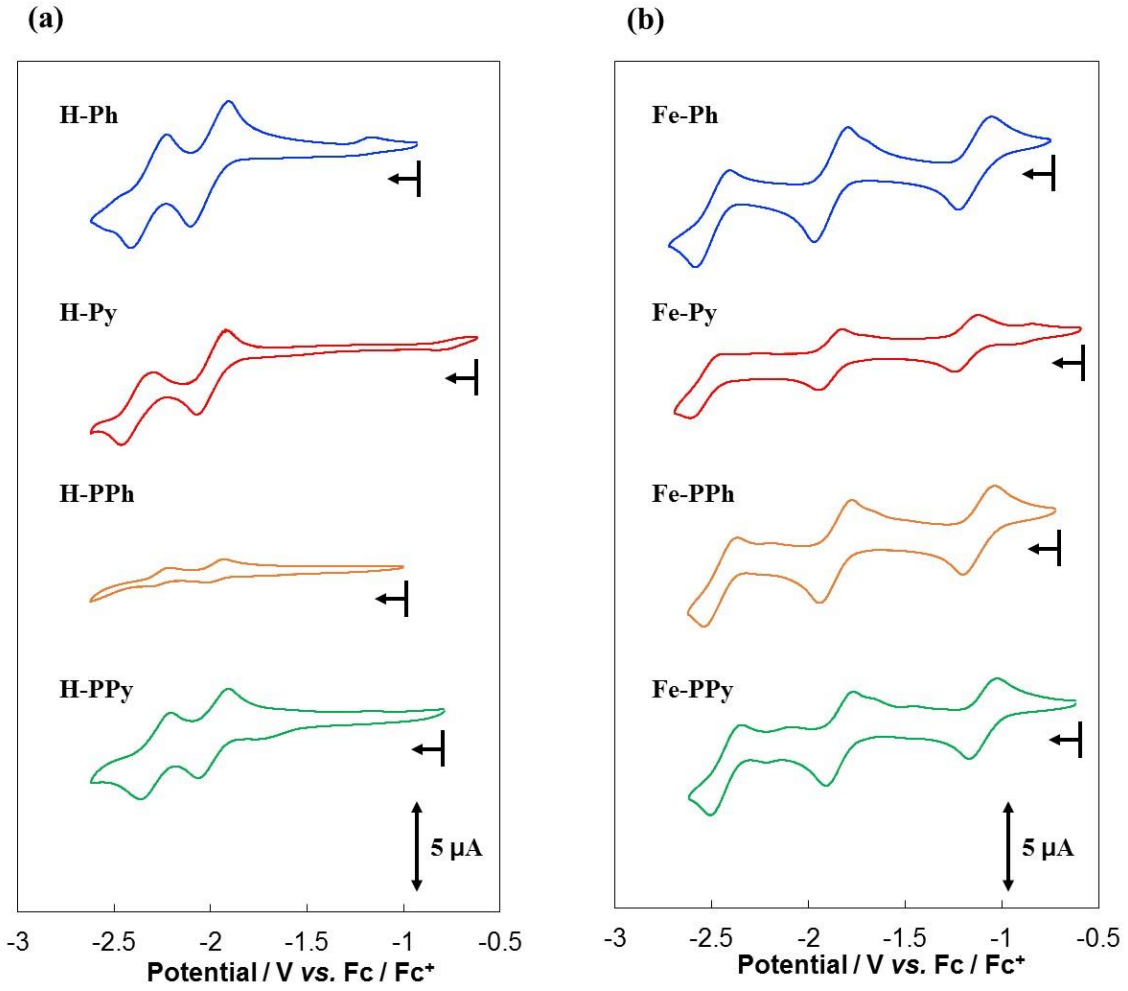

Figure 4. Cyclic voltammograms of the free-base porphyrins (**H-Ph, H-Py,** and **H-PPy,** 1.0 mM) and the iron porphyrin complexes (**Fe-Ph, Fe-Py, Fe-PPy and Fe-PPy,** 1.0 mM) in a 0.1 M TBAP/1,2-dichlorobenzene solution under an Ar atmosphere (WE: GC; CE: Pt wire; RE: Ag^{+}/Ag; scan rate: 20 mV s^{-1}). Note that the measurement of **H-PPh** was performed using a saturated solution due to its low solubility in the electrolyte solution. Potential sweeps were started from the open circuit potential −0.93 V (**H-Ph**), −0.62 V (**H-Py**), −1.00 V (**H-PPh**), −0.79 V (**H-PPy**), −0.75 V (**Fe-Ph**), −0.59 V (**Fe-Py**), −0.72 V(**Fe-PPh**) and −0.62 V (**Fe-PPy**). Arrows in the voltammograms indicate the direction of potential sweep.

Catalytic activity

Iron porphyrin complexes are known to catalyze the CO_2 reduction reaction to generate CO under electrochemical conditions [7, 8]. In the cyclic voltammograms of the complexes under a CO_2 atmosphere, an increase of the irreversible current coupled with the third reduction wave was observed. This irreversible current is called the catalytic current and indicates the occurrence of the electrocatalytic reduction of CO_2. It is also known that the intensity of the catalytic current basically is correlated to the rate of the catalytic reaction [7b, 25, 26]. Therefore, the electrochemical measurements of the newly synthesized complexes were also conducted under a CO_2 atmosphere to investigate the catalytic activity.

Initially, the measurements were performed using 0.1 M TBAP/1,2-dichlorobenzene solution. The results of the measurements are shown in Figure 5. Under a CO_2 atmosphere, an increase of the irreversible currents was observed at a potential close to the third redox wave for all compounds, suggesting the electrocatalytic reduction of CO_2 [7, 8]. However, the intensities of these catalytic currents were very small. In the CO_2 reduction catalyzed by iron-porphyrin complexes, the existence of proton source is essential to promote the reaction [7b]. It is also reported that water contained in the solvent is known to serve as a proton source [6e, 8d]. However, the concentration of water is low in 1,2-diclorobenzene due to its hydrophobicity, which may result in the small catalytic current [27]. Therefore, we measured the CVs of the iron complexes using a more hydrophilic solvent, DMF. The results of the measurements and a summary of the electrochemical data are shown in Figure 6 and Table 3, respectively. It should be noted the CV measurement of **Fe-PPh** was unsuccessful due to the low solubility of the complex in DMF. **Fe-Ph** and **Fe-Py** exhibited three reversible redox waves (–0.63, –1.51, and –2.15 V for **Fe-Ph**, and –0.63, –1.47, –2.08 V for **Fe-Py**) under an Ar atmosphere, which is in good agreement with the CVs measured in 1,2-dichlorobenzene. For **Fe-PPy**, in addition to the three reversible redox waves (–0.62, –1.50, and –2.11 V), one new reversible redox peak appeared at –2.43 V. This additional peak was assigned to the reduction of the 1-phenylpyrene substituents by comparing the CVs of related compounds (Figure 7). Under a CO_2 atmosphere, **Fe-Ph** exhibited large irreversible cathodic currents attributed to the catalytic reduction of CO_2 to CO at a potential close to the third redox

couple (−2.1 V vs. Fc/Fc^+), and the result is consistent with the previous report [8d]. Similarly, an irreversible current in a similar potential region was observed in the CV of **Fe-Py** under CO_2. To confirm the origin of the irreversible current, controlled potential electrolysis of **Fe-Py** and **Fe-Ph** was performed. Solutions containing 1.0 mM of the complexes were electrolyzed at −2.2 V (vs. Fc/Fc^+) for 1 h. After the electrolysis, both the gas and the liquid phases were analyzed and CO as a major product and small amount of dihydrogen (H_2) as a minor product were detected. The formation of formic acid was not detected. The faradaic efficiencies for the conversion of CO_2 to CO were determined to be 87 (**Fe-Py**) and 93 (**Fe-Ph**)% (Table 4 and Figure 11). These results clearly indicate the irreversible current is attributed to the electrocatalytic CO_2 reduction by the complexes. In the case of **Fe-PPy**, an increase of the irreversible current was observed both at the Fe(I)/Fe(0) redox couple (−2.11 V) and the reduction of the substituent (–2.43 V). Among the three complexes, **Fe-Py** exhibited the largest catalytic current under our experimental conditions, which suggests that the introduction of π-expanded substituents can improve the catalytic activity. Additionally, the controlled potential electrolysis revealed that the amounts of CO evolved during the electrolysis for were 2978 and 1999 μL for **Fe-Py** and **Fe-Ph**, respectively (Table 4). We also calculated the turnover frequency (TOF) and turnover number (TON) of the reaction for each complex based on the result of CPE experiments. TOF values were 120 (**Fe-Py**) and 60 (**Fe-Ph**) s^{-1} and TON values were 4.3×10^5 (**Fe-Py**) and 2.2×10^5 (**Fe-Ph**) s^{-1} for 1 h (for details of the calculation of TOF and TON values, see the Experimental section). These results clearly indicate that the reaction rate of **Fe-Py** is approximately 2.0 times higher than that of **Fe-Ph**. Based on these observations, we can conclude that the introduction of π-expanded substituents can improve the catalytic activity. Given that the redox potentials attributed to the iron porphyrin complexes are quite similar in these complexes (Table 3), the substituents rarely affected the electronic structure of the iron centers. It should be also noted that the adsorption of **Fe-Py** on the GC electrode rarely occur under the experimental conditions employed in this study (Figures 8-10 and 12). One possible explanation for the difference in the catalytic activity is that the hydrophobic space created by the substituents could promote the accumulation of the substrate, CO_2, and the faster supply of the substrate during catalysis resulted in a larger reaction rate.

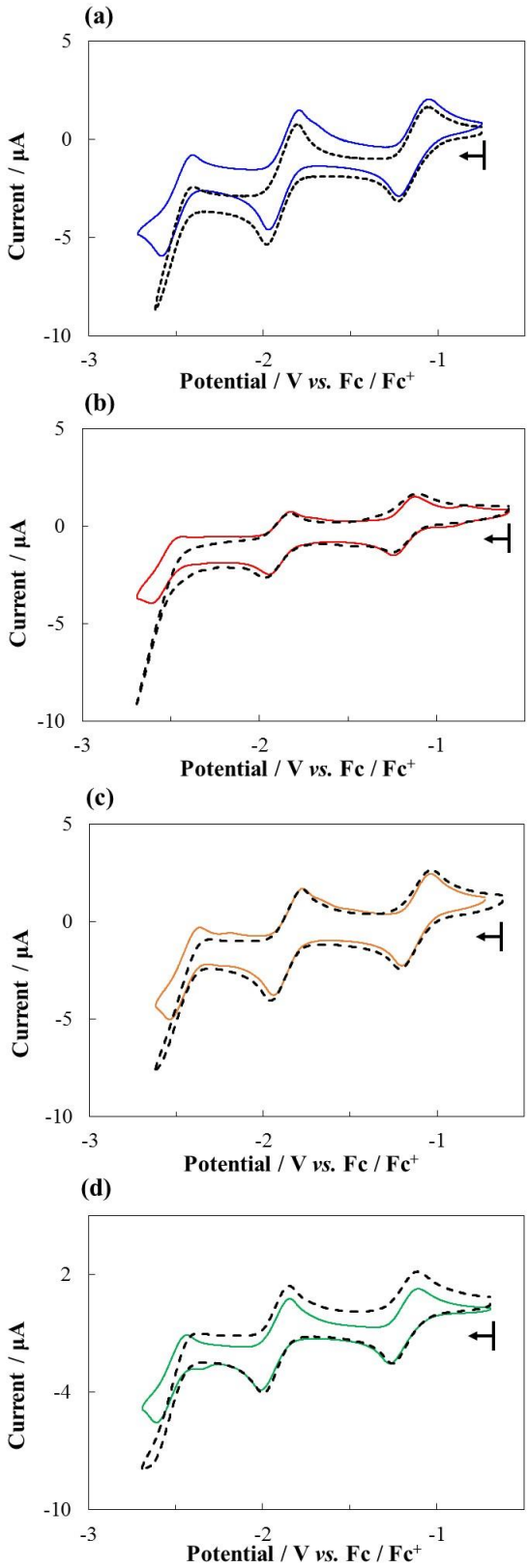

Figure 5. Cyclic voltammograms of the iron porphyrin complexes ((a) **Fe-Ph,** (b) **Fe-Py,** (c) **Fe-PPy** and (d) **Fe-PPy**, 1.0 mM) in a 0.1 M TBAP/1,2-dichlorobenzene solution

under Ar (solid lines) and CO_2 (dotted lines) atmospheres. (WE: GC; CE: Pt wire; RE: Ag^+/Ag; scan rate: 20 mV s^{-1}). The solutions were saturated with Ar or CO_2 prior to the experiments. Potential sweeps were started from the open circuit potential −0.75 V (**Fe-Ph**), −0.59 V (**Fe-Py**), −0.72 V (**Fe-PPh**) and −0.62 V (**Fe-PPy**). Arrows in the voltammograms indicate the direction of potential sweep.

Table 3. Redox potential for the prepared iron porphyrin complexes ($E_{1/2}$ / V vs. Fc/Fc^+) in a 0.1 M TBAP/DMF solution under Ar atmosphere.

Compound	$E_{1/2}(1)$ / V	$E_{1/2}(2)$ / V	$E_{1/2}(3)$ / V
Fe-Ph	−0.63	−1.51	-2.15
Fe-Py	−0.63	−1.47	−2.08
Fe-PPy	−0.62	−1.50	−2.11

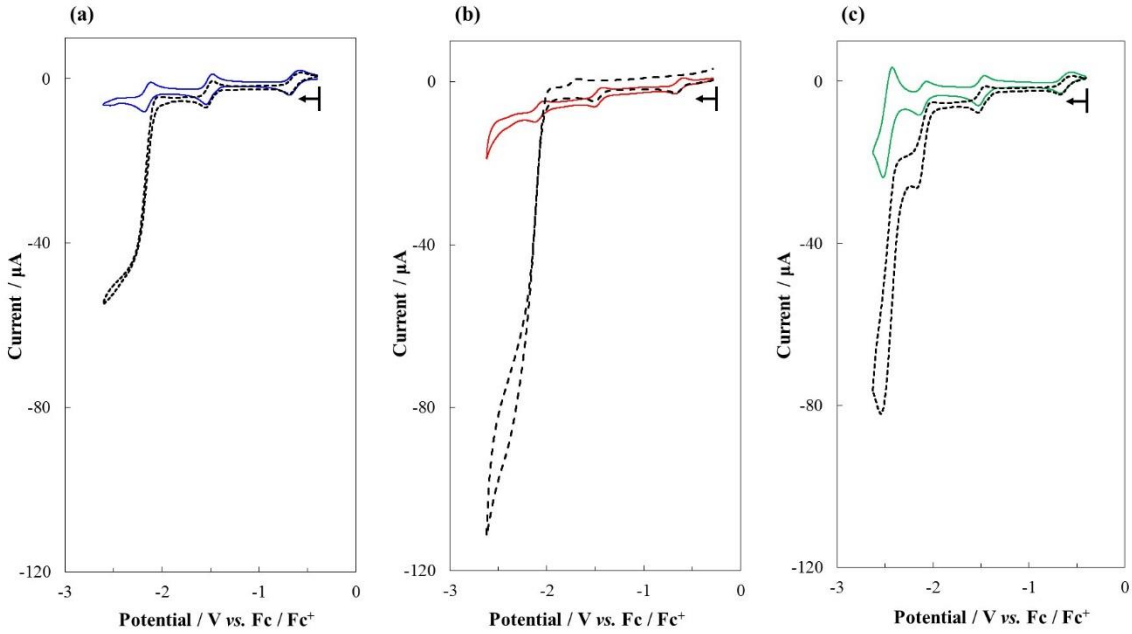

Figure 6. Cyclic voltammograms of (a) **Fe-Ph**, (b) **Fe-Py** and (c) **Fe-PPy** (1.0 mM) in a 0.1 M TBAP/DMF solution under Ar (solid lines) and CO_2 (dotted lines) atmospheres. (WE: GC; CE: Pt wire; RE: Ag^+/Ag; scan rate: 20 mV s^{-1}) The solutions were saturated with Ar or CO_2 prior to the experiments. The concentration of CO_2 in a 0.1 M TBAP/DMF solution is approximately 0.23 M [28]. Potential sweeps were started from the open circuit potential −0.40 V (**Fe-Ph**), −0.28 V (**Fe-Py**) and −0.41 V (**Fe-PPy**). Arrows in the voltammograms indicate the direction of potential sweep.

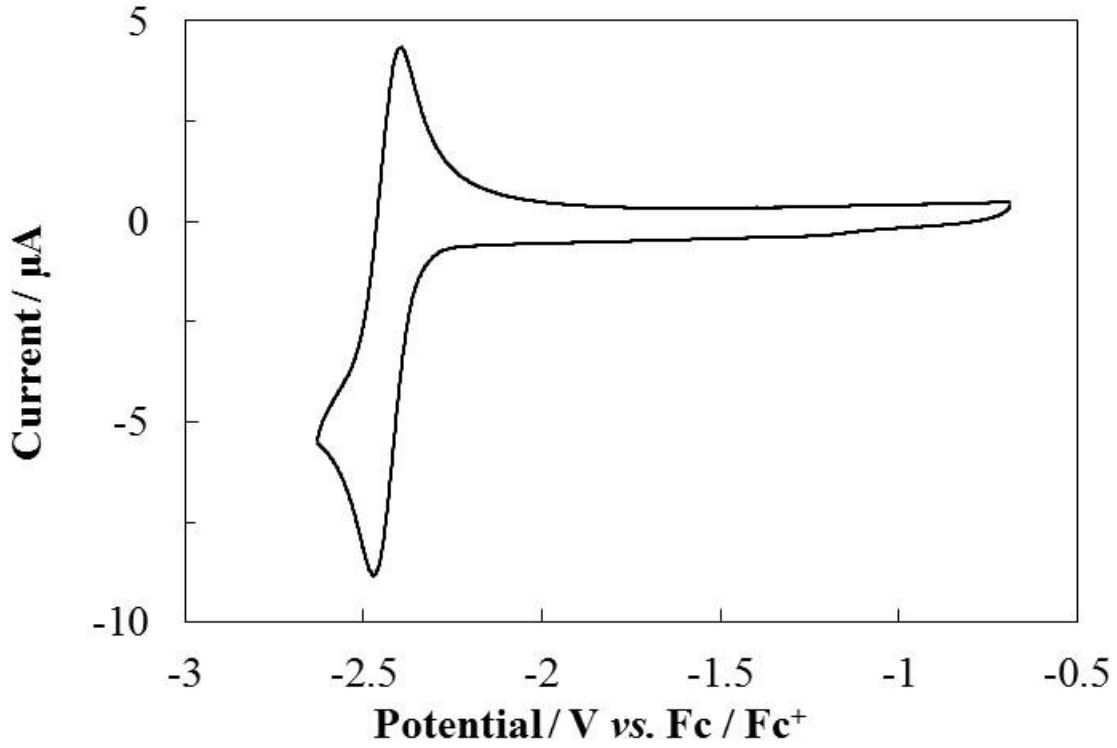

Figure 7. A cyclic voltammogram of 1-phenylpyrene (1.0 mM) in a 0.1 M TBAP/DMF solution under an Ar atmosphere (WE: GC; CE: Pt wire; RE: Ag^{+}/Ag; scan rate: 20 mV s^{-1}).

Table 4. Summary of the controlled potential electrolysis.

cat.	[cat], mM	Time, h	Applied potential, V vs. Fc/Fc^+	Charge, C	Evolved CO,μL	Faradaic efficiency, %			
						CO	H_2	HCOOH	Total
Fe-Py	1.0	1	–2.2 V	27.6	2978	87	5	n.d.	92
Fe-Ph	1.0	1	–2.2 V	17.2	1999	93	trace	n.d.	93

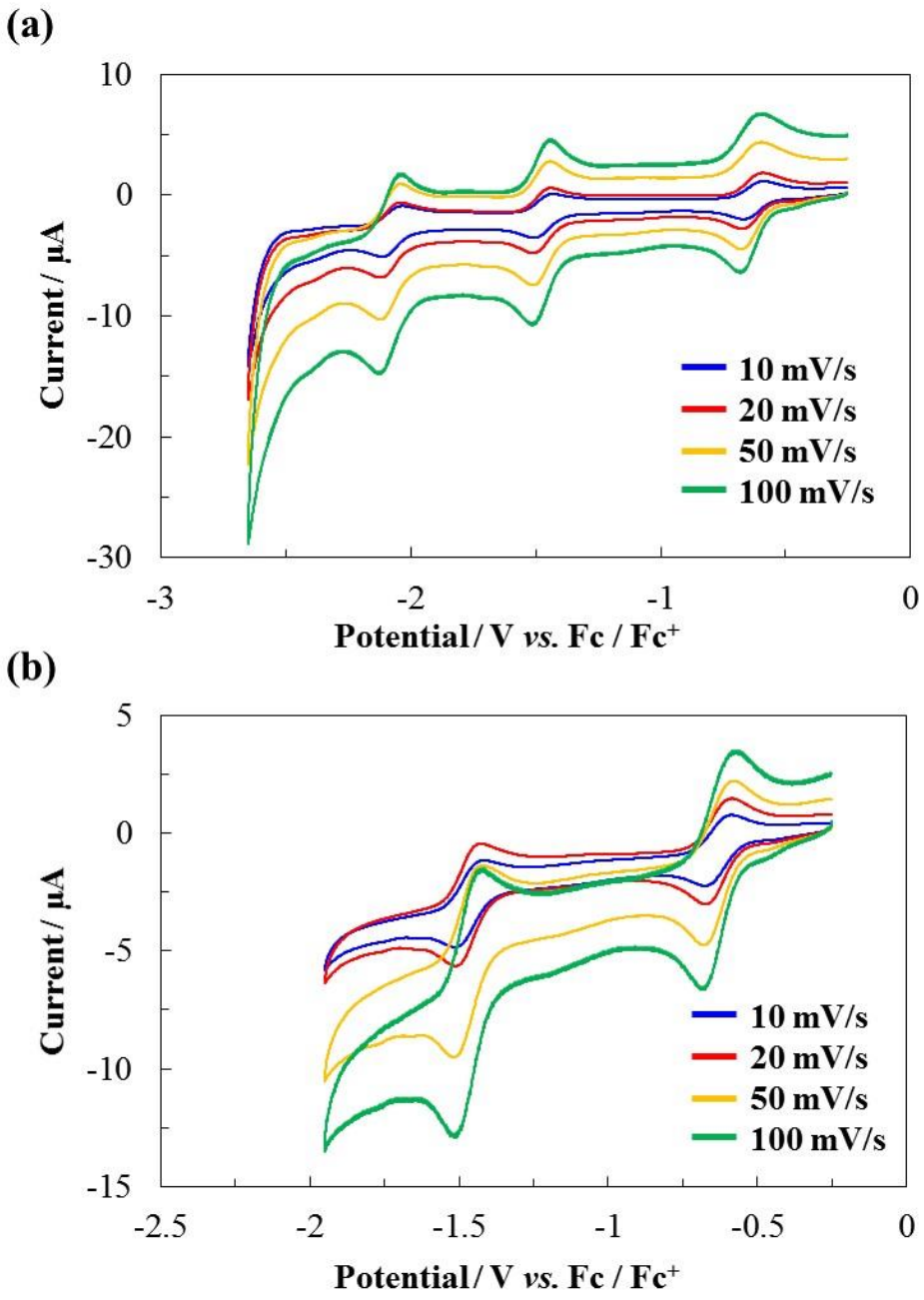

Figure 8. Cyclic voltammograms of **Fe-Py** (1.0 mM) in a 0.1 M TBAP/DMF solution under (a) Ar and (b) CO_2 atmosphere at various scan rates (WE: GC; CE: Pt wire; RE: Ag^+/Ag).

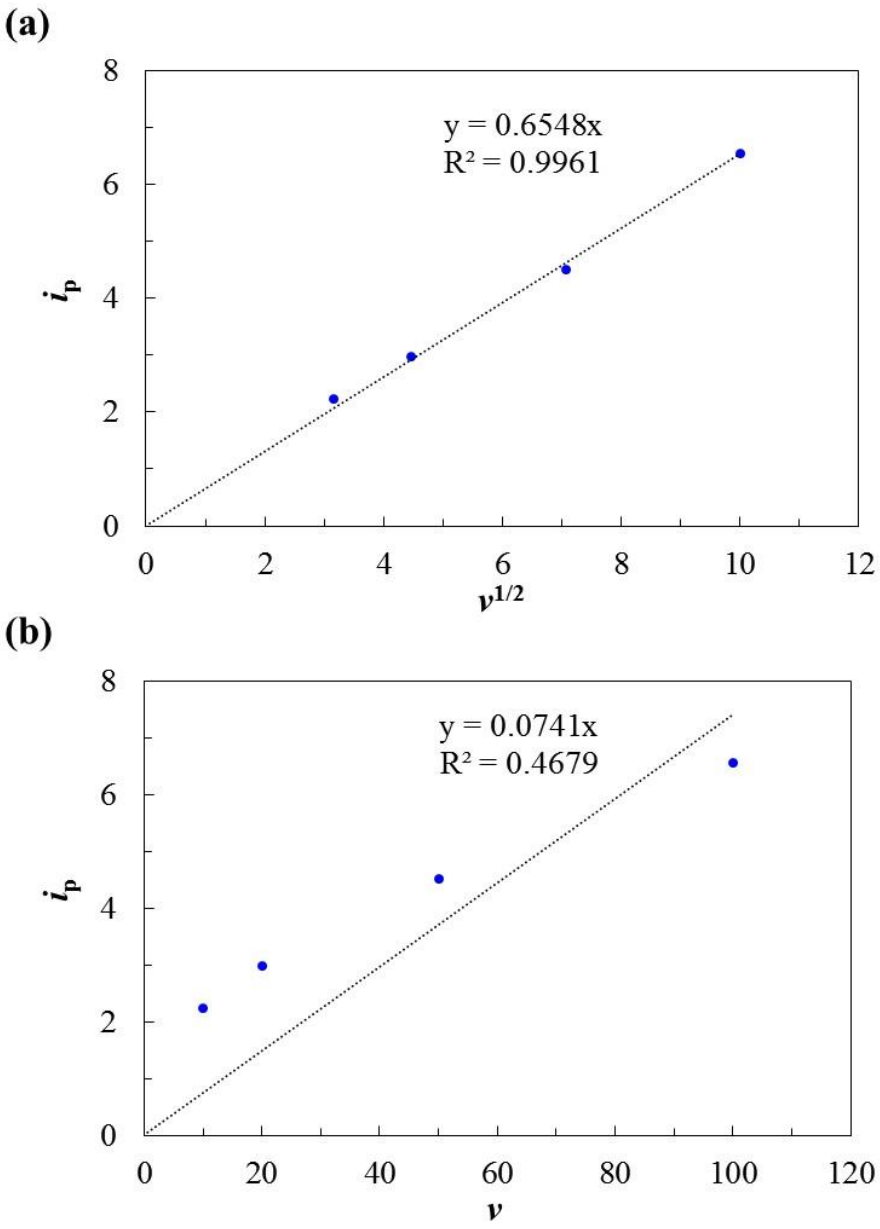

Figure 9. Plots of (a) i_p *vs.* $v^{½}$ and (b) i_p *vs.* v. Measurements were performed under an Ar atmosphere. The original voltammograms are shown in Figure 8a. The cathodic current of the third reduction wave in Figure 8a was used as i_p. The linear relationship between i_p and $v^{½}$ indicates the diffusion limited electron transfer process (Randles-Sevcik equation), suggesting that no adsorption of **Fe-Py** on the electrode.

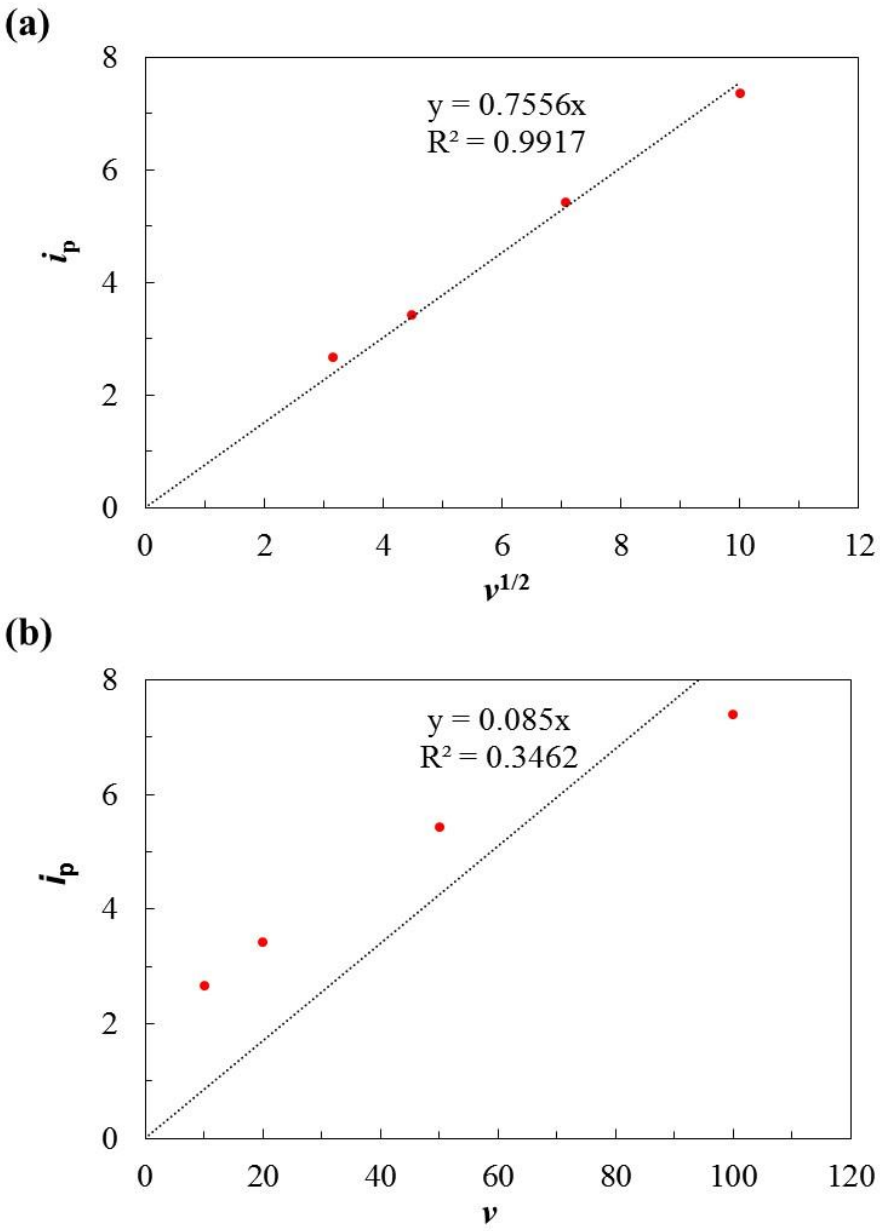

Figure 10. Plots of (a) i_p *vs.* $v^{½}$ and (b) i_p *vs.* v. Measurements were performed under a CO_2 atmosphere. The original voltammograms are shown in Figure 8b. The cathodic current of the second reduction wave in Figure 8b was used as i_p. The linear relationship between i_p and $v^{½}$ indicates the diffusion limited electron transfer process (Randles-Sevcik equation), suggesting that no adsorption of **Fe-Py** on the electrode.

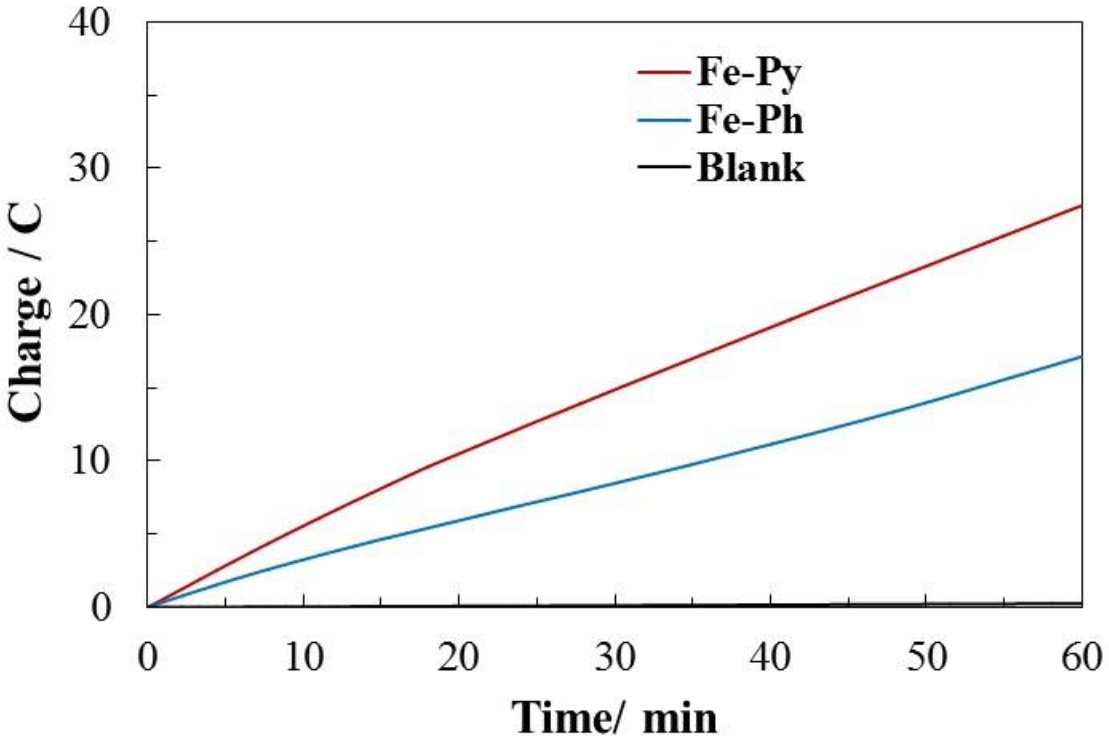

Figure 11. Electrolysis data in DMF/water (10 : 1) mixed solutions containing *n*Bu$_4$NClO$_4$ (0.1 M) at a potential of –2.2 V vs. Fc/Fc$^+$ with 1.0 mM of **Fe-Py** (red line) and **Fe-Ph** (blue line) and without catalyst (black line).

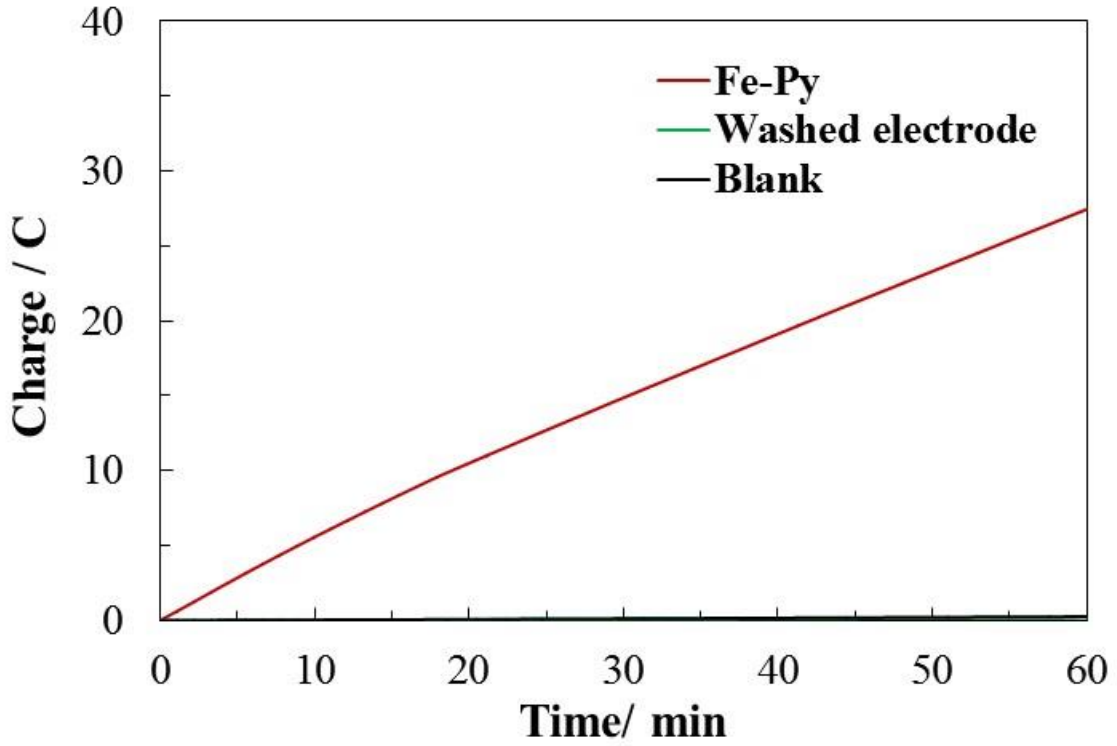

Figure 12. The result of the first electrolysis using a fresh glassy carbon electrode in 1.0 mM of **Fe-Py** (red line, same data as shown in Figure 11, red line) and that of second round of electrolysis without **Fe-Py** (green line), and the electrolysis data of a blank solution (black line, same data as shown in Figure 11, black line). In the second round of electrolysis, the glassy carbon electrode utilized in first electrolysis was gently washed with electrolyte solution prior to the experiment and used without polishing. Condition: DMF/water (10 : 1) mixed solution with nBu$_4$NClO$_4$ (0.1 M) at a potential of −2.2 V *vs.* Fc/Fc$^+$. The charge observed in the second round of electrolysis is comparable to that of blank, which suggests that the deposition of **Fe-Py** on the electrode did not occur during the first electrolysis.

Conclusion

This study describes the syntheses and the spectroscopic and electrochemical properties of iron porphyrin complexes with π-conjugated substituents at the *meso*-position. Three novel iron complexes, **Fe-Py**, **Fe-PPh**, and **Fe-PPy,** were synthesized by the reaction of the corresponding free-base porphyrins (**H-Py**, **H-PPh**, and **H-PPy**) with iron(II) chloride tetrahydrate in DMF or NMP and characterized by elemental analyses and UV-vis absorption spectroscopy. The electrochemical analysis of the complexes under an Ar atmosphere indicated that the introduction of the π-conjugated substituents rarely affects the electronic structures of the iron porphyrin complexes. However, the catalytic activity of **Fe-Py** was found to be much higher than that of **Fe-Ph**. These results indicate that the introduction of large π-conjugated substituents directly to the *meso*-positions of a porphyrin moiety could provide a hydrophobic space suitable for the accumulation of CO_2 molecules.

Experimental

Materials and Methods

Pyrrole was purchased from Sigma-Aldrich Co., LLC. 1,2-dichlorobenzene, ferrocene (Fc), 4-formylphenylboronic acid, iron(II) chloride tetrahydrate, 1-methylpyrrolidin-2-one (NMP), 1-pyrenecarbaldehyde, triethylamine (TEA), trifluoroacetic acid (TFA), bis(triphenylphosphine)palladium(II) dichloride and tripotassium phosphate were purchased from Wako Pure Chemical Industries, Ltd. Hexane (Hex) and *N*,*N*-dimethylformamide (DMF) were purchased from Kanto Chemical Co., Inc. Tetra(*n*-butyl)ammonium perchlorate (TBAP), 1-bromopyrene, 2,3-dichloro-5,6-dicyano-1,4-benzoquinone and 4-phenylbenzaldehyde were purchased from Tokyo Chemical Industry Co., Ltd. $CDCl_3$ was obtained from Cambridge Isotopes, Inc. All reagents were used without further purification. TBAP was recrystallized from absolute ethanol and dried in vacuo. Dichloromethane (DCM) and tetrahydrofuran (THF) were degassed and purified under an N_2 atmosphere using a GlassContour solvent system (Nikko Hansen Co., Ltd.).

^{1}H NMR spectra were recorded on a JEOL 400 MHz instrument. All ^{1}H NMR spectra were referenced against residual proton signals. Elemental analyses were measured on a MICRO CORDER JM10. Electrochemical experiments were performed under argon and CO_2 atmospheres using a BAS ALS Model 650DKMP electrochemical analyzer. Cyclic voltammograms were recorded in 1,2-dichlorobenzene ([complex] = 1.0 mM; 0.1 M TBAP) using a glassy carbon disk, a platinum wire and an Ag^+/Ag electrode (Ag/0.01 M $AgNO_3$) that were used as the working, auxiliary, and reference electrodes, respectively. The redox potentials of the samples were calibrated against the redox signal for the ferrocene/ferrocenium (Fc/Fc^+) couple. UV-vis absorption measurements were performed on a Shimadzu UV-1800 spectrometer at room temperature.

Controlled-potential electrolysis was performed in a gas-tight two-compartment electrochemical cell. The first compartment held the carbon rod working electrode (3.9 cm^2 surface area) and Ag/AgCl reference electrode in DMF/water (10 : 1) mixed solution containing 0.1 M TBAP (5 ml) with 1.0 mM catalyst, while the second compartment held the Pt auxiliary electrode containing 0.4 M $Et_4N^+CH_3CO_2^-$ + 0.1 M TBAP/DMF (5 ml). The role of $Et_4N^+CH_3CO_2^-$ is to function as reactant at anode to produce CO_2 and ethane

(Kolbe reaction).[7b] The two compartments were separated by Nafion® membrane. The solution was purged with CO_2 for 1 h prior to electrolysis. The electrolysis experiment was performed under constant stirring. The amount of CO and H_2 produced was quantified from an analysis of the headspace with Shimadzu GC-8A with TCD detector equipped with capillary column with Molecular Sieve 13X-S 60/80. Calibration curves were made by sampling known amounts of H_2 and CO. On the other hand, liquid product was quantified by using Shimadzu LC-20AD with SPD-20A and RID-10A detectors equipped with Shim-pack SCR102H column. A calibration curve was made by sampling known amounts of HCOOH.

Estimation of TOF and TON from controlled potential electrolysis

The TOF and TON values of **Fe-Py** and **Fe-Ph** were estimated using the results of controlled potential electrolysis based on the previously reported analysis (Equations 1-4) by Costentin and Savéant [29].

$$\frac{i}{F\,\mathrm{A}} = \frac{\sqrt{k_{cat}\,D}\,[\mathrm{cat}]}{1+\exp\left[\frac{F}{RT}\left(E_{applied}-E^{0}_{\mathrm{cat}}\right)\right]} \qquad (1)$$

$$k_{\mathrm{cat}} = \frac{i^{2}\left(1+exp\left[\frac{F}{RT}\left(E_{applied}-E^{0}_{\mathrm{cat}}\right)\right]\right)^{2}}{F^{2}\,\mathrm{A}^{2}\,D\,[cat]^{2}} \qquad (2)$$

$$\mathrm{TOF} = \frac{k_{cat}}{1+\exp\left[\frac{F}{RT}\left(E_{applied}-E^{0}_{\mathrm{cat}}\right)\right]} \qquad (3)$$

$$\mathrm{TON} = \mathrm{TOF} \times \mathrm{time} \qquad (4)$$

In these equations, i represents the stable current transferred during CPE, F is Faraday's constant (96485 C/mol), A is the surface area of the GC electrode (3.9 cm^2), k_{cat} is the overall rate constant of the catalytic CO_2 reduction reaction, D is the diffusion coefficient, which is assumed to be ~2.6×10^{-6} cm^2/s based on the previous report (*J. Am. Chem. Soc*. **2012**, *134*, 11235−11242), [cat] is the initial concentration of the catalyst (1.0 mM = 1×10^{-6} mol/cm^3, R is the universal gas constant (8.31 J K^{-1} mol^{-1}), T is temperature (298.15 K), $E_{applied}$ is the applied potential during CPE (−2.2 V vs. Fc/Fc^+), E^0_{cat} is the standard potential of the catalyst (−2.08 **(Fe-Py**) and −2.15 (**Fe-Ph**) V vs. Fc/Fc^+), and TOF is the turnover frequency. This leads to calculated values of TOF = 120 s^{-1} and TON = 4.3×10^5 for **Fe-Py** and TOF = 60 s^{-1} and TON = 2.2×10^5 for **Fe-Ph**.

Syntheses

Synthesis of 5,10,15,20-tetrakis(phenyl)porphyrin (H-Ph): **H-Ph** was synthesized according to the published method (yield 19%). ^{1}H NMR (400 MHz, $CDCl_3$) δ 8.82 (s, 8H), 8.19-8.21 (m, 8H), 7.71-7.78 (m, 12H), –2.80 (s, 2H) ppm. Anal. Calcd for $C_{44}H_{30}N_4$: C, 85.97; H, 4.92; N, 9.11. Found: C, 85.90; H, 5.02; N, 9.04%.

Synthesis of 5,10,15,20-tetrakis(pyren-1-yl)porphyrin (H-Py): To a solution of 1-pyrenecarbaldehyde (0.93 g, 4.05 mmol) in dry DCM (600 mL) was added pyrrole (0.28 mL, 4.05 mmol) in one portion at rt. After stirring for 5 min, to the reaction mixture was added TFA (0.93 mL, 12.2 mmol) at rt. The mixture was stirred for 21 h at rt and then DDQ (1.1 g, 4.9 mmol) was added. After 90 min, the reaction was quenched by TEA (1.7 mL, 12.2 mmol). The resulting mixture was passed through a silica short column to give a black solution. The resulting residue was purified by column chromatography (DCM/Hex) to afford a dark purple solution. The desired product was recrystallized from a tiny amount of THF and diethyl ether to give a purple solid, and the product was washed with several portions of methanol and diethyl ether (73 mg, yield 6%). ^{1}H NMR (400 MHz, $CDCl_3$) δ 8.75-8.86 (m, 4H), 8.46 (d, J = 7.9 Hz, 4H), 8.39-8.42 (m, 8H), 8.33 (d, J = 9.2 Hz, 4H), 8.24-8.29 (m, 8H), 8.08 (d, J = 6.4 Hz, 4H), 7.98-8.04 (m, 4H), 7.70-7.76 (m, 4H), 7.59-7.64 (m, 1H), 7.56 (dd, J = 9.2, 5.8 Hz, 2H), 7.47-7.51 (m, 1H), –1.98 (s, 2H) ppm. Anal. Calcd for $C_{84}H_{46}N_4 \cdot H_2O$: C, 89.34; H, 4.28; N, 4.96. Found: C, 89.61; H, 4.70; N, 4.95%.

Synthesis of 5,10,15,20-tetrakis((1,1'-biphenyl)-4-yl)porphyrin (H-PPh): To a solution of 4-phenylbenzaldehyde (1.2 g, 6.6 mmol) in dry DCM (300 mL) was added pyrrole (0.46 mL, 6.6 mmol) in one portion at rt. After stirring for 5 min, to the reaction mixture was added TFA (1.5 mL, 20 mmol) at rt. The mixture was stirred for 1 h at rt and then DDQ (1.8 g, 8.0 mmol) was added. After 90 min, the reaction was quenched by TEA (2.8 mL, 20 mmol). The resulting mixture was purified by column chromatography (DCM/Hex) to afford a dark purple solution. The desired product was recrystallized from a tiny amount of THF and diethyl ether to give a purple solid (0.108 mg, yield 7%). ^{1}H NMR (400 MHz, $CDCl_3$) δ 8.96 (s, 8H), 8.31 (d, J = 8.2 Hz, 8H), 8.00 (d, J = 8.2 Hz,

8H), 7.93 (d, *J* = 7.0 Hz, 8H), 7.60 (t, *J* = 7.6 Hz, 8H), 7.47 (t, *J* = 7.5 Hz, 4H), –2.69 (s, 2H) ppm. Anal. Calcd for $C_{68}H_{46}N_4 \cdot H_2O$: C, 87.15; H, 5.16; N, 5.98. Found: C, 87.45; H, 5.62; N, 5.71%.

Synthesis of 4-(pyren-1-yl)benzaldehyde: To the mixture of 1-bromopyrene (4.5 g, 16 mmol), 4-formylphenylboronic acid (2.5 g, 17 mmol), tripotassium phosphate (10 g, 48 mmol) and bis(triphenylphosphine)palladium(II) dichloride (0.56 g, 0.80 mmol) was added dry THF (160 mL) and water (21 mL). The mixture was refluxed with stirring for 19 h. After evaporation of THF, the precipitate was washed by water and methanol. The mixture was purified by column chromatography (DCM: Hex = 1:1) to afford the desired product (4.3 g, yield 88%). ^{1}H NMR (400 MHz, $CDCl_3$) δ 10.15 (s, 1H), 8.17-8.24 (m, 3H), 8.01-8.13 (m, 7H), 7.96 (d, *J* = 7.9 Hz, 1H), 7.80 (dt, *J* = 8.0, 1.6 Hz, 2H) ppm.

Synthesis of 5,10,15,20-tetrakis(4-(pyren-1-yl)phenyl)porphyrin (H-PPy): To a solution of 4-(pyren-1-yl)benzaldehyde (2.03 g, 6.6 mmol) in dry DCM (300 mL) was added pyrrole (0.46 mL, 6.6 mmol) in one portion at rt. After stirring for 5 min, to the reaction mixture was added TFA (1.5 mL, 20 mmol) at rt. The mixture was stirred for 1 h at rt and then DDQ (1.8 g, 8.0 mmol) was added. After 90 min, the reaction was quenched by TEA (2.8 mL, 20 mmol). The resulting mixture was purified by column chromatography (DCM) to afford a dark purple solution. The desired product was recrystallized from a tiny amount of THF and diethyl ether to give a purple solid (0.38 mg, yield 16%). ^{1}H NMR (400 MHz, $CDCl_3$) δ 9.21 (s, 8H), 8.66 (d, *J* = 9.2 Hz, 4H), 8.52 (d, *J* = 7.9 Hz, 8H), 8.40 (dd, *J* = 13.0, 7.8 Hz, 8H), 8.17-8.28 (m, 20H), 8.06-8.11 (m, 12H), –2.51 (s, 2H) ppm. Anal. Calcd for $C_{108}H_{62}N_4 \cdot 2.5H_2O$: C, 88.80; H, 4.62; N, 3.84. Found: C, 88.87; H, 4.57; N, 3.71%.

Synthesis of 5,10,15,20-tetrakis(phenyl)porphyrinato iron(III) chloride (Fe-Ph): Fe-Ph was prepared by the modification of a previous report. To a solution of **H-Ph** (0.50 g, 0.81 mmol) in DMF (60 mL), a DMF (21 mL) solution of $FeCl_2 \cdot 4H_2O$ (0.97 g, 4.9 mmol) was added dropwise at room temperature. The mixture was refluxed for 30 min and then cooled to room temperature. After evaporating all the solvent, the resulting mixture was

extracted with DCM. The extract was dried over anhydrous Na_2SO_4, and concentrated under reduced pressure. The desired product was precipitated from DCM and Hex to give a purple solid that was collected by filtration (0.53 g, yield 93%). Anal. Calcd for $C_{44}H_{28}ClFeN_4$: C, 75.06; H, 4.01; N, 7.96. Found: C, 75.19; H, 4.31; N, 7.82%.

Synthesis of 5,10,15,20-tetrakis(pyren-1-yl)porphyrinato iron(III) chloride (Fe-Py): To a solution of **H-Py** (0.63 g, 0.56 mmol) in DMF (41 mL), a DMF (15 mL) solution of $FeCl_2 \cdot 4H_2O$ (0.67 g, 3.4 mmol) was added dropwise at room temperature. The mixture was refluxed for 3 h and then cooled to room temperature. After evaporating all the solvent, the resulting mixture was extracted with DCM. The extract was dried over anhydrous Na_2SO_4, and concentrated under reduced pressure. The desired product was precipitated from DCM and Hex to give a dark brown (0.68 g, yield quant.). Anal. Calcd for $C_{84}H_{44}ClFeN_4 \cdot 2.5H_2O$: C, 81.00; H, 3.97; N, 4.50. Found: C, 81.33; H, 4.06; N, 4.19%.

Synthesis of 5,10,15,20-tetrakis((1,1'-biphenyl)-4-yl)porphyrinato iron(III) chloride (Fe-PPh): To the mixture of **H-PPh** (41 mg, 0.045 mmol) and $FeCl_2 \cdot 4H_2O$ (89 mg, 0.45 mmol) was added NMP (9 mL). The mixture was refluxed for 1 h and then cooled to room temperature. After evaporating all the solvent, the resulting mixture was extracted with DCM. The extract was dried over anhydrous Na_2SO_4, and concentrated under reduced pressure. The desired product was recrystallized from a tiny amount of THF and diethyl ether to give a dark purple solid (30 mg, yield 66%). Anal. Calcd for $C_{68}H_{44}ClFeN_4 \cdot 1.75H_2O$: C, 78.54; H, 4.60; N, 5.39. Found: C, 78.53; H, 4.80; N, 5.38%.

Synthesis of 5,10,15,20-tetrakis(4-(pyren-1-yl)phenyl)porphyrinato iron(III) chloride (Fe-PPy): To the mixture of **H-PPy** (0.10 g, 0.071 mmol) and $FeCl_2 \cdot 4H_2O$ (0.14 g, 0.71 mmol) was added NMP (14 mL). The mixture was refluxed for 1 h and then cooled to room temperature. After evaporating all the solvent, the resulting mixture was extracted with DCM. The extract was dried over anhydrous Na_2SO_4, and concentrated under reduced pressure. The desired product was recrystallized from a tiny amount of THF and diethyl ether to give a dark purple solid (92 mg, yield 87%). Anal. Calcd for $C_{108}H_{60}ClFeN_4 \cdot 2.25H_2O$: C, 83.93; H, 4.21; N, 3.63. Found: C, 83.80; H, 4.31; N, 3.86%.

References

1. N.S. Lewis, D. G. Nocera, *Proc. Natl. Acad. Sci. U.S.A.*, **2006**, *103*, 15729.
2. H. B. Gray, *Nat. Chem*., **2009**, *1*, 7.
3. (a) K. Tanaka, D. Ooyama, *Coord. Chem. Rev*., **2002**, *226*, 211. (b) J-M. Savéant, *Chem. Rev*., **2008**, *108*, 2348. (c) H. Takeda, O. Ishitani, *Coord. Chem. Rev*., **2010**, *254*, 346. (d) J. Schneider, H. Jia, J .T. Muckermana, E. Fujita, *Chem. Soc. Rev*., **2012**, *41*, 2036. (e) C. D. Windle, R. N. Perutz, *Coord. Chem. Rev*., **2012**, *256*, 2562. (f) P. Kang, Z. Chen, M. Brookhart, T. J. Meyer, *Top. Catal*., **2015**, *58*, 30.
4. (a) M. Beley, J. P. Collin, R. Ruppert, J. P. Sauvage, *J. Am. Chem. Soc*., **1986**, *108*, 7461. (b) H. Nagao, T. Mizukawa, K. Tanaka, *Inorg. Chem.* 1994, *33*, 3415. (c) Z. Chen, C. Chen , D. R. Weinberg, J. J. Concepcion, D. P. Harrison, M. S. Brookhart, T. J. Meyer, *Chem. Commun*., **2011**, *47*, 12607. (d) J. M. Smieja, E. E. Benson, B. Kumar, K. A. Grice, C. S. Seu, A. J. M. Miller, J. M. Mayer, C. P. Kubiak, *Proc. Natl. Acad. Sci. U.S.A.*, **2012**, *109*, 15646. (e) J. A. Keith, K. A. Grice, C. P. Kubiak, E. A. Carter, *J. Am. Chem. Soc*., **2013**, *135*, 15823. (f) M. S. Jeletic, M. T. Mock, A. M. Appel, J. C. Linehan, *J. Am. Chem. Soc.*, **2013**, *135*, 11533. (g) K. Kobayashi, K. Tanaka, *Phys. Chem. Chem. Phys*., **2014**, *16*, 2240. (h) Z. Chen, P. Kang, M-T. Zhang, T. J. Meyer, *Chem. Commun*., **2014**, *50*, 335. (i) P. Kang, S. Zhang, T. J. Meyer, M. Brookhart, *Angew. Chem. Int. Ed*., **2014**, *53*, 8709. (j) B. A. Johnson, H. Agarwala, T. A. White, E. Mijangos, S. Maji, S. Ott, *Chem. Eur. J*., **2016**, *22*, 14870. (k) J. Kothandaraman, A. Goeppert, M. Czaun, G. A. Olah, G. K. S. Prakash, *J. Am. Chem. Soc.*, **2016**, *138*, 778. (l) G. Sahara, H. Kumagai, K. Maeda, N. Kaeffer, V. Artero, M. Higuchi, R. Abe, O. Ishitani, *J. Am. Chem. Soc*. **2016**, *138*, 14152.
5. (a) A. J. Morria, G. J. Meyer, E. Fujita, *Acc. Chem. Res*., **2009**, *42*, 1983. (b) C. Costentin, M. Robert, J-M. Savéant, *Chem. Soc. Rev*., **2013**, *42*, 2423. (c) C. Costentin, M. Robert, J-M. Savéant, *Acc. Chem. Res*. **2015**, *48*, 2996.
6. (a) J. Grodkowski, D. Behar, P. Neta, P. Hambright, *J. Phys. Chem. A*, **1997**, *101*, 248. (b) T. Dhanasekaran, J. Grodkowski, P. Neta, P. Hambright, E. Fujita, *J. Phys. Chem. A*, **1999**, 103, 7742. (c) E. A. Mohamed, Z. N. Zahran, Y. Naruta, *Chem. Commun*. **2015**, *51*, 16900. (d) B. Mondal, A. Rana, P. Sen, A. Dey, *J. Am. Chem. Soc*., **2015**, *137*, 11214. (e) A. Fukatsu, M. Kondo, Y. Okabe, S. Masaoka, *J. Photochem.*

Photobiol. A: Chem., **2015**, 313, 143.

7. (a) M. Hammouche, D. Lexa, M. Momenteau, J-M. Savéant, *J. Am. Chem. Soc*., **1991**, *113*, 8455. (b) C. Costentin, S. Drouet, M. Robert, J-M. Savéant, *Science*, **2012**, *338*, 90. (c) C. Costentin, G. Passard, M. Robert, J-M. Savéant, *J. Am. Chem. Soc*., **2014**, *136*, 11821.
8. (a) I. Bhugun, D. Lexa, J-M. Savéant, *J. Am. Chem. Soc*., **1994**, *116*, 5015. (b) I. Bhugun, D. Lexa, J-M. Savéant, *J. Am. Chem. Soc*., **1996**, *118*, 1769. (c) I. Bhugun, D. Lexa, J-M. Savéant, *J. Phys. Chem*., **1996**, *100*, 19981. (d) C. Costentin, S. Drouet, G. Passard, M. Robert, J-M. Savéant, *J. Am. Chem. Soc*., **2013**, *135*, 9023.
9. A. D. Adler, F. R. Longo, W. Shergalis, *J. Am. Chem. Soc*., **1964**, *86*, 3145.
10. G. Knör, *Inorg. Chem. Commun*., **2001**, *4*, 160.
11. O. Penon, F. Marsico, D. Santucci, L. Rodriguez, D. B. Amabilino, L. Pérez-García, *J. Porphyrins Phthalocyanines*, **2012**, *16*, 1293.
12. J. S. Lindsey, H. C. Hsu, I. C. Schreiman, *Tetrahedron Lett*., **1986**, *27*, 4969.
13. J. S. Lindsey, R. W. Wagner, *J. Org. Chem.*, **1989**, *54*, 828.
14. R. Ishikawa, K. Katoh, B. K. Breedlove, M. Yamashita, *Inorg. Chem*., **2012**, *51*, 9123.
15. H. Kobayashi, T. Higuchi, Y. Kaizu, H. Osada, M. Aoki, *Bull. Chem. Soc. Jpn*., **1975**, *48*, 3137.
16. Z-C. Sun, Y-B. She, Y. Zhou, X-F. Song, K. Li, *Molecules*, **2011**, *16*, 2960.
17. M. Gouterman, *J. Chemi. Phys*., **1959**, *30*, 1139.
18. M. Gouterman, *J. Mol. Spectrosc*., **1961**, *6*, 138.
19. A. Stockmann, J. Kurzawa, N. Fritz, N. Acar, S. Schneider, J. Daub, R. Engl, T. Clark, *J. Phys. Chem. A*, **2002**, *106*, 7958.
20. M. Raytchev, E. Pandurski, I. Buchvarov, C. Modrakowski, T. Fiebig, *J. Phys. Chem. A*, **2003**, 107, 4592.
21. W. Weigel, W. Rwttig, M. Dekhtyar, C. Modrakowski, M. Beinhoff, A. D. Schlüter, *J. Phys. Chem. A*, **2003**, *107*, 5941.
22. W. Wu, W. Wu, , S. Ji, H. Guo, X. Wang, J. Zhao, *Dyes Pigments*, **2011**, *89*, 199.
23. J. Mack, M. J. Stillman, The Porphyrin Handbook (Eds. K. Kadish, K. M. Smith, R. Guilard) **2003**, *16*, Elsevier Science, San Diego USA, 43.
24. (a) In the iron porphyrin complexes, there are several possible resonant forms to

describe the electronic structure of the reduced species, and all resonant forms presumably contribute to the electronic structure of the complexes. In the case of **Fe-Ph**, previous reports suggested that the three electron reduced species should be best formulated as a Fe(0) complex, based on the results of UV-vis and resonance Raman spectroscopy and studies on electrocatalytic reactions (reference 8b, 24b and 24c). Given that redox potentials of the newly synthesized complexes (**Fe-Py**, **Fe-PPh** and **Fe-PPy**) are quite similar to the reported complex, **Fe-Ph**, the nature of the redox processes and the electronic structure of the reduced species are probably similar. Therefore, we have assigned the redox processes of the newly synthesized complexes to be Fe(III)/Fe(II), Fe(II)/Fe(I) and Fe(I)/Fe(0) according to the previous reports. (b) D. Lexa, J-M. Savéant, K-B. Su, D-L. Wang, *J. Am. Chem. Soc*. **1988**, *110*, 7617. (c) É. Anxolabéhère, G. Chottard, D. Lexa, *New J. Chem*., **1994**, *18*, 889.

25. E. S. Rountree, B. D. McCarthy, T. T. Eisenhart, J. L. Dempsey, *Inorg. Chem*., **2014**, *53*, 9983.
26. Okamura M. , M. Kondo, R. Kuga, Y. Kurashige, T. Yanai, S. Hayami, V. K. K. Praneeth, M. Yoshida, K. Yoneda, S. Kawata, S. Masaoka, *Nature*, **2016**, *530*, 465.
27. It should be noted that the concentration of CO_2 in solution can be an important factor to affect the reaction rate. In our experiments, CO_2-saturated solutions were employed in all the electrochemical measurements under a CO_2 atmosphere although the exact concentration of CO_2 in the 1,2-diclorobenzene solutions was unknown.
28. A. Gennaro, A. A. Isse, E. Vianello, *J. Electroanal. Chem*., **1990**, *289*, 203.
29. C. Costentin, S. Drouet, M. Robert, J-M. Savéant, *J. Am. Chem. Soc.* **2012**, *134*, 11235.

Chapter 3

Construction of framework structure based on metalloporphyrin catalysts via intermolecular non-covalent interaction between pyrene units

Introduction

Metalloporphyrin derivatives are known to serve as catalysts for CO_2 reduction.[1] Recently, two important keys to improve the catalytic activity of metalloporphyrin derivatives for CO_2 reduction have independently been proposed. The first key is adjacent metal centers. Naruta *et al.* reported that the catalyst which has two iron porphyrin moieties bridged by a *o*-phenylene linker exhibits superior activity than a relevant derivative which has a *m*-phenylene linker.[2] They concluded that the suitable separation of the two iron ions can facilitate the strong binding of CO_2 molecules, which results in the high activity, selectivity, and stability of the catalyst. The second key is the formation of hydrophobic space to accommodate non-polar CO_2 molecules. Yaghi *et al.* has succeeded in developing efficient CO_2 reduction system based on a covalent organic framework (COF)[3] containing cobalt porphyrin complexes as catalytic centers.[4] The COF developed by the group has porous structure and can adsorb CO_2 gas inside the cavity. By utilizing the COF, the selective CO_2 reduction in aqueous media was achieved, and the performance of the catalytic system was much better than the corresponding discrete system.

Encouraged by these pioneering works, I assume that the construction of the framework structure which has adjacent catalytic centres to activate CO_2 and a hydrophobic cavity to accumulate CO_2 can be a new strategy to develop highly efficient CO_2 reduction system. In order to obtain such a framework structure, the self-assembly of the catalyst with intermolecular interaction sites via the non-covalent interaction is a

valuable approach.[5] In this context, I focused on a planar polyaromatic molecule, pyrene. Pyrene derivatives are known to exhibit both face-to-face (π-π) interaction and face-to-edge (CH-π) interaction (Scheme 1) between molecules and easily form the relatively strong assembled structure with close distance of molecules.[6] Therefore, it is expected that the robust framework structure with adjacent catalytic centres can be constructed by introducing of pyrene moiety to catalyst molecules. Note that use of non-covalent interaction is attractive because the assembled structure can be constructed under milder conditions than the construction of metal-organic frameworks (MOFs) or COFs, which often requires solvothermal conditions.[7]

Based on the aforementioned consideration, I newly design a porphyrin compound, 5,10,15,20-tetrakis(4-(7-(*tert*-butyl)pyren-2-yl)phenyl)porphyrin (**H-BPPy,** Scheme 2). **H-BPPy** possesses four pyrenylphenyl moieties at the *meso*-positions of a porphyrin ring. This molecule has four-fold symmetry and is expected to show high planarity, which are advantageous for the construction of a highly ordered framework structure. *tert*-Butyl group was introduced at the 7-position of the pyrene moiety to increase the solubility of the molecule. It should be also noted that the catalytic activity can also be controlled by the alternation of a metal ion.

In this chapter, syntheses of **H-BPPy** and **H-BPPy** based metal complexes, 5,10,15,20-tetrakis(4-(7-(*tert*-butyl)pyren-2-yl)phenyl)porphyrinato cobalt(II) (**Co-BPPy**) and 5,10,15,20-tetrakis(4-(7-(*tert*-butyl)pyren-2-yl)phenyl)porphyrinato iron(III) chloride (**Fe-BBPy**) are described. Physical properties of the obtained porphyrin derivatives were investigated by UV-vis absorption and electrochemical measurements, and the catalytic activity of metal complexes was studied. The self-assembly of the catalyst was examined using **Co-BPPy** and the formation of framework structure was confirmed by single crystal X-ray diffraction study.

i) π-π interaction

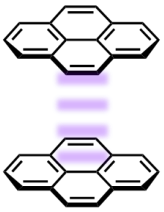

ii) CH-π interaction

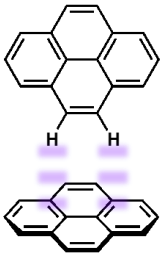

Scheme 1 (i) Face-to-face (π-π) interaction and (ii) face-to-edge (CH-π) interaction between pyrene units.

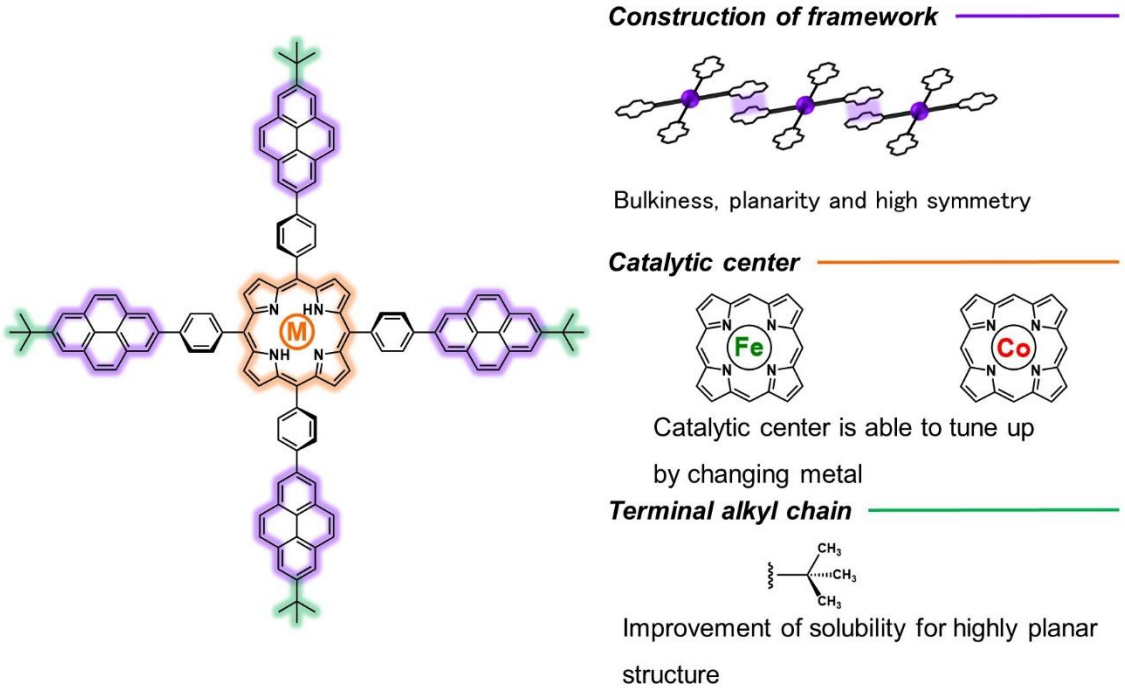

Scheme 2 Molecular design of **H-BPPy**.

Results and Discussion

Syntheses

Synthesis of a free-base porphyrin is described in Scheme 3. 2-bromo-7-*tert*-butylpyrene was employed as a building block of intermolecular interaction site, and was reacted with 4-formylphenylboronic acid in Suzuki-Miyaura coupling condition to give 4-(7-(tert-butyl)pyrene-2-yl)benzaldehyde in 77% yield. The obtained aldehyde derivative was reacted with pyrrole under an acidic condition to give macrocyclic structure. Further oxidation of the porphyrinogen afforded the desired porphyrin, 5,10,15,20-tetrakis(4-(7-(*tert*-butyl)pyren-2-yl)phenyl)porphyrin (**H-BPPy**), in 33% yield. The product was characterized by ^{1}H NMR spectroscopy and elemental analysis.

A ^{1}H NMR spectrum of **H-BPPy** indicated that highly symmetrical tetra-substituted structure of the molecule. The signal attributed to the protons at the *β*-position of pyrrole rings was observed as a singlet peak (Figure 1, 9.08 ppm). Two doublet signals from 4, 5, 9 and 10 positions of pyrene moieties (8.46 and 8.32 ppm) and two singlet signals from 1, 3, 6 and 8 position of pyrene moieties (8.72 and 8.27 ppm) appeared at upper field than pyrrole protons. Additionally, protons from phenyl linker moiety was observed in the vicinal region as two doublet peaks (8.23 and 8.15 ppm). Standard aliphatic hydrocarbons shows their signal approximately at 0 to 2 ppm, thus signal located at 1.61 ppm can be assigned to the protons of terminal alkyl chain of *tert*-butyl group. Finally, the inner imino proton showed their singlet broaden peak at 2.58 ppm due to ring current effect of porphyrin macrocycle.

The metal insertion reaction to **H-BPPy** was performed using iron and cobalt as metal source. Cobalt(II) acetate tetrahydrate (10 eq.) was used as a cobalt metal source and was reacted with **H-BPPy** in *N*-methylpyrrolidinone (NMP) at 210 ℃ by using microwave instrument (Scheme 3). Note that reaction at high tempterature (210 ℃) is crucial to proceed the metal insertion reaction, and several attempts using the reported synthetic conditions[8] at lower reaction temperature (< 200 ℃) were not successful. After 24 h, the generation of the desired cobalt porphyrin complex, 5,10,15,20-tetrakis(4-(7-(tert-butyl)pyren-2-yl)phenyl)porphyrinato cobalt(II) (**Co-BPPy**), was checked by UV-vis absorption spectroscopy. **Co-BPPy** was purified by column chromatography of the reaction mixture, and was obtained as a pure product in 11% yield. The product was

characterized by UV-vis absorption spectroscopy and elemental analysis. I also attempted the iron insertion reaction using iron(II) chloride tetrahydrate as a metal source in the same condition as employed in the synthesis of the cobalt complex. However, the formation of the desired product was not detected and only the consumption of starting material proceeded. Based on this observation, I designed an alternative synthetic route shown in Scheme 4. In this synthetic route, the iron insertion reaction is performed at an initial stage and the pyrene moieties are introduced by Suzuki-Miyaura coupling. The details of the synthesis are as follows. 4-iodobenzaldehyde was used as a starting material for condensation reaction with pyrrole in propionic acid. 5,10,15,20-tetrakis(4-iodophenyl)porphyrin (**H-PI**) was obtained as a major product in 65% yield. Subsequently, **H-PI** and iron(II) chloride tetrahydrate (5.9 eq.) was refluxed in *N*, *N*-dimethylformamide (DMF) for 1.5 h, which affords 5,10,15,20-tetrakis(4-iodophenyl)porphyrinato iron(III) chloride (**Fe-PI**) in 96% yield. Generation of the iron complex was checked by UV-vis absorption spectroscopy. As a final step, the desired iron porphyrin complex, 5,10,15,20-tetrakis(4-(7-(tert-butyl)pyren-2-yl)phenyl)porphyrinato iron(III) chloride (**Fe-BBPy**), was synthesized from **Fe-PI** by Suzuki-Miyaura coupling reaction with (7-(tert-butyl)pyren-2-yl)boronic acid (Yield: 6%). **Fe-BBPy** was characterized by UV-vis absorption spectroscopy and elemental analysis.

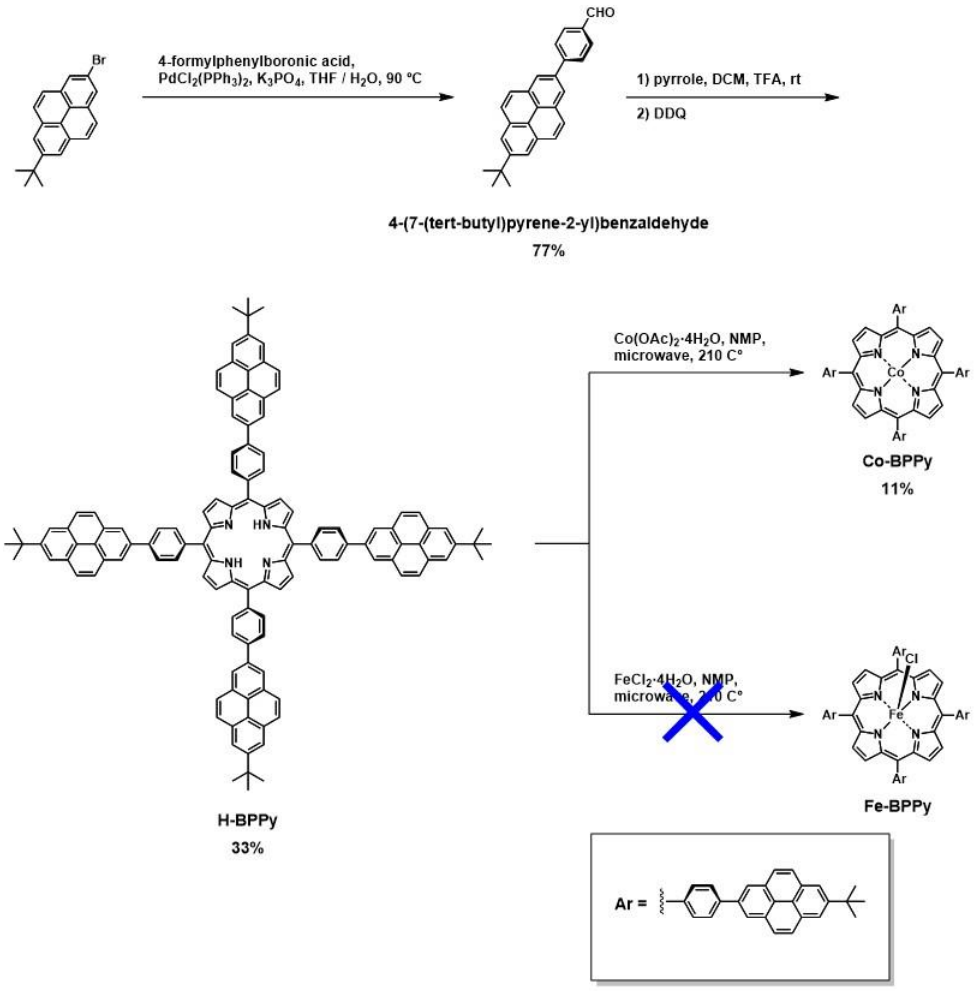

Scheme 3. Synthetic routes for the free-base porphyrin (**H-BPPy**) and the cobalt porphyrin complex (**Co-BPPy**).

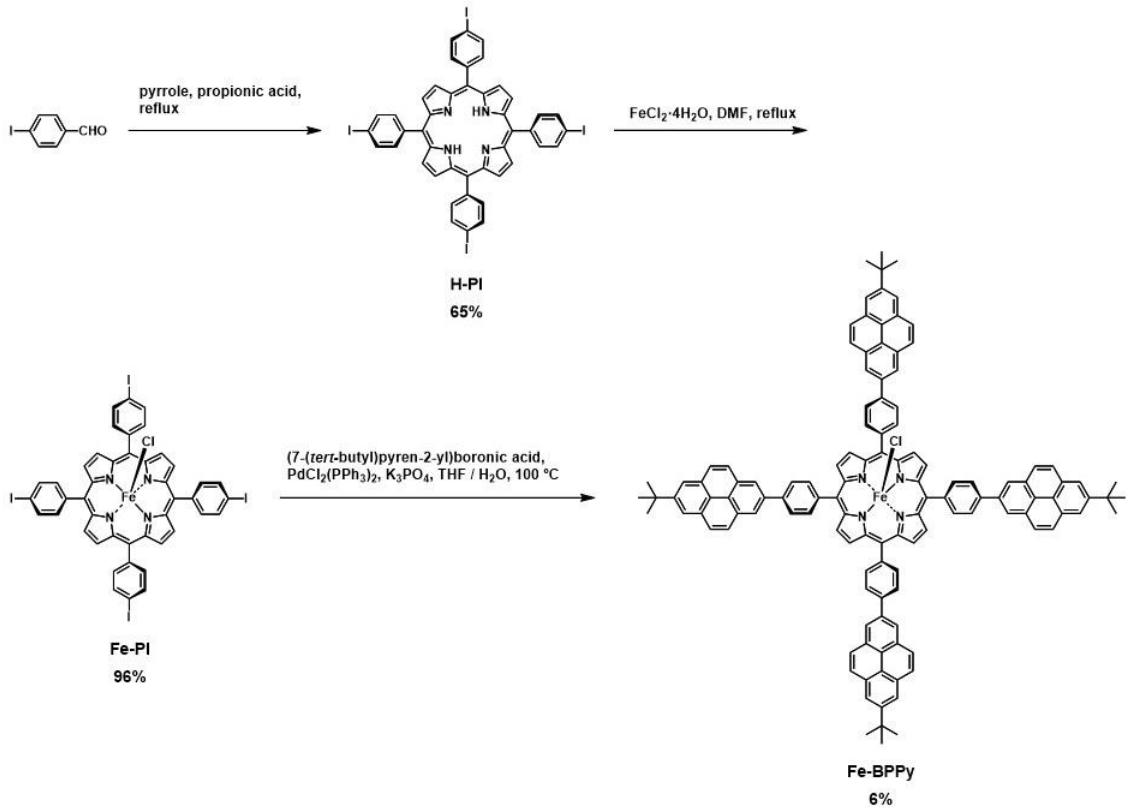

Scheme 4. Synthetic routes for the iron porphyrin complex (**Fe-BPPy**).

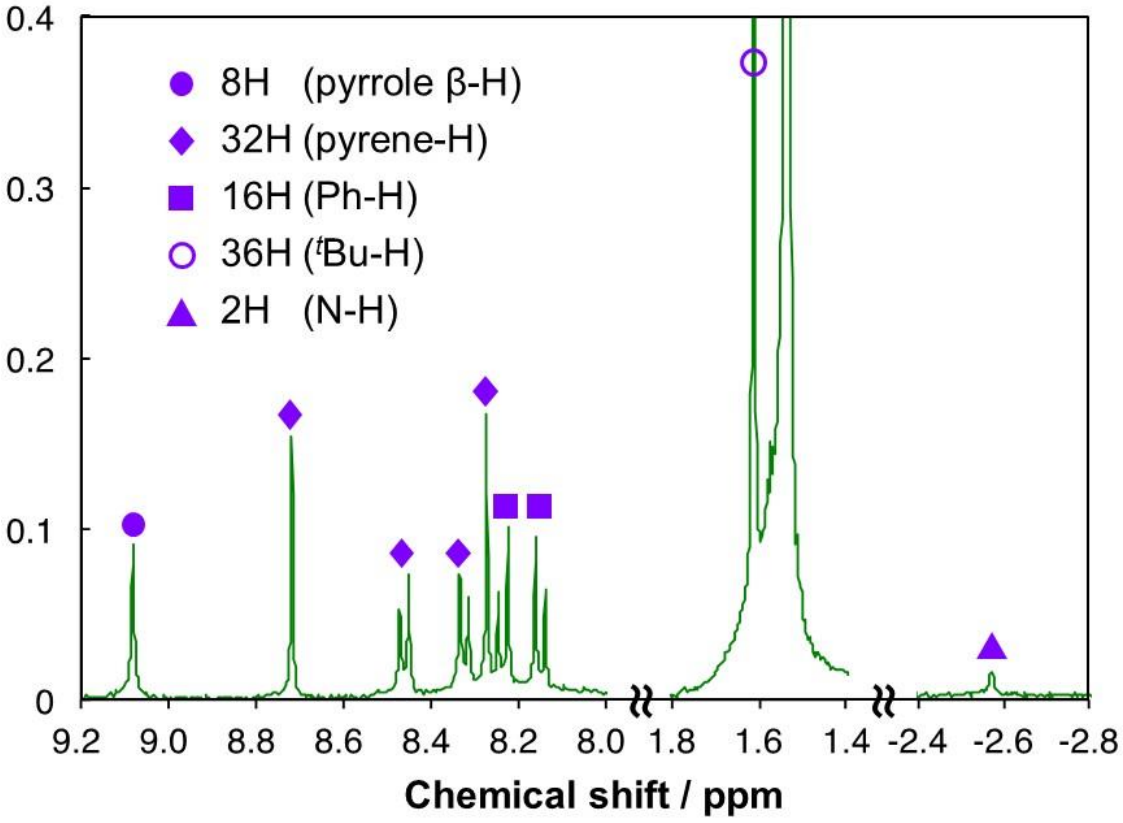

Figure 1. A ^{1}H NMR spectrum of **H-BPPy** (400 MHz, $CDCl_3$).

UV-vis Absorption Spectroscopy

UV-vis absorption spectra of free-base porphyrin and metalloporphyrin complexes were measured in 1,2-dichlorobenzene (Figure 2 and Table 1). For all compounds, sharp and intense bands assignable to *tert*-pyrene units were observed in the UV region,[9] and the peak positions of these bands were almost identical for all compounds (Table 1). At around 420−430 nm, Soret bands of porphyrin moiety was observed. The positions of the bands were similar for **H-BPPy** (429 nm) and **Fe-BPPy** (428.5 nm), whereas the slight blue shift of the band was observed for **Co-BPPy** (422 nm). The intensity of the band largely decreased upon the insertion of metal ions as previously reported.[10] In the visible region, four Q-bands of porphyrin moiety appeared for **H-BPPy** (521, 558, 595.5, and 652 nm). In contrast, the smaller number of Q-bands were observed for **Co-BPPy** and **Fe-BPPy** due to the degeneration of the HOMO and the HOMO–1 upon the generation of more symmetric structures via metalation.[11]

Table 1. Summary of the absorption spectra for the free-base porphyrins and the iron porphyrin complexes in 1,2-dichlorobenzene.

Compound	λ_{max} / nm ($\varepsilon/10^4$ M^{-1} cm^{-1})		
	Substituent's bands	**Soret-band**	**Q-bands**
H-BPPy	313.5 (7.04), 328 (10.24), 343.5 (14.8)	429 (47.52)	521 (1.84), 558 (1.56) 595.5 (0.62), 652 (0.60)
Co-BPPy	312.5 (6.34), 328.5 (7.74), 344.5 (10.14)	422 (9.7)	530.5 (1.34), br
Fe-BPPy	313.5 (8.52), 328.5 (11.34), 344.5 (16.28)	428.5 (10.48)	511.5 (1.44), 692.5 (0.36)

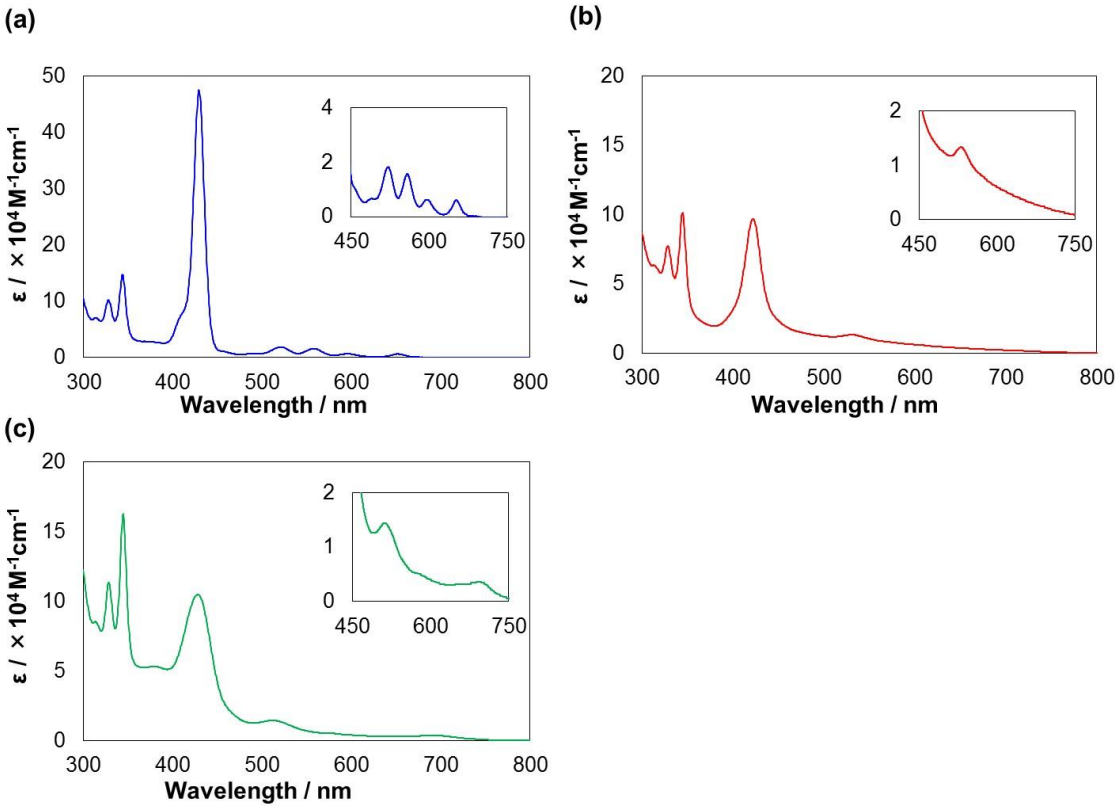

Figure 2. UV-vis absorption spectra of the porphyrin derivatives in 1,2-dichlorobenzene (a) **H-BPPy**, (b) **Co-BPPy**, and (c) **Fe-BPPy**. (Insets) Enlarged UV-vis absorption spectra at Q-band regions.

Cyclic Voltammetry

The cyclic voltammograms (CVs) of the free-base porphyrin (**H-BPPy**) and the metal porphyrin complexes (**Co-BPPy**, **Fe-BPPy**) are shown in Figure 3 and the redox potentials of these compounds are summarized in Table 2. The **H-BPPy** was soluble in 1,2-dichlorobenzene in spite of their highly planar structure and showed two redox waves corresponding to the reduction of porphyrin ring (Figure 3 (a)). The half wave potentials ($E_{1/2}$ (1) / V vs. ferrocene/ferrocenium (Fc/Fc^+)) for the first reduction was –2.10 V and that for the second reduction ($E_{1/2}$ (2)) was –2.40 V. For cobalt porphyrin complex (**Co-BPPy**), a half wave potential was observed at –2.40 V. In the case of **Fe-BPPy**, three reversible redox waves were observed at –1.17, –1.92 and –2.51 V, which are possibly assigned to be Fe(III)/Fe(II), Fe(II)/Fe(I) and Fe(I)/Fe(0) redox couples according to the previous report.[12]

For metal porphyrin complexes, the cyclic voltammograms were also measured under a CO_2 atmosphere. As shown in Figure 4 (a), the increase of the current was observed at around −2 V for **Co-BPPy**. In the case of **Fe-BPPy**, an increase of the irreversible current was observed both at the Fe(I)/Fe(0) redox couple (−2.51 V, Figure 4 (b)). These increase of the irreversible current is possible to due to the conversion of CO_2 to CO, which implies that both **Co-BPPy** and **Fe-BPPy** can serve as catalysts for CO_2 reduction.

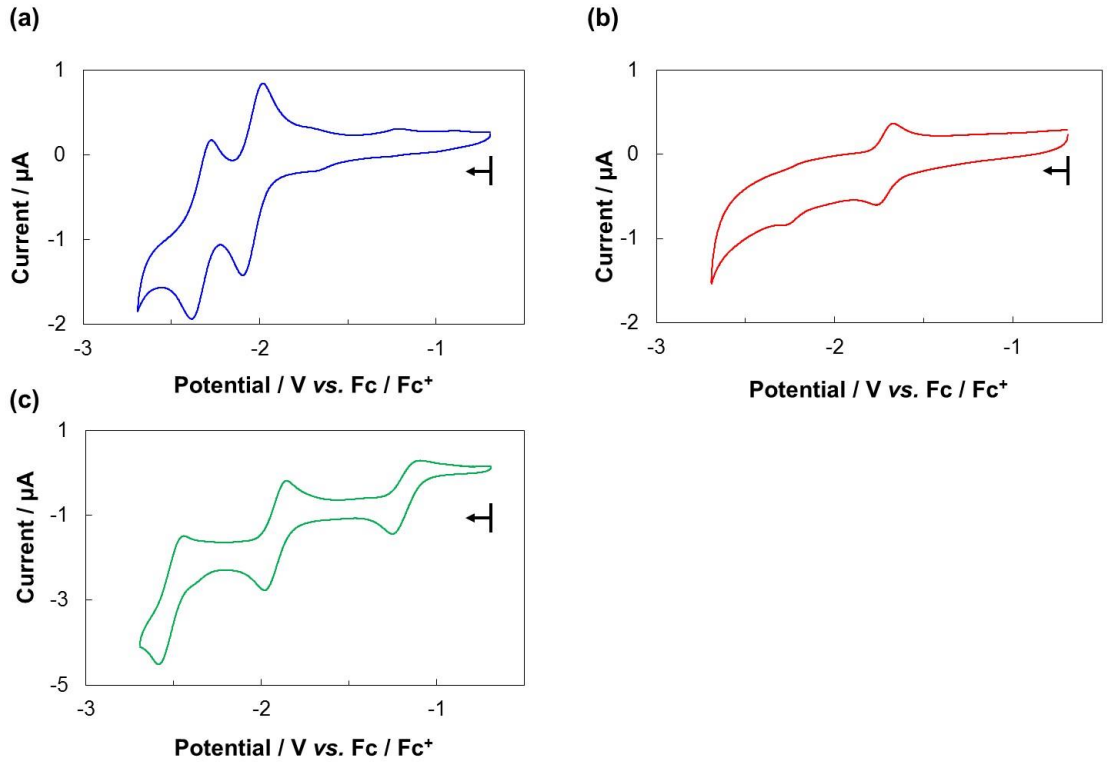

Figure 3. Cyclic voltammograms of the free-base porphyrin (a) **H-BPPy** (1.0 mM) and the metal porphyrin complexes (b) **Co-BPPy** (1.0 mM) and (c) **Fe-BPPy** (1.0 mM) in a 0.1 M TBAP/1,2-dichlorobenzene solution under an Ar atmosphere (WE: GC; CE: Pt wire; RE: Ag^{+}/Ag; scan rate: 20 mV s^{-1}). Potential sweeps of all compounds were started from the open circuit potential of −0.69 V. Arrows in the voltammograms indicate the direction of potential sweep.

Table 2. Redox potentials of the prepared free-base porphyrin (**H-BPPy**) and the metal porphyrin complexes (**Co-BPPy**) and (**Fe-BPPy**) ($E_{1/2}$ / V vs. Fc/Fc^{+}) in 1,2-dichlorobenzene under an Ar atmosphere.

Compound	$E_{1/2}(1)$ / V	$E_{1/2}(2)$ / V	$E_{1/2}(3)$ / V
H-BPPy	−2.04	−2.34	–
Co-BPPy	−1.72	–	–
Fe-BPPy	−1.17	−1.92	−2.51

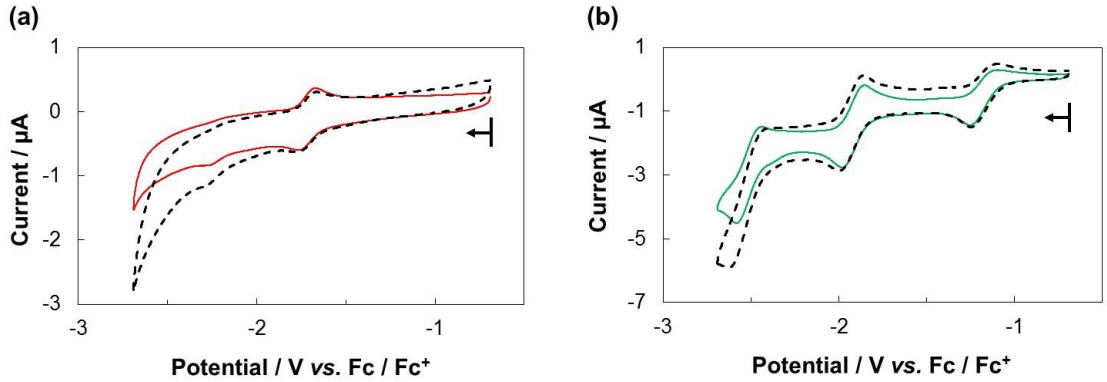

Figure 4. Cyclic voltammograms of the metal porphyrin complexes (a) **Co-BPPy** (1.0 mM) and (b) **Fe-BPPy** (1.0 mM) in a 0.1 M TBAP/1,2-dichlorobenzene solution under an Ar (solid lines) and CO_2 (dotted lines) atmosphere (WE: GC; CE: Pt wire; RE: Ag^+/Ag; scan rate: 20 mV s^{-1}). Potential sweeps of all compounds were started from the open circuit potential −0.69 V. Arrows in the voltammograms indicate the direction of potential sweep.

Crystal Structure

Single crystals of **Co-BPPy** were obtained by liquid diffusion of hexane to the THF solution of the complex and the crystal structure was determined by single crystal X-ray diffraction analysis. An ORTEP drawing and the summary of the crystallographic data of **Co-BPPy** are shown in Figure 5 and Table 3, respectively. The complex crystallized in a triclinic $P\bar{1}$ space group and one crystallographically independent **Co-BPPy** molecule was observed in the structure. The π planes of the phenyl moieties are slightly tilted against those of the pyrene moieties. The dihedral angles between the phenyl and pyrene moieties are in the range of 13.6−36.3 deg. The porphyrin moiety of the complex has distorted structure. Note that the occupancy of the cobalt center is approximately 24%, indicating that the structure is the co-crystal of the free-base porphyrin (**H-BPPy**) and the cobalt complex (**Co-BPPy**). In the ESI-MS spectrum of the crystals, a major peak at around 1640 m/z and a minor peak at around 1700 m/z were observed (Figure 6). These peaks can be assigned to **H-BPPy** and **Co-BPPy**, respectively. The UV-vis absorption spectrum of the crystals dissolved in 1,2-dichlorobenzene shown in Figure 7 exhibited Soret band and Q bands attributed to **H-BPPy**. These experimental results suggest the existence of **H-BPPy** in the structure and are consistent with the result of single crystal X-ray structural analysis.

The packing of the structure is shown in Figures 8−9. In this structure, the one-dimensional column stabilized by head-to-head CH-π interaction between pyrenyl moieties along the *a* axis was observed (Figure 8). The averaged distance between pyrene moieties was 2.90 Å. As a result, the distance between metal centres becomes relatively short (5.46 Å, Figure 9), which is expected to be close enough to function as adjacent reaction centres for CO_2 reduction. Additionally, these one-dimensional columns are connected via head-to-tail CH-π interaction with the distance of 2.68 Å (Figure 8), which results in the formation of porous structure (Figure 9). The pore entrance size was estimated to be 9.03 × 8.64 $Å^2$ by considering the van der Waals radii of the constituent atoms. In this pore, solvent molecules used in the recrystallization was observed.[13] These pores are expected to function as channels to accumulate CO_2 molecules because the pores should exhibit hydrophobic nature surrounded by aromatic ring and the size of pores is large enough to accommodate CO_2. It is also that the metal centres do not affect the

packing structure because this structure is obtained as the co-crystal of the free-base porphyrin and the cobalt complex.

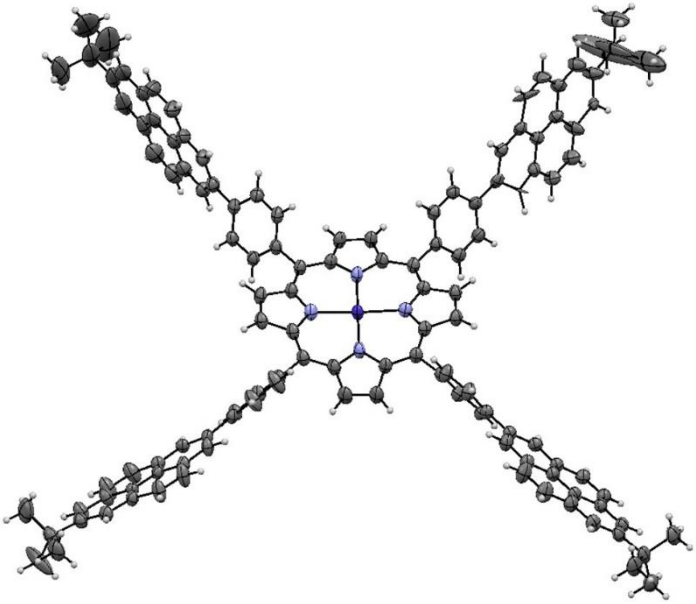

Figure 5. An ORTEP drawing of **Co-BPPy**. A disordered pyrene moiety was omitted for clarity. The occupancy of the cobalt ion is approximately 24%. Thermal ellipsoids are shown at the 50% probability level. C = gray, N = pale blue, Co = blue, and H = white.

Table 3. Summary of crystallographic data for **Co-BPPy**.

Formula	$C_{124}H_{92}Co_{0.24}N_4$
Fw	1652.3
Color, habit	red, platelet
Crystal size, mm	0.74 × 0.06 × 0.06
Crystal system	triclinic
Space group	*P*-1
a (Å)	12.8312(11)
b (Å)	19.1501(16)
c (Å)	22.182(2)
α (deg)	76.796(4)
β (deg)	89.726(5)
γ (deg)	78.659(4)
V (Å^3)	5198.2(8)
Z	2
T (K)	123(2)
R_1	0.0626
wR_2	0.1765
GOF	0.877

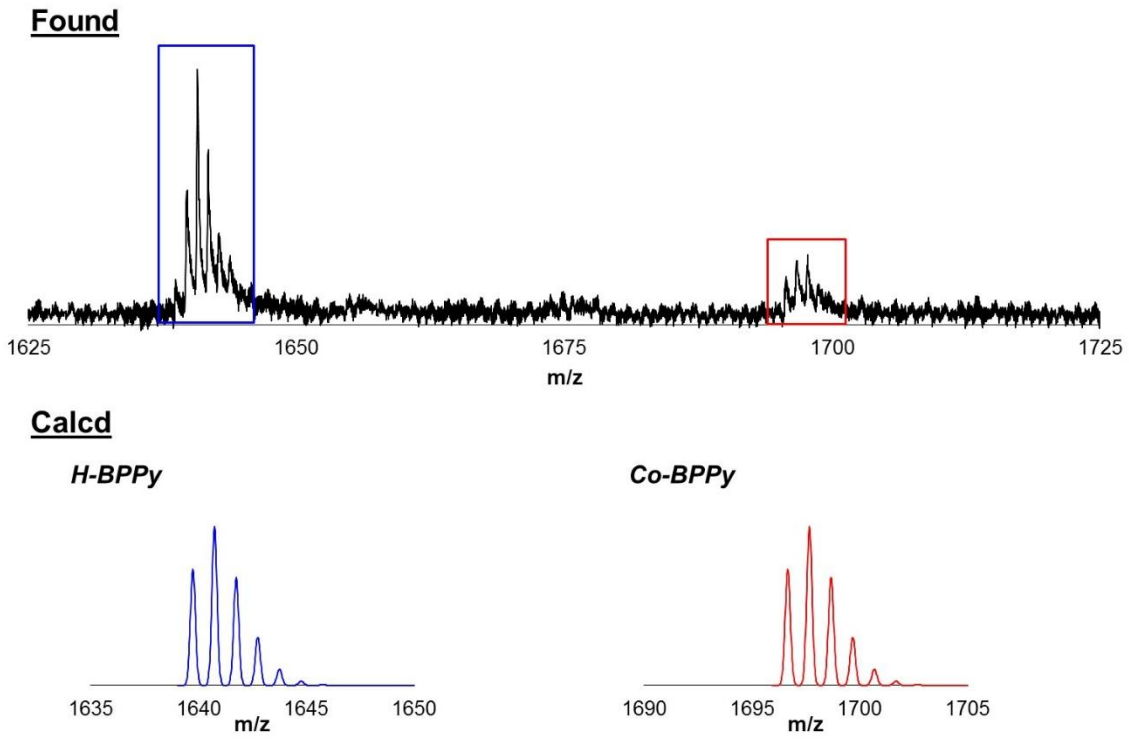

Figure 6. An ESI-TOF mass spectrum of single crystals of **Co-BPPy** (top) and simulated spectra for **H-BPPy** and **Co-BPPy** (bottom).

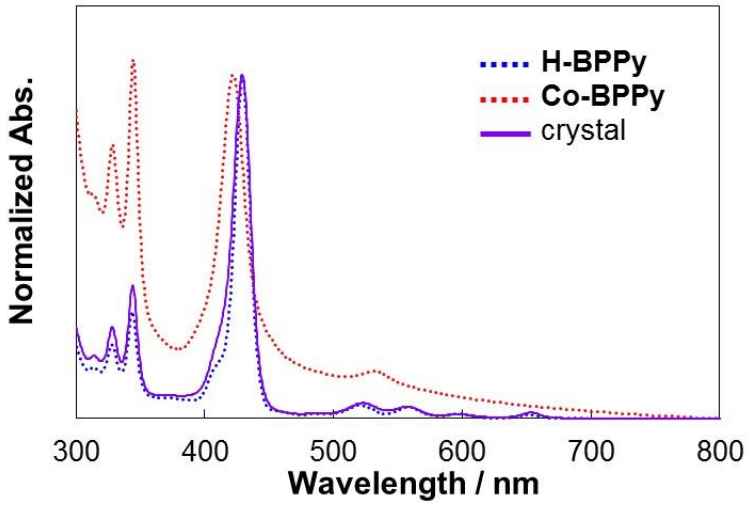

Figure 7. UV-vis absorption spectra of single crystals of **Co-BPPy** (purple solid line), **H-BPPy** (blue dotted line) and **Co-BPPy** (red dotted line) in 1,2-dichlorobenzen.

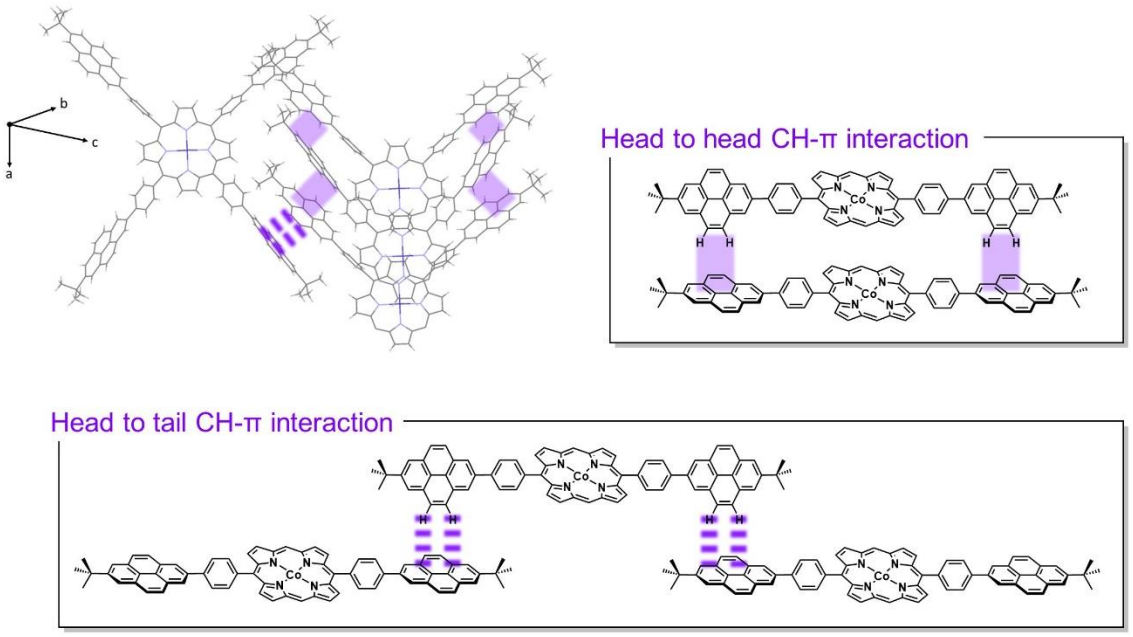

Figure 8. Packing structure of **Co-BPPy** and schematic figure of CH-π interaction between pyrene units.

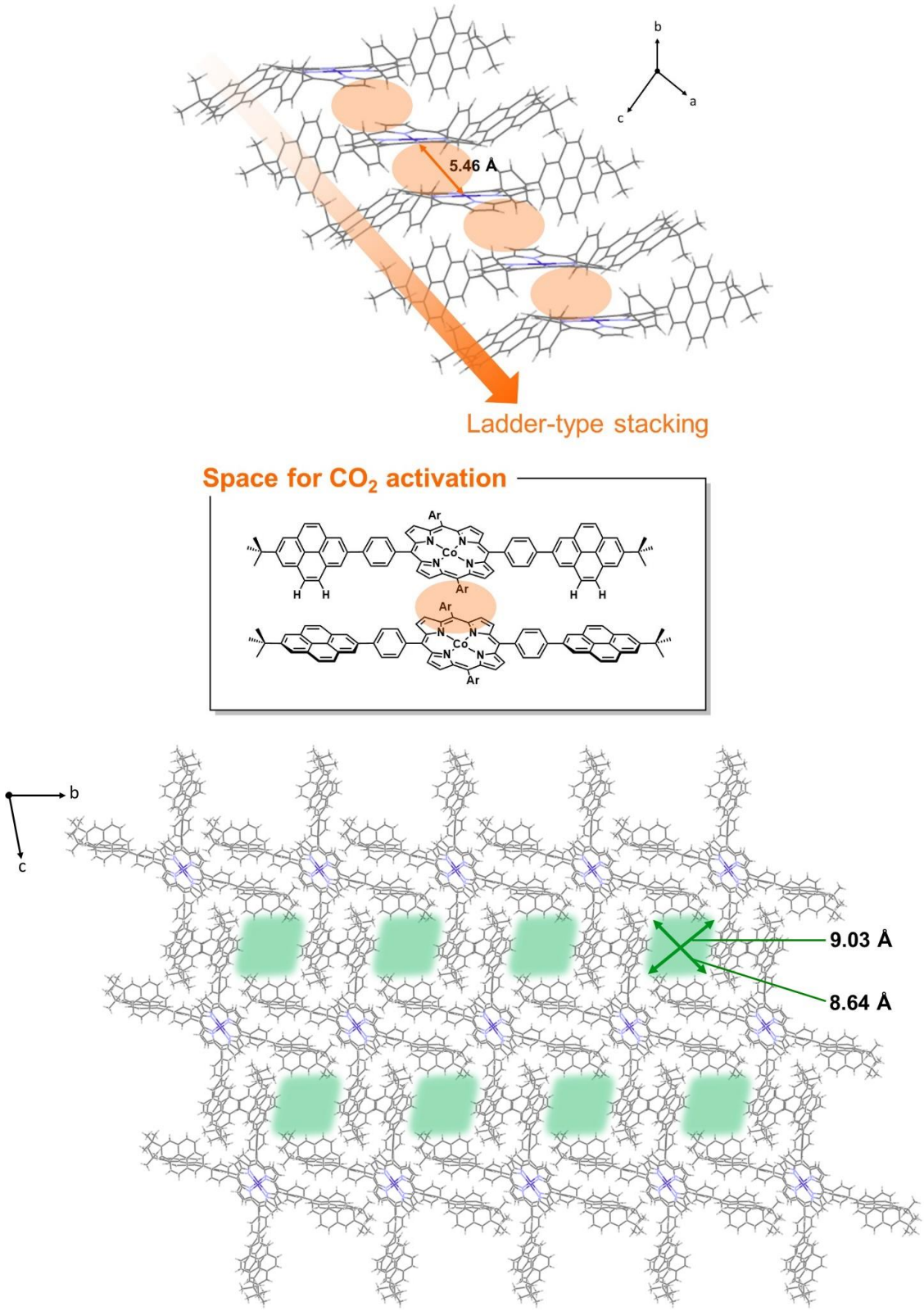

Figure 9. Packing structures of **Co-BPPy**.

Conclusion

As a summary of this study, highly symmetric and novel free-base porphyrin, cobalt and iron porphyrin complexes which have pyrene substituents for anticipation of construction of framework were successfully synthesized. The electrochemical measurement in solution under a CO_2 atmosphere indicated that the cobalt complex, **Co-BPPy**, can act as CO_2 reduction catalyst. The single crystal X-ray analysis of **Co-BPPy** was performed, and they have pores (9.03×8.64 Å^2) large enough than the size of CO_2 molecule in their packing structure. Moreover, the pore is hydrophobic because crystallization solvents existed in the void, thus it is expected to be the channel of CO_2 condensation. It should be also noted that the similar structure probably be obtained when the complex with different metal ions are used because the metal centres do not participate in the formation of porous structure. The catalytic activity of the framework as a heterogeneous catalyst should be investigated in the future.

Experimental

Materials and Methods

Pyrrole was purchased from Sigma-Aldrich Co., LLC. 1,2-dichlorobenzene, diethyl ether, ferrocene (Fc), 4-formylphenylboronic acid, HCl, iron(II) chloride tetrahydrate, MeOH, 1-methylpyrrolidin-2-one (NMP), triethylamine (TEA), trifluoroacetic acid (TFA), bis(triphenylphosphine)palladium(II) dichloride and tripotassium phosphate were purchased from Wako Pure Chemical Industries, Ltd. Hexane (Hex) and *N*,*N*-dimethylformamide (DMF) were purchased from Kanto Chemical Co., Inc. Tetra(*n*-butyl)ammonium perchlorate (TBAP), 1-bromopyrene, 2,3-dichloro-5,6-dicyano-1,4-benzoquinone, 4-phenylbenzaldehyde and triisopropyl borate were purchased from Tokyo Chemical Industry Co., Ltd. $CDCl_3$ was obtained from Cambridge Isotopes, Inc. All reagents were used without further purification. TBAP was recrystallized from absolute ethanol and dried in vacuo. Dichloromethane (DCM) and tetrahydrofuran (THF) were degassed and purified under an N_2 atmosphere using a GlassContour solvent system (Nikko Hansen Co., Ltd.).

Biotage INITIATER+ was used as microwave reactor for metal insertion reaction. ^{1}H NMR spectra were recorded on a JEOL 400 MHz instrument. All ^{1}H NMR spectra were referenced against residual proton signals. Elemental analyses were measured on a MICRO CORDER JM10. Electrochemical experiments were performed under argon and CO_2 atmospheres using a BAS ALS Model 650DKMP electrochemical analyzer. Cyclic voltammograms were recorded in 1,2-dichlorobenzene ([complex] = 1.0 mM; 0.1 M TBAP) using a glassy carbon disk, a platinum wire and an Ag^+/Ag electrode (Ag/0.01 M $AgNO_3$) that were used as the working, auxiliary, and reference electrodes, respectively. The redox potentials of the samples were calibrated against the redox signal for the ferrocene/ferrocenium (Fc/Fc^+) couple. UV-vis absorption measurements were performed on a Shimadzu UV-1800 spectrometer at room temperature. ESI-TOF mass spectra were recorded on a JEOL JMS-T100LP mass spectrometer. All the ESI-TOF mass spectrometric measurements were recorded in the positive ion mode at a cone voltage of 20 V. Typically, each sample solution was introduced in the spectrometer at a flow rate of 10 mL min^{-1} using a syringe pump.

Syntheses

Synthesis of 4-(7-(*tert*-butyl)pyren-2-yl)benzaldehyde: To the mixture of 2-bromo-7-*tert*-butylpyrene (1.2 g, 3.6 mmol), 4-formylphenylboronic acid (0.81 g, 5.4 mmol), tripotassium phosphate (2.3 g, 11 mmol) and bis(triphenylphosphine)palladium(II) dichloride (0.25 mg, 0.36 mmol) was added dry THF (36 mL) and water (5 mL). The mixture was refluxed with stirring for 19 h. The resulting mixture was extracted with DCM. The extract was dried over anhydrous Na_2SO_4, and concentrated under reduced pressure. The mixture was purified by column chromatography (DCM: Hex = 1:1) to afford the desired product (1.0 g, yield 77%). ^{1}H NMR (400 MHz, $CDCl_3$) δ 10.11 (s, 1H), 8.39 (s, 2H), 8.23 (s, 2H), 8.07 (d, J = 18.9 Hz, 8H), 1.58 (s, 9H) ppm.

Synthesis of 5,10,15,20-tetrakis(4-(7-(*tert*-butyl)pyren-2-yl)phenyl)porphyrin (H-BPPy): To a solution of 4-(7-(*tert*-butyl)pyren-2-yl)benzaldehyde (0.49 g, 1.4 mmol) in dry DCM (200 mL) was added pyrrole (0.094 mL, 1.4 mmol) in one portion at rt. After stirring for 5 min, to the reaction mixture was added TFA (0.207 mL, 2.7 mmol) at rt. The mixture was stirred for 19.5 h at rt and then DDQ (0.37 g, 1.6 mmol) was added. After 90 min, the reaction was quenched by TEA (0.38 mL, 2.7 mmol). The resulting mixture was purified by column chromatography (DCM) to afford a dark purple solution. The desired product was recrystallized from a tiny amount of THF and diethyl ether to give a purple solid (0.18 mg, yield 33%). ^{1}H NMR (400 MHz, $CDCl_3$) δ 9.08 (s, 8H), 8.72 (s, 8H), 8.46 (d, J = 7.9 Hz, 8H), 8.32 (d, J = 8.2 Hz, 8H), 8.27 (s, 8H), 8.23 (d, J = 9.2 Hz, 8H), 8.15 (d, J = 8.9 Hz, 8H), 1.61 (s, 36H), −2.58 (s, 2H) ppm. Anal. Calcd for $C_{124}H_{94}N_4 \cdot 1.25H_2O$: C, 89.58; H, 5.85; N, 3.37. Found: C, 89.67; H, 5.93; N, 3.41%.

Synthesis of 5,10,15,20-tetrakis(4-(7-(*tert*-butyl)pyren-2-yl)phenyl)porphyrinato cobalt(II) (Co-BPPy): To the mixture of **H-BPPy** (30 mg, 0.018 mmol) and $Co(OAc)_2 \cdot 4H_2O$ (46 mg, 0.18 mmol) was added NMP (18 mL). The mixture was refluxed for 12 h in microwave condition and then cooled to room temperature. After evaporating all the solvent, the resulting mixture was purified by column chromatography (DCM: MeOH = 19:1) to afford a red purple solution. The desired product was recrystallized from a tiny amount of THF and diethyl ether to give a red purple solid (3.5 mg, yield

11%). Anal. Calcd for $C_{124}H_{92}CoN_4 \cdot 5H_2O$: C, 83. 34; H, 5.75; N, 3.14. Found: C, 83.06; H, 5.68; N, 3.55%

Synthesis of 5,10,15,20-tetrakis(4-iodophenyl)porphyrin (H-PI): A solution of 4-iodobenzaldehyde (1.0 g, 4.3 mmol) and pyrrole (0.30 mL, 4.3 mmol) was refluxed in propionic acid (14 mL) for 3 h and then cooled to room temperature. The resulting mixture was filtrate and washed by MeOH to give a dark purple solid (0.78 g, yield 65%). ^{1}H NMR (400 MHz, $CDCl_3$) δ 8.82 (s, 8H), 8.09 (d, J = 7.9 Hz, 8H), 7.91 (d, J = 8.2 Hz, 8H), −2.91 (s, 2H) ppm.

Synthesis of 5,10,15,20-tetrakis(4-iodophenyl)porphyrinato iron(III) chloride (Fe-PI): To the mixture of **H-PI** (0.30 g, 0.27 mmol) and $FeCl_2 \cdot 4H_2O$ (0.32 g, 1.6 mmol) was added DMF (27 mL). The mixture was refluxed for 1.5 h and then cooled to room temperature. After evaporating all the solvent, the desired product was recrystallized from DCM and MeOH to give a dark purple solid (0.31 g, yield 96%).

Synthesis of (7-(*tert*-butyl)pyren-2-yl)boronic acid: To a solution of 2-bromo-7-*tert*-butylpyrene (1.0 g, 3.0 mmol) in THF (7.4 mL) ^{n}BuLi (2.8 mL, 4.4 mmol) was dropwisely added at −78 ℃. After stirring for 1 h, to the reaction mixture was added triisopropyl borate (1.4 mL, 5.9 mmol) at the same temperature. The mixture was stirred for 1.5 h at rt and then quenched by 1M HCl. After 90 min, the reaction was quenched by TEA (0.38 mL, 2.7 mmol). The resulting mixture was extracted with DCM, water and brine. The extract was dried over anhydrous Na_2SO_4, and concentrated under reduced pressure to afford the desired product (0.47 g, yield 52%).

Synthesis of 5,10,15,20-tetrakis(4-(7-(*tert*-butyl)pyren-2-yl)phenyl)porphyrinato iron(III) chloride (Fe-BBPy): To the mixture of **Fe-PI** (50 mg, 0.041 mmol), (7-(*tert*-butyl)pyren-2-yl)boronic acid (25 mg, 0.083 mmol), tripotassium phosphate (26 mg, 0.12 mmol) and bis(triphenylphosphine)palladium(II) dichloride (5.8 mg, 0.0083 mmol) was added dry THF (41 mL) and water (5.5 mL). The mixture was refluxed with stirring for 15 h. After evaporation of THF, the precipitate was washed by water and methanol. The

mixture was purified by column chromatography (DCM: Hex = 2:3) to give a green solid (4.4 mg, yield 6%). Anal. Calcd for $C_{124}H_{92}ClFeN_4 \cdot 5H_2O$: C, 81.86; H, 5.65; N, 3.08. Found: C, 82.05; H, 5.95; N, 3.03%.

References

1. M. Hammouche, D. Lexa, J-M. Savéant, M. Momenteau, *J. Electroanal. Chem. Interfacial Electrochem.*, **1988**, *249*, 347. (b) C. Costentin, G. Passard, M. Robert, J-M. Savéant, *Proc. Natl. Acad. Sci. U.S.A.*, **2014**, *111*, 14990. (c) T. Atoguchi, A. Aramata, A. Kazusaka, M. Enyo, *J. Chem. Soc., Chem. Commun.*, **1991**, 156. (d) D. Behar, T. Dhanasekaran, P. Neta, C. M. Hosten, D. Ejeh, P Hambright, E. Fujita, *J. Phys. Chem. A*, **1998**, *102*, 2870.
2. E. A. Mohamed, Z. N. Zaharan, Y. Naruta, *Chem. Commun.*, **2015**, *51*, 16900.
3. (a) I. Goldberga, *Chem. Commun.*, **2005**, 1243. (b) S-Y. Ding, W. Wang, *Chem. Soc. Rev.*, **2013**, *42*, 548. (c) N. U. Day, C. C. Wamser, M. G. Walter, *Polym. Int*., **2015**, *64*, 833.
4. S. Lin, C. S. Diercks, Y-B. Zhang, N. Kornienko, E. M. Nichols, Y. Zhao, A. R. Paris, D. Kim, P. Yang, O. M. Yaghi, C. J. Chang, *Science*, **2015**, *349*, 6253.
5. (a) T. Itoh, M. Kondo, M. Kanaike, S. Masaoka, *CrystEngComm*., **2013**, *15*, 6122. (b) T. Itoh, M. Kondo, H. Sakamoto, K. Wakabayashi, M. Kanaike, K. Itami, S. Masaoka, *Dalton Trans.*, **2015**, *44*, 15334.
6. (a) D. P. Lydon, P. Li, A. C. Benniston, W. McFarlane, R. W. Harrington, W. Clegg, *Eur. J. Org. Chem*., **2007**, *10*, 1653. (b) B. B. Shrestha, S. Higashibayashi, H. Sakurai, *Beilstein J. Org. Chem*., **2014**, *10*, 841. (c) M. A. Dobrowolski, G. Garbarino, M. Mezouar, A. Ciesielski, M. K. Cyrański, *CrystEngComm*., **2014**, *16*, 415. (d) A. Nagai, Y. Okabe, *Chem. Commun*., **2014**, *50*, 10052.
7. (a) N. Stock, S. Biswas, *Chem. Rev*., **2012**, *112*, 933. (b) T. R. Cook, Y-R. Zheng, P. J Stang, *Chem. Rev*., **2013**, *113*, 734. (c) U. Diaz, A. Corma, *Coord. Chem. Rev*., **2016**, *311*, 85. (d) J. L. Segura, M. J. Mancheñoa, F. Zamora, *Chem. Soc. Rev*., **2016**, *45*, 5635.
8. (a) T. Nakazono, A. R. Parent, K. Sakai, *Chem. Commun*., **2013**, *49*, 6325. (b) T. Nakazono, A. R. Parent, K. Sakai, *Chem. Eur. J*., **2015**, *21*, 6723. (a) A. Stockmann, J. Kurzawa, N. Fritz, N. Acar, S. Schneider, J. Daub, R. Engl, T. Clark, *J. Phys. Chem. A*, **2002**, *106*, 7958. (b) M. Raytchev, E. Pandurski, I. Buchvarov, C. Modrakowski, T. Fiebig, *J. Phys. Chem. A*, **2003**, *107*, 4592. (c) W. Weigel, W. Rwttig, M. Dekhtyar, C. Modrakowski, M. Beinhoff, A. D. Schlüter, *J. Phys. Chem. A*, **2003**, *107*, 5941.

(d) W. Wu, W. Wu, S. Ji, H. Guo, X. Wang, J. Zhao, *Dyes Pigments*, **2011**, *89*, 199.

9. Z-C. Sun, Y-B. She, Y. Zhou, X-F. Song, K. Li, *Molecules*, **2011**, *16*, 2960.
10. J. Mack, M. J. Stillman, The Porphyrin Handbook (Eds. K. M. Kadish, K. M. Smith, R. Guilard), **2003**, *16*, Elsevier Science, San Diego USA, 43.
11. (a) D. Lexa, J-M. Savéant, K-B. Su, D-L. Wang, *J. Am. Chem. Soc*., **1988**, *110*, 7617. (b) I. Bhugun, D. Lexa, J-M. Savéant, *J. Am. Chem. Soc*., **1996**, *118*, 1769. (c) É. Anxolabéhère, G. Chottard, D. Lexa, *New J. Chem*., **1994**, *18*, 889.
12. The diffused electron densities resulting from disordered solvent molecules in the pores were removed from the data set using the SQUEEZE routine of PLATON (A. L. Spek, Structure validation in chemical crystallography, *Acta Cryst*., **2009**, *D65*, 148).

Acknowledgements

I have been studied from April 2014 to March 2017 under the direction of Associate Professor Shigeyuki Masaoka in the Institute for Molecular Science and I would like to express my gratitude to him for his passionate encouragement, valuable and appropriate mentorship. I would like to show my greatest appreciation to Assistant Professor Mio Kondo for considerable encouragement, incisive advice, fruitful discussion and tremendous support. Without her encouragement, this dissertation would not have materialized. I would like to thank Designated Assistant Professor Masaya Okamura in Nagoya University for giving me instructive advices of chemistry.

I owe my deepest gratitude to Professor Hidehiro Sakurai in Osaka University for giving the chance to build up my English ability. I would like to express my gratitude to Assistant Professor Shuhei Higashibayashi in the Institute for Molecular Science for constructive and in-depth discussion. I learned a lot of techniques in organic synthesis field by his incisive tutelage. I am deeply grateful to Professor Shigeru Ishikawa in Tokai University for teaching of quantum chemical calculation.

I wish to thank our members in the Institute for Molecular Science, Dr. Vijayendran K. K. Praneeth, Mr. Takahiro Itoh, Ms. Pondchanok Chinapang, Ms. Arisa Fukatsu, Mr. Sze Koon Lee, Mr. Takafumi Enomoto, Mr. Hitoshi Izu (an amazing chef of I'z kitchen), Mr. Riku Ushijima, Ms. Chihiro Matsui, Ms. Reiko Kuga, Ms. Mari Kanaike and Ms. Akane Shibata, for the kind support, encouragement, valuable discussion, and friendship. I also wishes to express sincere thanks to our graduated member, Dr. Go Nakamura, Mr. Ke Liu, Ms. Yukino Fukahori. I also grateful to Ms. Mayuko Taniwake and Ms. Kyoko Nogawa for their clerical support.

I have greatly benefited from Sakurai group member, Dr. Qi-TaoTan, Dr. Tsuyuka Sugiishi, Dr. Yuki Morita, Dr. Raghu Nath Dhital, Dr. Binod B. Shrestha, Dr. Sangita Karanjit, Dr. Setsiri Haesuwannakij, Dr. Palash Pandit, Dr. Prasenjit Maity, Dr. Bernd Schmidt, Dr. Berit Topolinski, Dr. Gautam Panda, Dr. Sudipta Kumar Manna,

Mr. Satoru Onogi, Mr. Niti Ngamsomprasert, Ms. Patcharin, Ms. Paweena Pongpipatt, Ms. Jin Young Koo, Ms. Atchaleeya Jinasan, Mr. I-Chang Tsai, Mr. Jompol Thongpaen, Mr. Fabian F. Everle for their support and fruitful discussion.

I gratefully acknowledge Professor Kenichiro Itami and Dr. Hirotoshi Sakamoto in Nagoya University for the measurement of the single-crystal X-ray diffraction, Mr. Seiji Makita in the Institute for molecular Science for the elemental analysis and mass spectroscopy.

I appreciate Professor Tetsuro Murahashi, Assistant Professor Koji Yamamoto in Tokyo Institute of Technology, Assistant Professor Shinnosuke Horiuchi in Nagasaki University and Professor Masahiro Hiramoto in the Institute for molecular Science and Associate Professor Toshihiko Kaji in Tokyo University of Agriculture and Technology for precious experiences in different field in the lab rotation program.

I also gratefully acknowledge Professor Toshi Nagata in Meijo University, Associate Professor Norie Momiyama, Assistant Professor Atsuto Izumiseki, Assistant Professor Takuya, Kurahashi in the Institute for molecular Science, Designated Assistant Professor Koji Yamamoto in Tokyo Institute of Technology and the other members in the Yamate Joint Seminar for a meaningful discussion of chemistry.

Finally, I would like to thank my father Yoshifumi Okabe, mother Michiko Okabe, younger sister Riho Okabe, younger sister Saeko Okabe, all relatives and girlfriend Kyoko Imatsu for giving me the opportunity to learn chemistry, constant encouragement and tremendous supporting for my life.

Yuki Okabe

March, 2017

List of Publications

Chapter 1

Yuki Okabe, Mio Kondo, Akane Shibata, and Shigeyuki Masaoka
"Co-crystal structure of unsymmetric porphyrin with TCNE as acceptor molecule"
Manuscript in preparation.

Chapter 2

Yuki Okabe, Sze Koon Lee, Mio Kondo, and Shigeyuki Masaoka
"Synthesis and CO_2 reduction activities of π-expanded/extended iron porphyrin complexes"
J. Biol. Inorg. Chem., **2017**, *in press.* DOI: 10.1007/s00775-017-1438-3

Chapter 3

Yuki Okabe, Mio Kondo, Akane Shibata, and Shigeyuki Masaoka
"TBA"
Manuscript in preparation.

Other Publications

Atsushi Nagai and **Yuki Okabe**
"Charge transfer (CT) mechanochromism: dramatic CT absorption change of crystalline π-conjugated oligomers containing TCNQ upon mechanical grinding"
Chem. Commun., **2014**, *50*, 10052-10054.

Arisa Fukatsu, Mio Kondo, **Yuki Okabe** and Shigeyuki Masaoka
"Electrochemical analysis of iron-porphyrin-catalyzed CO2 reduction under photoirradiation"
J. Photochem. Photobiol. A: Chem., **2015**, *313*, 143-148.